Springer Theses
Recognizing Outstanding Ph.D. Research

Chengyuan Li

Not-So-Simple Stellar Populations in Star Clusters

Springer

Springer Theses

Recognizing Outstanding Ph.D. Research

Aims and Scope

The series "Springer Theses" brings together a selection of the very best Ph.D. theses from around the world and across the physical sciences. Nominated and endorsed by two recognized specialists, each published volume has been selected for its scientific excellence and the high impact of its contents for the pertinent field of research. For greater accessibility to non-specialists, the published versions include an extended introduction, as well as a foreword by the student's supervisor explaining the special relevance of the work for the field. As a whole, the series will provide a valuable resource both for newcomers to the research fields described, and for other scientists seeking detailed background information on special questions. Finally, it provides an accredited documentation of the valuable contributions made by today's younger generation of scientists.

Theses are accepted into the series by invited nomination only and must fulfill all of the following criteria

- They must be written in good English.
- The topic should fall within the confines of Chemistry, Physics, Earth Sciences, Engineering and related interdisciplinary fields such as Materials, Nanoscience, Chemical Engineering, Complex Systems and Biophysics.
- The work reported in the thesis must represent a significant scientific advance.
- If the thesis includes previously published material, permission to reproduce this must be gained from the respective copyright holder.
- They must have been examined and passed during the 12 months prior to nomination.
- Each thesis should include a foreword by the supervisor outlining the significance of its content.
- The theses should have a clearly defined structure including an introduction accessible to scientists not expert in that particular field.

More information about this series at http://www.springer.com/series/8790

Chengyuan Li

Not-So-Simple Stellar Populations in Star Clusters

Doctoral Thesis accepted by
the Department of Astronomy at Peking University,
Beijing, China.

Springer

Author
Dr. Chengyuan Li
Department of Physics and Astronomy
Macquarie University
Beijing
China

Supervisor
Prof. Richard de Grijs
Kavli Institute for Astronomy
and Astrophysics
Peking University
Beijing
China

ISSN 2190-5053 ISSN 2190-5061 (electronic)
Springer Theses
ISBN 978-981-10-5680-2 ISBN 978-981-10-5681-9 (eBook)
DOI 10.1007/978-981-10-5681-9

Library of Congress Control Number: 2017948204

Printed on acid-free paper

This Springer imprint is published by Springer Nature
The registered company is Springer Nature Singapore Pte Ltd.
The registered company address is: 152 Beach Road, #21-01/04 Gateway East, Singapore 189721, Singapore

Memorial to my grandfather

Supervisor's Foreword

Until about a decade ago, star clusters were considered 'simple' stellar populations. That is, it was generally agreed that all member stars in a given cluster formed at approximately the same time from the same progenitor gas cloud. As a consequence, all stars in a cluster were thought to have similar ages (within a few hundred thousand years, that is, the difference in formation timescales between low- and high-mass stars) and the same metallicity. Only the individual stellar masses were thought to vary, but the community also agreed that this variation was fairly well understood, given that the stellar initial mass function was thought to be universal, at least in the local Universe.

Over the past decade, this situation has changed dramatically, with a key consequence that star clusters can no longer be considered simple stellar populations. Yet, at the same time, they are among the brightest stellar population components and, as such, they are visible out to much greater distances than individual stars, even the brightest, so that understanding the intricacies of star cluster composition and their evolution is imperative for understanding stellar populations and the evolution of galaxies as a whole.

Chengyuan Li's Ph.D. thesis work collected in this book represents one of the first systematic analyses of deviations from the simple stellar population approximation for massive, well-populated star clusters with ages of up to a few billion years. In addition to a broad review of the subject suitable for non-experts, his work presented here addresses the dynamical importance of the presence of significant fractions of binary systems in the youngest star clusters, as well as their interaction products—blue straggler stars—in the much older globular clusters that are ubiquitous in most large spiral and elliptical galaxies.

At ages in excess of a few hundred million years, our interpretation of the observational Hertzsprung–Russell diagrams of the nearest massive star clusters becomes rather complicated. Suggestions put forward to explain the extended main-sequence turn-off regions observed in the colour–magnitude diagrams of such intermediate-age clusters include the presence of stellar populations characterized by a significant spread in age (≥ 300 million years) or metal abundance, or the presence of a population of rapidly rotating stars. Rapidly rotating stars can retain

hydrostatic equilibrium at lower temperatures than their equal-mass, non-rotating counterparts, thus resulting in cooler stellar atmospheres and, hence, redder colours in the colour–magnitude diagram for approximately the same luminosities.

Chengyuan Li set out to disentangle the effects of age/metallicity spreads and stellar rotation using the innovative idea to focus on post-main-sequence evolutionary stages, that is, clusters' subgiant and red giant branches. He produced ground-breaking results, leading to publication in *Nature* on two occasions, concluding that an extended main-sequence turn-off does not necessarily imply the presence of a significant age or metallicity spread. He showed conclusively that a population of rapidly rotating stars could explain the observational results equally well or even better.

His research also led to rather puzzling and as yet unexplained results, showing the apparent presence of single-age *younger* stellar populations associated with a number of intermediate-age clusters in the Milky Way's nearest companion galaxies, the Large and Small Magellanic Clouds. While this has led to vigorous debate within the astronomical community, this result appears to have stood the test of careful scrutiny. The implications of his work are exciting: we now understand the formation and subsequent evolution of massive star clusters much better than even a few years ago, yet many open questions remain. This, however, is the nature of the pursuit of high-level science: new answers tend to raise even more follow-up questions, and Chengyuan Li is now well placed to make his mark in this fast-moving field!

Beijing, China
October 2016

Richard de Grijs
Professor of Astrophysics

Preface

Scope

Almost all stars initially stayed in clustered environment, they formed from following the turbulent structure. These structures will quickly collapse into bound clusters within very short period. Current consensus of formations of star clusters suggests that their star-forming processes should behave as a star burst mode: the initially segregated protostars and the secondary protostars will lead the central region of a cluster to be shielded from further gas accretion, they will quickly dominate the cluster region and expel their surrounding gas through strong stellar feedback, stoping the subsequent star formation. This is the simple stellar population scenario, which means in a star cluster, all of its member stars should form in the same era (therefore have the same age) and share similar helium abundance and metallicity. However, the discoveries of stellar age spreads and chemical anomalies of stellar populations in lots of massive clusters have made the notion of star clusters as true samples of simple stellar populations had to face a serious challenge. This book aims to introduce the stellar population properties of star clusters with various ages. The history and progress of researches in this field as well as most recent improvements, including observational results and related scenarios that were proposed to explain the observations, are also present.

Content

This book consists of three parts: Part I contains the background knowledges of star formation and evolution, as well as an introduction of current consensus of stellar populations in star clusters. Part II covers the latest researches related to this topic, including the observational results of young massive star clusters, 1–2 Gyr intermediate-age star clusters as well as old globular clusters. The relevant scenarios that proposed to explain the observations are also present. Part III gives a

comprehensive discussion based on all the observations and explanations: Where do we stand in this field? How can we shed light on the stellar population problems in the future? What is the impact on other astrophysical aspects once we improved our understanding on this topic?

This book is mainly based on my Ph.D. thesis that was submitted to Peking University of China in 2015, it also includes some of our subsequent researches and reviews, as this active field really changes rapidly. Because of this, we cannot guarantee that all the conclusions appearing in this book are exactly correct, we suggest that readers inherit the knowledges of this book in a critical way.

Audience

This book is designed for junior researchers who are interested in stellar populations in star clusters. For those who are senior experts in this field, we hope this book can serve as a reference for scientific discussions and debates. For readers who want to get a quick start on this field, we encourage them to focus on Part I, Part III and the main conclusions in Part II. The Chaps. 1 and 2 in Part I mainly focus on the basic knowledges of star formation and evolution, readers who already have this base level foundation can skip this part and directly enter the Part II, which introduces our latest research results related to this field. Any comment about our works in this book is welcome.

Acknowledgements

I want to thank Dr. Mark Gieles at the University of Cambridge, UK, Dr. Simon F. Portegies Zwart at the Leiden Observatory, the Netherlands and Dr. Wuming Yang at the Beijing Normal University, China, for sharing their data with us. I also want to express my gratitude to Dr. Wong Mek, who was my psychiatrist when I was a Ph.D. student in Peking University, she supported in any aspect during that period.

Macquarie University, Sydney Chengyuan Li

Contents

Part I Star Formation, Evolution and Stellar Populations in Star Clusters

1 Stellar Evolution and Populations 3
1.1 The Early History of Researches on Star Clusters 3
1.2 A Simple Introduction on Stellar Evolution 6
1.2.1 The Main Sequence 6
1.2.2 The Turn-Off and Sub-giant Stage 8
1.2.3 The Red-Giant Stage 9
1.2.4 Stellar Age Versus Its Initial Mass 10
1.3 Simple Stellar Populations 11
1.3.1 Describing the Simple Stellar Population 12
1.4 Not-So-Simple Stellar Populations: Multiple Stellar Populations 13
1.4.1 Describing the Multiple Stellar Populations 14

2 Researches of Stellar Populations in Star Clusters 19
2.1 Stellar Populations: We Think We Know Until Everything Change 19
2.1.1 Why Most Clusters Should be Simple Stellar Populations? 19
2.1.2 Complicated Stellar Populations in Star Clusters 22
2.2 Proposed Scenarios 26
2.2.1 The Extended Main Sequence Turn-Off Regions in Star Clusters 26
2.2.2 Multiple Stellar Populations in Old Globular Clusters 29

Part II Researches on Stellar Populations in Massive Star Clusters

3 Binary Fraction in Young Massive Star Clusters 35
3.1 Introduction 35
3.2 Data Reduction 36
3.3 Isochrone Fitting 38
3.3.1 Detect Binary Stars in the CMD 40
3.3.2 Determine the Coordinates of Cluster Center 41
3.3.3 Artificial-Star Tests 42
3.4 Results Based on χ^2 Minimization 45
3.5 Physical Implications 49
3.5.1 Binary Segregation 49
3.5.2 Binary Dynamical Disruption 51
3.6 Summary on This Work 53

4 The Formation and Evolution of Blue Straggler Stars in Globular Cluster 55
4.1 Introduction 55
4.2 Data Reduction 57
4.3 Analysis and Results 58
4.4 Physical Implications 61
4.5 Conclusion 62

5 Multiple Stellar Populations in the Giant Branches of Galactic Globular Clusters 65
5.1 Introduction 65
5.2 Data Reduction and Analysis 66
5.3 Main Results 71
5.3.1 Sub-giant Branch Stars 71
5.3.2 Red-Giant Branch Stars 74
5.4 Physical Inplications 78
5.5 Conclusion 85

6 Do Intermediate-Age Star Clusters Have Extended Star Formation Histories? 89
6.1 Introduction 89
6.2 Data Reduction 90
6.3 Main Results 91
6.3.1 NGC1651 91
6.3.2 NGC411 94
6.3.3 NGC419 99
6.4 Physical Discussion 102
6.5 Conclusion 104

Part III Not-So-Simple Stellar Populations in Massive Star Clusters, Where Do We Stand?

7 Lessons Learned from This Thesis 109
7.1 Do the Young Massive Clusters Harbor Multiple Stellar Populations? 109
7.2 No Evidence of Multiple Stellar Populations in Intermediate-Age Star Clusters 111
7.3 Do Globular Clusters have Another Origin? 112
7.4 Epilogue 115

References 119

Acronyms

AS	Artificial Star
AU	Astronomical Unit
BSS	Blue Straggler Star
GC	Globular Cluster
GMC	Giant Molecular Cloud
HRD	Hertzsprung–Russell Diagram
HST	Hubble Space Telescope
ISM	Interstellar Medium
LF	Luminosity Function
MS	Main Sequence
MSP	Multiple Stellar Population
MSTO	Main-Sequence Turn-Off
MW	Milky Way
NIR	Near Infrared
PSF	Point Spread Function
RGB	Red giant branch
SFH	Star Formation History
SGB	Subgiant Branch
SSP	Simple Stellar Population
UV	Ultraviolet
VISTA	Visible and Infrared Survey Telescope for Astronomy
YMC	Young Massive Cluster
ZAMS	Zero Age Main Sequence

Part I
Star Formation, Evolution and Stellar Populations in Star Clusters

Chapter 1
Stellar Evolution and Populations

1.1 The Early History of Researches on Star Clusters

Assume you live in the northern hemisphere. On a clear summer night, with no cloud or light pollution from urban areas, you go outside and watch the sky, and you will see stars fully distributed around the whole sky. If you stare at them long enough, you will resolve that most of them seem associated with a stripe, which we call the Milky Way (MW), the galaxy that we live in. At first glance, you may think stars are roughly homogeneously distributed in the MW, with large 'void' regions between them like the stars that in our solar neighborhood. But if you have a excellent vision or use a small telescope, you will find that some stars seem to be distributed as clumps. Most of these clumps are called 'star clusters' (SCs). The discovery of SCs can date back to the Renaissance. Galileo Galilei, wrote "the galaxy is nothing else but a mass of innumerable stars planted together in clusters." in his treatise *Sidereus Nuncius* [1], and it has been realized that the stars in a SC are physically related since 1767 [2]. Now people believe that clusters are the basic units for star formation [3]: almost all stars form in clustered environments, most of them will dissipate into the galactic field over time [4], This scenario seems to not only hold for our MW, but also for other galaxies [4, 5]. Because of this, understanding stellar evolution in SCs and the evolution of SCs themselves hence becomes important for understanding galaxy evolution as a whole.

The number of stars that are contained in SC can be span from less than 10 to several millions, and with the average age from extremely young (several million years, Myr) to the cosmic age (more than 10 billion years, Gyr). SCs in the MW can be classified as Open Clusters (OCs) and Globular Clusters (GCs). These two types of SCs are very different in both configuration as well as their spatial distribution in the Galaxy. OCs usually contain up to hundreds of stars, sometimes even only several tens, like **the Pleiades** (see Fig. 1.1). Since the observed 'strip' in the night sky is just the disk structure of our MW, OCs are usually associated with the MW disk. Since SCs often contains lots of stars, it hence becomes clearly difficult to define the age of SCs. However, as the next section will introduce, stars in SCs are believed to

C. Li, *Not-So-Simple Stellar Populations in Star Clusters*, Springer Theses,
DOI 10.1007/978-981-10-5681-9_1

Fig. 1.1 The open cluster pleiades (messier 45). Credit: NASA (Roberto Colombari)

form in the same era, so it is often not a problem to set those stars' average age as the age of a SC. OCs are often very young, at least in the MW, with ages of several Myr. Only a few rare exceptions can reach several Gyrs, like **Messier 67** (M67) [6]. Compared to the GCs, whose age normally can reach the cosmic age (more than 10 billion years), the OCs were just born yesterday.

GCs may more deserve to be called 'cluster'. They often contain more than 10,000 stars, some even reach millions of stars, and, almost all of them exhibit a spherical appearance (see **Messier 80** as an example in Fig. 1.2). Unlike the OCs, which are often associated with the MW disk, GCs are often found in the Galactic halo, which is a spheroidal structure that surround the disk. The Galactic GCs are the oldest objects in the Universe, whose ages are often greater than 10 Gyr. This indicates that their member stars should more or less belong to the earliest stellar generation. However, it seems that the first stars (population III stars) still did not formed in these GCs [7]. Currently 158 GCs are known in the MW [8].

It is still unclear if GCs and OCs have the same origin. This is because, as the OC evolve, most of its member stars will escape from SCs. This process is called 'evaporation' (for more details, see [9]). It was estimated that the typical number of member stars for SCs that can survive to the cosmic age (>10 Gyr) should be at least 10^5 [10]. Clearly, rarely OCs can contain enough member stars to that reach this number. Also the lack of intermediate-age SCs (with ages between $\sim$1 and 10 Gyr) in the MW makes investigation of the continues evolution of SCs difficult. Because of this, the sample of extragalactic (like Large Magellanic Cloud, LMC) SCs, ideally compensates this disadvantage.

Fig. 1.2 The globular cluster messier 80. Credit: HST/NASA/ESA

Table 1.1 Comparison of fundamental parameters of Open Clusters (OC), Globular Clusters (GC), and young massive clusters (YMC), credit: [10]

Cluster type	Age [Gyr]	Mass [$M_{\odot}$[a]]	Central density [$M_{\odot}$ pc^{-3}]	Metallicity[b] [$Z_{\odot}$]
OC	$\leq$0.3	$\leq 10^3$	$\leq 10^3$	$\sim$1
GC	$\geq$10	$\geq 10^5$	$\geq 10^3$	$\leq$1
YMC	$\leq$0.1	$\leq 10^4$	$\geq 10^3$	$\geq$1

[a]The solar mass.
[b]The mass fraction for element that heavier than helium, it has been normalized to the solar metallicity

There is another type of young massive clusters (YMCs), which is rare in the MW, but common in some other galaxies. The YMCs are as young as OCs, but unlike the OCs, they always contain large numbers of stars, hence they are as compact as GCs. The basic features of OCs, YMCs and GCs, including their typical age, total mass, metallicity (the mass fraction of elements that are heavier than helium (He), indicated by "Z" [for sun, the latest $Z \sim 0.0152$ [11]) and core density, are present in Table 1.1 (derived from [10]). Compared to OCs, the YMCs seem to prefer to be candidate of 'young GCs'. Since they contain more stars than OCs and are compact, the probability for them survive to the cosmic age is high. Figure 1.3 shows the configuration of the YMC NGC1818.

In any case, SCs are the most important objects in a galaxy. It is important to investigate their formation, interaction and evolution if one wants to understand the fate of a galaxy as a whole. For a SC, its stellar populations contain the most

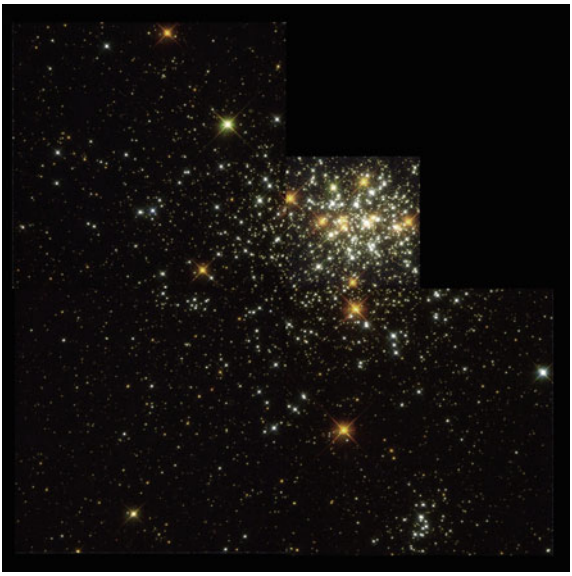

Fig. 1.3 The young massive cluster NGC1818. Credit: HST/NASA/ESA

important information about its formation and evolution. The basic tool to study the stellar populations in star clusters is the theory of star formation and evolution, which has been well established in last century. Although today there are lots of well-established stellar evolutionary models, in Part II, we will see that there are still some physical parameters that will affect our understanding of the stellar populations in a SC.

1.2 A Simple Introduction on Stellar Evolution

1.2.1 The Main Sequence

We begin our story on the "main sequence" (MS), i.e., stars have already formed, continually burning their core hydrogen. Because the core region's nuclear reactions heat the whole star, its radiation pressure can balance the stellar self-gravity, the whole star therefore reaches hydrostatic equilibrium. Such kind of star is called a MS star. Most of the stars that we observe are MS stars, and they are quite simple, discovered by Hertzsprung Ejnar and Russell Henry Norris [12, 13]. They first investigated the relationship between the stellar luminosity and spectral types (now we call the diagram of this relationship "**Hertzsprung–Russell diagram (HRD)**", or equally, the "Color-magnitude diagram" (CMD)). They found that most of the stars are located in a stripe from blue-bright towards red-faint, and hence called them the MS stars.

The main sequence is also a mass sequence, with the massive stars being the brightest stars, while the less massive stars are relatively faint. The relationship between the MS stars' luminosity and mass can be approximately described as [14]:

$$L/L_{\odot} = 1.2(M/M_{\odot})^{4.0}, (0 \leq M_{\mathrm{bol}} \leq +7.5) \tag{1.1}$$

or

$$L/L_{\odot} = 0.67(M/M_{\odot})^{2.76}, (+7.5 \leq M_{\mathrm{bol}} \leq +11) \tag{1.2}$$

Here, L indicates the luminosity, and M is the stellar mass, the "$\odot$" subscript indicates values that correspond to the sun. M_{bol} is the bolometric magnitude, the magnitude that take into account the stellar radiation over all wavelengths (in observation, we only select a certain band to collect the radiation from stars over a given range of wavelength). The relationship between bolometric magnitude and luminosity is:

$$L/L_{\odot} = 10^{(M_{\mathrm{bol}} - M_{\mathrm{bol}_{\odot}})} \tag{1.3}$$

It is easy to find that the most massive stars are also the most luminous objects, while the less massive stars also belong to the faintest sample. Hence for the MS stars, we get a one-to-one relationship between their mass, luminosity and color: **the MS in fact describes a stellar sequence from massive, bright and blue to less massive, faint and red**. Another important conclusion is that the stellar radiation is very close to black-body behavior. This is because the stellar atmosphere is very opaque (so called optically thick). Photons radiating from the stellar core are hardly transported to the surface. The black-body radiation would fit the "Wien displacement law", which describes the relationship between the typical color and temperature for black-body radiation.

$$\lambda_{\mathrm{max}} = \frac{0.28978}{T} \ (\mathrm{cm\ K^{-1}}) \tag{1.4}$$

where λ_{max} indicates the wavelength placement of maximum radiation intensity, and T is the corresponding temperature of the black-body. It is hence clear that a black-body typically radiating in short-wavelengths should correspond to a high temperature, and black-body radiation that seems red indicates a low temperature. Since the MS stars is approximately radiate like a black-body, we hence connect their color to their surface temperature.

In one sentence, the stars on the MS should harbor such features: the more massive, the brighter, bluer, and hence with higher surface temperature; the less massive, the fainter, redder, with lower surface temperature. Figure 1.4 illustrates this relationship.

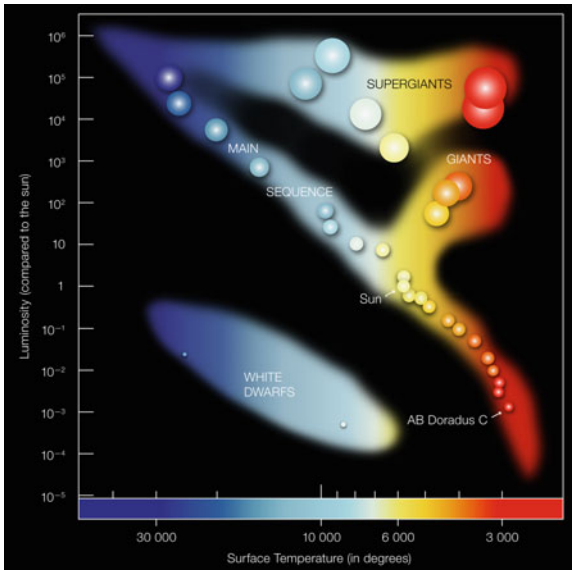

Fig. 1.4 An illustration of the stellar Hertzsprung–Russell diagram. The strip that runs across the whole diagram indicates the main sequence. The horizontal axis indicates their surface temperature (hence the color), the vertical axis indicate their luminosity relative to the sun (equal to the magnitude). Credit: ESO

1.2.2 The Turn-Off and Sub-giant Stage

Once stars have used all of their core hydrogen (all hydrogen has been transferred into helium), it lacks nuclear reactions to balance its self-gravity, so that the star begins to contract. It releases gravitational potential energy, which heats the surrounding hydrogen shell of the core, at this stage, the shell begins burning, stops the contraction and expands outwards. But the central temperature is still not high enough to trigger helium burning, so in the mean time, the stellar core keeps contracting, becoming denser and denser. Stars then enter the turn-off region, and evolve to the sub-giant phase.

Stars evolving from turn-off to the sub-giant stage would experience very complicated physical processes, since they expand in radius. From the well-known relationship between luminosity, temperature, and radius for a black-body, we get:

$$L = 4\pi R^2 \sigma T_{\text{eff}}^4 \tag{1.5}$$

where $\sigma \approx 5.67 \times 10^{-8}\,\text{Js}^{-1}\text{m}^{-2}\text{K}^{-4}$ is the Stefan-Boltzman constant. From (1.5) we get, if we keep the luminosity constant, the increase in radius would lead to a decrease in temperature. Hence this indicates that the stars in expansion would become redder. But of course, the energy released by the shell burning should not identical to that by core burning when stars are on the MS. For most low-mass stars ($M \leq 2.3 M_{\odot}$), their turn-off stage would experience a significant luminosity increase, because the shell burning lead to a increasing reaction rates, but changes little in color, while when star goes into the sub-giant stage, their expansion becomes important, and at this stage

it would vary more significant in color. From the view of the CMD, this means that stars at this stage would go across from the left towards the right, a significant change in their position along with color-axis. The sub-giant stage is a very short stage in the context of the whole stellar evolution. Stars would quickly travel across the sub-giant region and enter the red-giant stage. However, as we will see, the sub-giant stars are very important to study stellar populations in SCs.

1.2.3 The Red-Giant Stage

The burning converts the hydrogen shell into a helium shell. The helium shell then quenched and contracts towards the central core, and makes the core more and more massive. In the mean time, the core keeps contracting and hence becomes denser. The contraction of the more massive core again releases a larger amount of potential energy, and enhance the rate of hydrogen burning in the shell [15]. At this stage, almost the whole outer layer becomes convective. The convective shell soon penetrates so deeply that $\sim$70 % of the total mass is convective [16]. The star's luminosity has a monotonic positive correlation to its helium core mass. At this stage, the increased helium core would cause the stellar luminosity to increase by a factor of 1000–10000. In the mean time, the helium core is so dense that the electrons in the core are degenerate. The core become isothermal, releasing neutrino radiation, and further cooling the core surrounding temperature. Also the shell keeps expanding and decreasing the surface temperature. Hence a star would continually evolve towards the red direction in the CMD (in Fig. 1.4 the red-giant stars are indicated as "giant stars"). At this stage, the stellar radii would expand by several hundreds times compare to their radii on the MS. Our sun in the red-giant phase would expand to more than 1 astronomical unit (AU) in radius, swallow the orbit of the earth.

The behavior of the central isothermal, electron-degenerated helium core is very complicated. The contraction of such a helium core would cause the core temperature to vary, but this depend on the core mass. If the mass of the core less than the critical mass $M_{\rm ch}$ ($=0.45M_{\odot}$), the contraction would not increase the core temperature. But the burning shell would contribute additional materials to the core. If the star is massive enough ($\sim 1.3M_{\odot}$), the contraction would lead the core temperature to increase. Once the central temperature is high enough ($\sim 10^8$K), it would trigger core helium burning. This process is extremely short (timescales of seconds or minutes), called the "helium flash". The helium flash is the end of the red-giant stage. All these descriptions are only suit for relatively low-mass stars ($M \leq 2.3M_{\odot}$); more massive stars would experience different physical processes and hence become more complicated.

Figure 1.5 presents the theoretical stellar evolutionary track in the CMD for the sun. A $\rightarrow$ B is the MS stage, from B $\rightarrow$ C, stars enter the turn-off region, but still have central hydrogen burning, hence people also call this the main-sequence turn-off (MSTO). C $\rightarrow$ D is the sub-giant stage, while D $\rightarrow$ E (the helium flash) is the red-giant stage. Not all MS stars would experience all these stages, only stars that

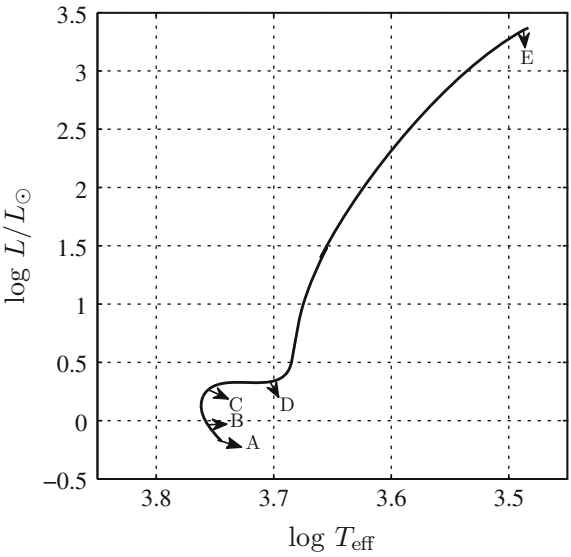

Fig. 1.5 The stellar evolutionary track for the sun, calculated by the PGPUC model [17, 226]

are initially massive enough to make a massive core can reach the helium flash. After the helium flash, stars would still experience some post-red-giant stages, and some of these stages are still poorly studied. To explore the content of this book, exploring the stellar evolution to the red-giant stage is sufficient.

1.2.4 Stellar Age Versus Its Initial Mass

Stellar luminosity is monotonically positively correlated to its mass. Generally speaking, their relationship can be described as:

$$\frac{L}{L_\odot} = a\left(\frac{M}{M_\odot}\right)^\gamma \tag{1.6}$$

where a is the coefficient and the index γ depends on the mass range. There is a good approximation for $M < 0.43M_\odot$, $\gamma = 2.3$, while for $0.43M_\odot < M < 2M_\odot$, $\gamma = 4$. Only for $M > 20M_\odot$, $\gamma = 1$, and for all other cases, $\gamma > 1$ [18, 19]. The luminosity is the result of nuclear fusion reactions from the stellar materials, hence $L \sim Mc^2 \propto M$ (here is a coefficient because only parts of the materials would participate in the nuclear reactions), where c indicates the speed of light in vacuum. Then the lifetime for a star should be the total mass of burning materials, βM $(0 < \beta < 1)$ divided by the burning rates, hence L. Then the lifetime for a star should be:

$$\tau \propto \frac{\beta M}{L} \propto \frac{M}{M^\gamma} = M^{1-\gamma} \tag{1.7}$$

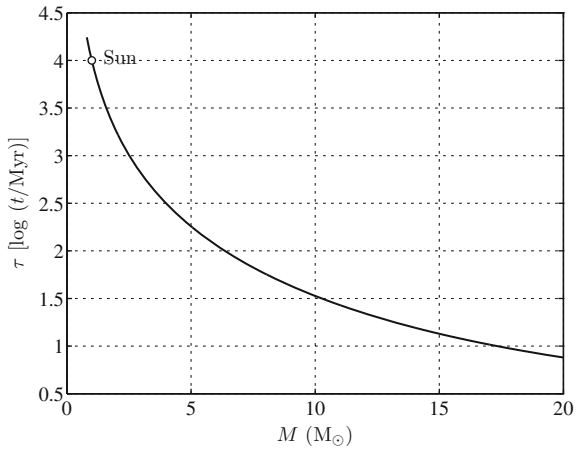

Fig. 1.6 Stellar lifetime (log (t/Myr)) versus stellar initial mass ($\mathrm{M}_\odot$) based on analytic model, the *open circle* represents the sun. Calculation based on the Astrophysical Multipurpose Software Environment (AMUSE) [21]

Since for most of the case, $\gamma > 1$, we obtain a very important conclusion: **the more massive the star, the shorter its lifetime**. The detailed relationship between stellar lifetime and initial mass is complicated, which depends on the metallicity as well. For their post-MS stages, this monotonic relationship would be broken, but since stars stay most of their lifetime in the MS ($\geq$90%), thus for their whole life, this tendency still holds. Figure 1.6 shows the relationship between stellar lifetime versus their initial mass, with the solar metallicity of $Z = 0.0152$, based on the analytic calculation, our sun will have a total lifetime of 10 Gyr.

1.3 Simple Stellar Populations

A simple stellar population (SSP), is an assumption that stars in SCs all originate from a common molecular cloud, formed in the same era, and share similar element composition—metallicity. It has been confirmed that their initial star forming process should behave approximately as a single burst [20]. Such a star-forming burst process is expected to quickly use all its progenitor gas in a molecular cloud [22]. Conceptually, SSPs are appealing. There is no exact SSP for any SC. Stars cannot form at exactly the same time. In addition, the SC progenitor molecular cloud (GMC) can spread from 5 to 200 parsecs (pc, 1 pc $\approx 3.09 \times 10^{16}$ m) [23]. The elemental composition of such a giant cloud will also vary depending on the spatial position. When we say a SC is a SSP, we mean their member stars' age should span a very narrow range, SCs whose typical age is significantly older than this time range can be ideally treated as SSPs. This statement is just like the primary students in grade 6, whose ages should roughly span 11 to 12 years old: this 1 year age dispersion will not affect the truth that they all belong to the same grade. The metallicity is always spread across a very narrow range for SSPs. No literature has determined how tight

this metallicity spread should be for typical SSPs SCs, because it seems that their internal metallicity spread is smaller than the measurement uncertainty.

To test if the stellar composition in SCs resembles that of SSPs, the simplest and most effective method is to investigate their CMDs. Because most stars are located on the MS, and all of them are formed in the same era, which means that the massive stars whose MS life is older than the bulk stars' common age would have evolved off the MS. If we put all the stars in an observed SC on the CMD,[1] one would expect to observe a narrow MS, leaving a uniquely, well-defined "cut-off" region on its bright-side. This is the MSTO region, the evolved-off stars may well populate a narrow sub-giant-branch (SGB), red-giant-branch (RGB), some later stages like horizontal-branch (HB). The faintest region like white-dwarf clump, may even just disappear from the CMD due to its very low luminosity at the final stage.

1.3.1 Describing the Simple Stellar Population

In a theoretical CMD, stars of SSPs are located along an **isochrone**, An isochrone is the line that connects SSP stars at different evolutionary stages at the same time. An isochrone that ideally fits the CMD should well describe the MS, MSTO, SGB, reach the bottom of the RGB, go across the RGB, for post-RGB stage, it should also fit the red clump (RC, which is considered the metal-rich counterpart to the horizontal branch). For stellar stages later than the helium flash, it should also fit the HB. In physical reality, not every sample can harbor all of these features, since the MS lifetime occupies a large fraction of the stellar whole life, in a given observation, the best populated sequence is the MS. Only samples that contain enough stars would display other features, for almost all young SCs, the most massive stars evolve so quickly that even a well-defined MSTO region does not exist. In that case we can only determine the upper limit for their age. GCs that contain large number of member stars usually show all these features in their CMDs. Figure 1.7 shows the CMD of a Small Magellanic Cloud (SMC) GC NGC339, which shows a dense strip representing the MS, as well as the well-populated SGB, RGB, RC and Asymptotic giant branch (AGB), respectively, all these parts can be ideally described by an isochrone. However, it also shows a population of blue straggler stars (BSSs, the points that beyond the bright side of the MSTO), as we will see, the presence of BSSs may explain the presences of genuine secondary stellar generations in lots of GCs.

For a SSP sample, all stars formed at the same time, share the same metallicity, and only vary in their initial masses. Since the massive stars would have evolved off the MS earlier, they would have left a well-defined MSTO region. The MSTO in SSPs is unique: which is unique, well-jointed to a narrow SGB. Since the sub-giant stage is extremely short, only a very small fraction of stars would be observed in the

[1] It is just like a snapshot for all these stars **at the same time**, readers should distinguish it from Fig. 1.5, which is the evolutionary track for single star **at different times**.

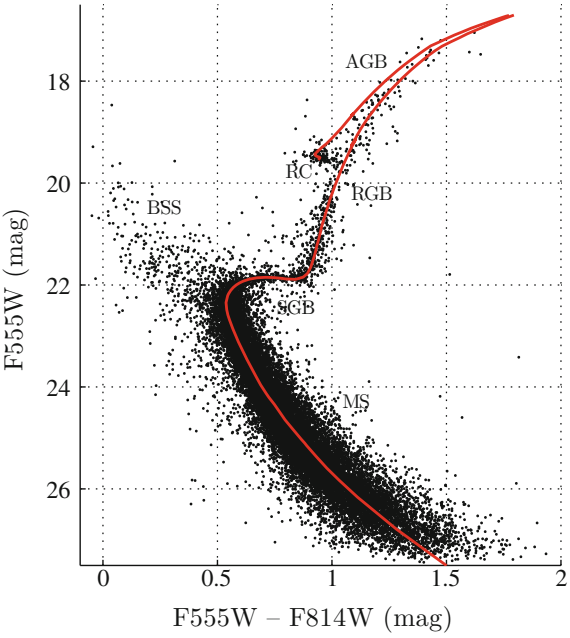

Fig. 1.7 The CMD of NGC339 with the best fitting isochrone (*red solid line*) [24], observations are based on *Hubble Space Telescope*/Advanced Camera for Surveys (HST/ACS) (Proposal ID: GO-10396, PI: J. S. Gallagher, III) filtered in F555W and F814W bands (which roughly correspond to the Johnson–Cousins *V* and *I* bands)

sub-giant region. Only SCs that contain large number of stars ($\geq 10^5$) would display a well-populated SGB. The next smoothly joined branch is the RGB. Again, SSP stars that pass the sub-giant stage would climb in luminosity along with a very narrow RGB. A SSP should also compose a compact RC in its CMD. In summary, stars in SSPs should present a narrow MS, a unique MSTO, a narrow and well-defined SGB and RGB, a compact RC, respectively, and all these features can be ideally described by a single isochrone with a given age and metallicity.

1.4 Not-So-Simple Stellar Populations: Multiple Stellar Populations

The SSP is a powerful conception. Based on SSPs, one can use the stellar population synthesis method to construct a stellar population model for more complicated stellar systems, like galaxies. A galaxy is not a SSP. It is composed of stars with different ages as well as helium abundances and metallicities, called 'multiple stellar populations' (MSPs). However, since it is assumed that SCs are the fundamental blocks that build a galaxy, combined with the SSPs assumption for SCs, we can ideally describe the stellar populations in galaxy as a combination of different SSPs for different initial conditions (age, helium abundance, metallicity).

If a stellar system is composed by MSPs, in contrast to SSPs, this means it should be composed of stars with **(1) different ages, (2) helium abundances, or (3) metallicities**. MSPs do not need to meet all these three criteria, normally people expect that they should show a spread in their combination.

A lots of mechanisms would lead SCs to become MSPs, some of the most popular scenarios include:

1. Some SCs are probably originally from the disrupted core of dwarf galaxies. These dwarf galaxies orbit to the MW, frequently go across the MW disk. The overdense MW disk region efficiently stripped the outer layer of the dwarf galaxy, in a process called "tidal shocking". Some enormous, massive GCs are assumed to be the nuclei of disrupted dwarf galaxies, like ω Centauri [25], some GCs in M81 (extragalactic) [26]. Since galaxies are often not SSPs, their remnant nucleus would exist as apparent GC composed of MSPs.
2. SCs could also live in clustered environments, called "cluster complexes" (CC). The dynamiced interactions between SCs would lead some of them merging into a giant SC. Some very massive SCs are suggested to be the results of SC mergers, like NGC 1023 [27], NGC 2419 [28], or even some YMCs: NGC 3603, Westerlund 1 & 2, and R136 [29].
3. For SCs, their member stars with masses less than 8 $M_{\odot}$ will undergo the the asymptotic-giant-branch (AGB) phase, during this very last evolutionary stage, the outer layer of the stars become unstable, eject large fraction of materials into the interstellar medium (ISM). The gas from the AGB ejecta can be retained within the SC, then converted into a second stellar generation [30, 31]. Another scenario regarding the contribution from the stellar wind of fast-rotating massive stars, the fast-rotating massive stars would shed their helium-rich materials (from more efficient hydrogen burning) into an equatorial disk, or radiatively drive them into the ISM via stellar winds. These helium-enhanced materials would pollute the low-mass stellar populations, hence broaden their internal helium (as well as some elemental abundance) spread [32, 33].
4. Stellar collisions or binary mergers would result in refreshed BSSs (for binary coalescence, see [34, 35]; for stellar collisions, see [36, 37]), BSSs would break the simplicity of the stellar age distribution in SCs, located in the region that bluer and brighter than the MSTO (that is the reason of their name—blue straggler stars). Both stellar collisions as well as binary mergers are non-negligible for dense, massive SCs, especially for GCs.

We will introduce some of these scenarios in more detail in Chap. 2.

1.4.1 Describing the Multiple Stellar Populations

Unlike for SSPs, describing MSPs is not-so-simple, but any feature that deviates from SSPs should be considered the result of a MSP (e.g., multiple-MSs, spread in the MSTO, broadened SGB or RGB). Below is a brief description of what would

happen to observations if stars are not SSPs (hence are no longer well described by a unique age, helium abundance, or metallicity).

1. **Stellar Populations with Dramatic Age Difference**.
   Stellar populations containing dramatic age differences would be significantly different in their MSTO as well as SGB regions. This is because, for a given observation, the difference in their ages would lead to changes in the stars that have evolved to the MSTO, hence makes the resulting luminosities different. The average luminosity of MSTO and SGB is the most important feature to learn about the age of a stellar population: when restricting the analyzed ages to greater than or of the order of 6 Gyr, the relationship between the age and luminosity of MSTO is roughly linearly dependent: $\mathrm{d}\log(L/L_{\odot}) \approx -4.1 \times 10^{-2}$ (dex/Gyr), [38]. Figure 1.8 presents theoretical isochrones with fixed chemical composition (helium abundance (Y), metallicity(Z) but different in age.).
   The effective temperature (color) of the MSTO increases with decreasing age because at the young stage of SC, the TO stars are more massive, hence hotter. In the mean time, the color of the base of RGB is almost unchanged.
   An extreme case of dramatic age differences is represented by the BSSs, which would lead to an age spread in SCs equal to the typical age of the SC itself, because people usually assume that all BSSs are associate with the zero-age MS, but we will see that the BSSs also evolve; tracing their formation and evolutionary history of BSSs is possible.
2. **Stellar Populations with Different Helium Abundance**.
   The stellar surface temperature is sensitive to its atmospheric opacity, defined as κ. Increasing κ would increase the interior absorption efficiency, especially for high-energy photons, hence short wavelengths. Since more short-wavelength photons have been absorbed than long-wavelength photons, the whole stellar spectrum would be re-distributed into black-body shape, which hence shifts the typical maximum wavelength of the spectrum towards the red direction, resulting in a decreased stellar surface temperature: **the higher the opacity, the more efficient the cooling, hence the lower the surface temperature is**.
   The stellar luminosity also depends on the mean molecular weight, $\mu(L_{\mathrm{H}} \propto \mu^7)$ [38]. This is because, as the mean molecular weight increases, the number of particles in the core that balance the self-gravity would decrease (because only hydrogen element would burning at the MS stage), which would lead the combination of local density and temperature, ρT, to increase, and so must the rate of nuclear reactions [39].
   For a fixed metallicity, Z, the increased helium abundance would lead the radiative opacity to decrease, because κ_{He} is lower than κ_{H} [38]. The enhanced Y would lead X (the mass fraction of hydrogen element) to decrease. The enhanced Y also increases the μ. The combination of these effects would make helium enhanced stars hotter and brighter at each stage, but the increased H-burning efficiency would shorten the stellar MS lifetime. If using isochrones for a given age to describe stellar populations with different Y, we would find both MS and RGB for high Y isochrones are hotter, but the TO is slightly fainter due to the shortened

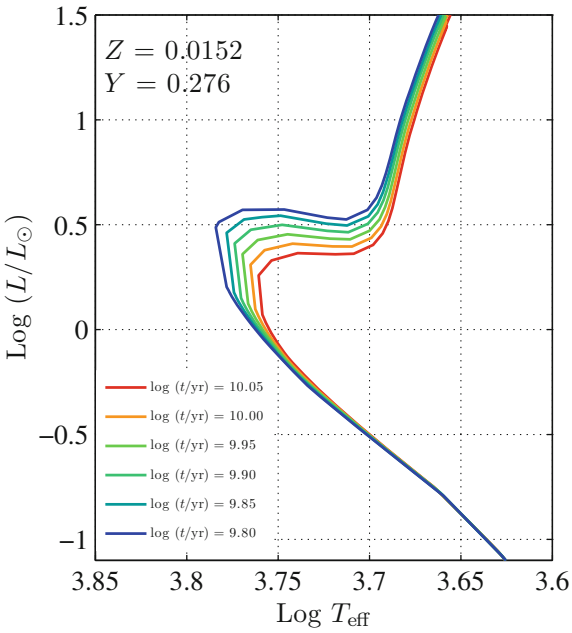

Fig. 1.8 Isochrones with fixed metallicity ($Z = Z_\odot$ 0.0152) and helium abundance ($Y = 0.276$), but differences in age, calculated by PARSEC code [24]

lifetimes of MS stars. Figure 1.9 illustrates the effect of helium abundance on stellar isochrones with fixed age and metallicity. The increased initial helium abundance would also lead the luminosity of RGB bump[2] to increase. More informations regard the RGB bump can be obtained from [38].

3. **Stellar Populations with Different Metallicities**.
   Increasing the metallicity would significantly contribute to the stellar opacity, for the same reason that was described for the last item. The enhanced opacity would lead to an increase in cooling efficiency, hence a decrease in the stellar surface temperature. In the mean time, the enhanced opacity would prevent the central energy from radiating towards the stellar surface, hence the stars with high metallicity are fainter than their low metallicity counterparts. Figure 1.10 presents the effects of varying metallicity on stellar isochrones with fixed age and helium abundance. It is clear that variations in metallicity would apparently affect the position of the RGB. This makes the RGB the best feature to trace the metallicity in stellar populations.

[2]The RGB bump is an intrinsic feature of the RGB. Its seems the RGB stars would peak in a very tight magnitude range. This is because during the RGB evolution, the H-burning shell crosses the chemical discontinuity left over by the convective envelope after the first dredge-up phase [40].

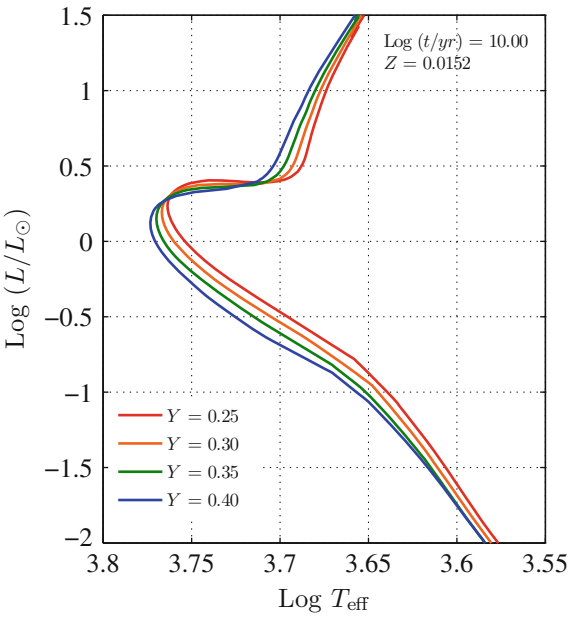

Fig. 1.9 Isochrones with fixed metallicity ($Z = Z_\odot$ 0.0152) and age (Log (t/yr) = 10.0), but differences in helium abundance, calculated by the model of [41]

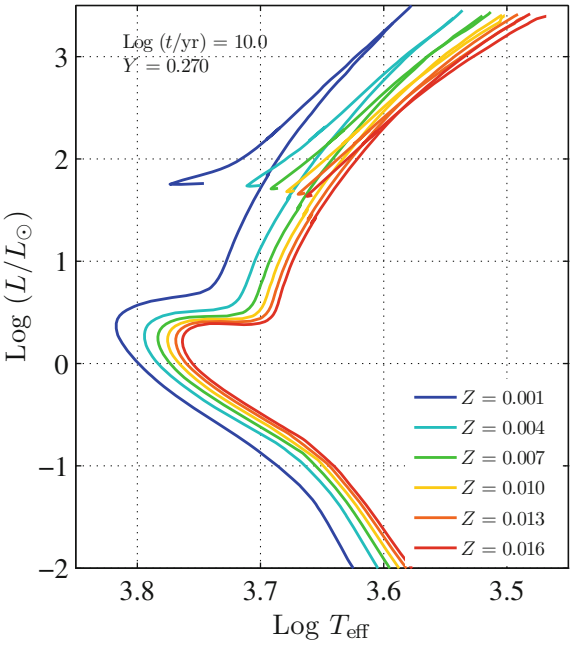

Fig. 1.10 Isochrones with fixed helium abundance (Y = 0.270) and age (Log (t/yr) = 10.0), but differences in metallicity, calculated by the model of [41]

Above are the three main causes that lead stellar population to no longer be simple. The stellar populations' features would be sensitive to all these three factors photometrically, but using spectroscopy, one can investigate different elements' information in detail.

Chapter 2
Researches of Stellar Populations in Star Clusters

2.1 Stellar Populations: We Think We Know Until Everything Change

SCs are the basic units for star formation [3]: almost all stars formed in clustered structures, most of them form following the turbulent structure of the interstellar medium (ISM) and collapse into bound clusters within a very short period (usually about one crossing time) [42, 43], a large fraction of those stars will gradually dissipate into the galactic field [4], populating the galactic stellar field. The SSP scenario assumes that this star forming process should resemble a single burst [20], this is because the strong initial stellar feedback, including the gas expulsion owing to energetic photons poured out from the most massive stars, strong stellar winds triggered by the first batch of Type II supernovae, will quickly exhaust all of the gas in the Giant Molecular Cloud (GMC), if a protocluster have exhausted its initial gas, its star forming process will stop rapidly.

2.1.1 Why Most Clusters Should be Simple Stellar Populations?

As introduced, the first topic confronting any underlying discussion of stellar populations is the initial star forming process in SCs. In principle, stars in a SCs should form in a single-burst channel unless they were initially extremely massive and compact: the strong stellar feedback would rapidly expel the initial gas, stoping the initial star-formation process. Timescale of the gas expulsion is very short, usually smaller than or comparable to the crossing time of a star cluster ($\sim$1 Myr), therefore the age range of first stellar population stars would be constrained in several million years as well. If there was a supernova explosion during the first several million years, all the gas will escape from the SC immediately, as a result, the clearance of molecular gas will quickly end the star formation in the SC. Assuming the typical time period for

C. Li, *Not-So-Simple Stellar Populations in Star Clusters*, Springer Theses,
DOI 10.1007/978-981-10-5681-9_2

the gas clearance is 1 Myr, given that the typical ages of most GCs (∼10 Gyr) and YMCs (10–100 Myr) are much longer than this timescale, the star forming process in a star cluster can be thus treated as a burst mode. Despite the supernova explosion, the typical escape velocity of the initial gas is about 10 km s^{-1} during this stage, which is the sound speed of the ionized hydrogen (HII) gas, sometimes this velocity can exceed 10 km s^{-1} if the gas expulsion process was dominated by radiation pressure, which usually occurs in massive clusters [45].

During the period from 3–10 Myr, most O-type stars with initial masses of ≥ 16 $M_\odot$ evolved off. These massive, quickly evolved stars will induce a large amount of energy into the ISM during their entire lifetime, which will unbind large amount of their surrounding gas. For example, A 15 $M_\odot$ star would be able to eject 3×10^{50} erg per 0.1 Myr into the ISM, which will unbind 10^4 $M_\odot$ gas within 1 pc region [46]. Because of this, a SC with age of ≥3 Myr should not contain a large fraction of residual gas, in addition, at this stage, the type II supernova explosion becomes frequent. The supernova explosions will expel its stellar material at a velocity of 10% of the speed of light (∼3×10^4 km s^{-1}), producing a shock wave through the ISM in their host SCs. Stimulated by the shock wave, the runaway velocity of the remaining gas in a SC will speed up to several hundreds or even thousands km s^{-1}. The multi-supernova explosions will sweep out all remanent gas in a SC immediately. Calculations have shown that only clusters who have their initial masses of 10^7 $M_\odot$ to 10^8 $M_\odot$ can survive the first series of supernova explosions [47].

Stars that are less massive than ∼ 8 $M_\odot$ will be able to undergo the AGB phase, the stellar feedback in this stage is believed the most important part for the formation of secondary stellar populations: the AGB stellar winds eject the stellar material into the ISM, these chemical enhanced materials build the body of new generation stars. However, at the stage of when there are intermediate mass AGB stars, a SC should already at least 30 Myr old, the gas expulsion and type II supernovae must have already exhausted a large amount of initial mass. In the meantime, the cluster itself should already be expanded, thus loss the capacity to capture the subsequent AGB stellar wind. Such a "self-circle" scenario is based on the assumption that clusters have the capacity to retain the AGB ejecta after the period of gas clearance, which means only the initially most massive and compact clusters will be able to form secondary stellar populations in this stage. The typical velocities of AGB stellar wind is about 10 km s^{-1} to 100 km s^{-1}, which is even faster than the velocity of initial gas expulsion (∼10 km s^{-1} [46]). Only a cluster whose escape velocity is larger than this value at the age of ≥30 Myr would be able to preserve a gas-rich environment. Assuming an average half-mass radii for young clusters is ∼1 pc, the escape velocity can be calculated through [48],

$$v_{\rm esc}(t) \approx 0.1\sqrt{\frac{M_{\rm cl}(t)}{r_{\rm h}(t)}} \quad {\rm km\,s^{-1}}. \tag{2.1}$$

It immediately tells us that only clusters whose initial mass are between $10^4\ M_\odot$ and $10^6\ M_\odot$ can retain the initial runaway stellar material in their gravitational potential wells.

Figure 2.1 shows the minimum mass for clusters to keep their initial runaway material versus their current mass, this diagram contains two sub-panels for two different escape velocities: 10 km s^{-1} (top; roughly equal to the gas-expulsion velocity and the slowest AGB ejecta), and 100 km s^{-1} (bottom; the **lowest** escape velocity driven by Type II supernovae).

Figure 2.1 tells us that all the OCs that we observed are not be able to have secondary star formation after their initial star formation terminate. About half of the observed YMCs in our MW will failed to retain the slowest AGB ejecta, and when the Supernova explosions further accelerate the remaining gas, all the YMCs will lose their initial ISM and stop the star formation permanently if no additional material can be fuelled. GCs seem more 'safe' than OCs and YMCs, but most of them would also not be able to keep the runaway gas once the Type II supernovae began to affect the environment. This is a conservative estimation, because the escape velocity of 100 km s^{-1} is only a lower limit to the velocities generated by supernova explosions.

However, Fig. 2.1 only compares the clusters' critical masses to their current masses not initial masses, for most OCs and all YMCs, this will not change anything because they may have unlikely undergone significant mass loss owning to their young age, but this may complicates the estimations of GCs' initial masses. Mass loss caused by two-body relaxation can be evaluated through the formula [50],

$$\dot{m} \approx 1100 \left(\frac{\rho_{\rm h}}{M_\odot\,{\rm pc}^{-3}} \right)^{1/2} M_\odot\,{\rm Gyr}^{-1}. \tag{2.2}$$

If assuming a typical age of 12 Gyr for GCs, then most GCs should be initially 10 to 15 times more massive than their current masses, that means they should have a strong capacity to keep their initial runaway gas in their infancy. It is unclear if young GCs could capture gas to form secondary stellar populations, because no observation has recorded a resolved YMC with this tremendous initial mass ($\geq 10^7\ M_\odot$).

This is why SCs should be initially SSPs: their initial star-formation episodes can only have lasted before all their initial gas being expelled, i.e., the first-generation stars should have a very narrow age range because they can only form over a short timescale. After this stage, a survived cluster will become less compact and less massive, thus loses its capacity to retain additional gas like the materials contributed by subsequent intermediate mass AGB stellar wind. The observations of young SCs with ages $\leq$10 Myr show that their member stars are usually embedded in a regions that are largely devoid of gas, while YMCs that are older than several tens of million years are all fully exposed.

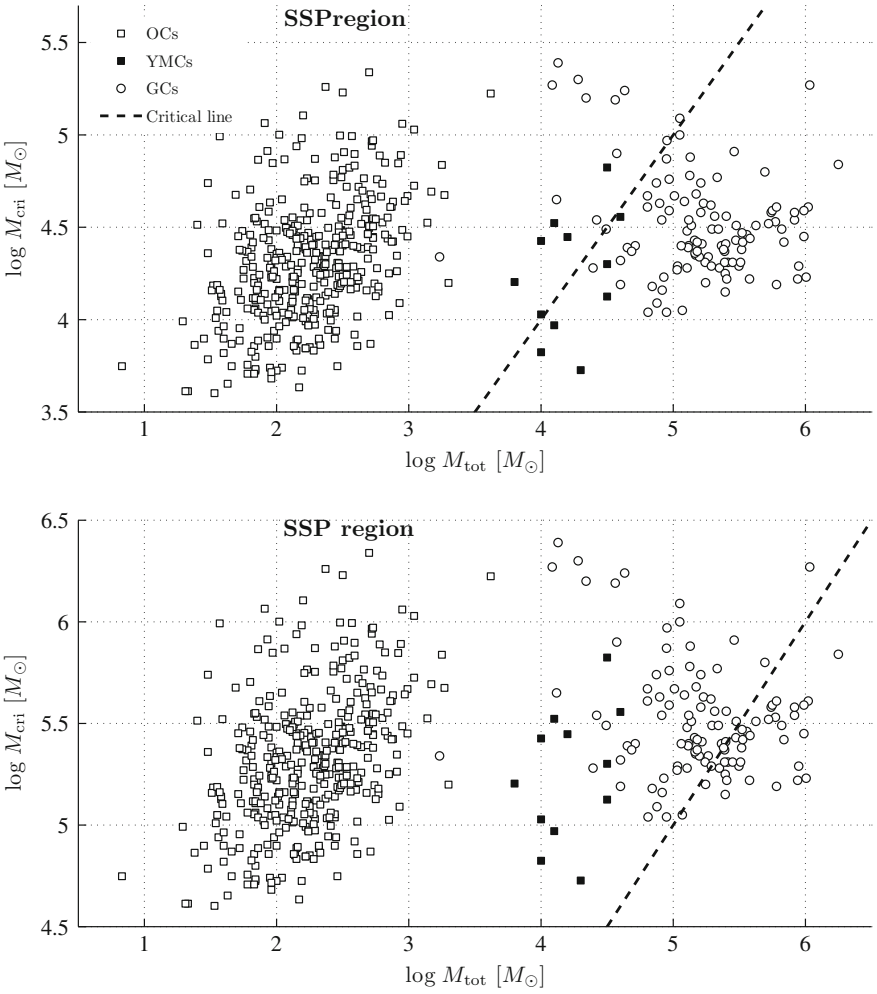

Fig. 2.1 Clusters' critical mass (log M_{cri}) versus their actual mass (log M_{tot}), here the critical mass is defined as the minimum mass that is required to capture the initial runaway gas for a cluster. Open squares, filled squares and *open circles* represent the Galactic OCs, YMCs, and GCs, respectively. OC and YMC data are from [10]. GC data are derived from [49]. The region that above the critical *lines* (*black dashed line*) represents the SSP region, that means SCs in this region will not be able to retain their initial runaway material based on their current masses. Escape velocities: (*top*) 10 km s^{-1}; (*bottom*) 100 km s^{-1}

2.1.2 Complicated Stellar Populations in Star Clusters

Almost all OCs are chemically homogeneous [51–53], this seems also hold for old OCs like NGC 188 [54], thus proving that their member stars were indeed coevally originated from a common GMC. Same conclusions also hold for stellar associations

and star-forming regions [55, 56], indicating a high degree of chemical homogeneity in primordial GMCs.

As introduced in Chap. 1, a direct method to examine if a SC is SSP is to study its CMD, the CMD of an SSP can be described by a single isochrone. However, because most OCs reside at the Galactic disk, their CMDs are usually messy owning to the extinction, making explorations of the age distributions of their member stars difficult. On the other hand, measuring a single star's age is still challenging based on current facilities and methods: no single approach can work for a broad range of stellar types in various ages, but this situation may change in the next few years once the technique of asteroseismology were improved [57].

Currently a main approach to study a single star's age is measuring its surface lithium abundance, because the lithium abundance is suggested to decrease with increasing stellar age. Studies based on this method have revealed that some stars seem to have ages that exceed the host OCs' isochronal ages [58, 59], but these exceptions only occupy a very small fraction of the first population stars, therefore they may not be able to resemble a large-scale ongoing star formation. To study the age range of a large stellar sample, a more promising approach is to explore the color-magnitude distribution of MSTO stars. The OCs Hyades and Praesepe, seem to possess their MSTO regions with apparent luminosity spread, indicating that their member stars may have age ranges span several hundred million years [60]. A similar result was found in the Orion Nebula Cluster, which seems harbor an internal age spread on the order of 10 Myr [61]. Similar results also appear in extragalactic YMCs, a recent study has found that a LMC YMCs, NGC 1856, displays an apparent extended MSTO (eMSTO) region [62], suggesting an initial SFH last for ∼150 Myr. Another LMC YMC, NGC 1850, was also found to harbor an eMSTO, indicating an age spread of ∼70 Myr [63]. Because both NGC 1850 and NGC 1856 belong to the LMC, differential extinction can not be responsible for their eMSTO regions, the discovery of broadened MSTO regions in YMCs seems to be a 'smoking gun' that supports stars in SCs can form continuously rather than born in an single star-burst.

For the CMDs of intermediate-age (1–2 Gyr) SCs in the LMC and SMC, the eMSTO is an ordinary feature: for instance, the LMC cluster NGC 1846 was found to possess a split in its MSTO region, indicating the presence of two stellar populations with ages of 1.5 Gyr and 1.8 Gyr, respectively [64], similar results were also found in LMC cluster NGC 1783 and NGC 1806 [65], with indications of their age dispersions should be at least 300 Myr. A comprehensive study shows that about 70% of the LMC intermediate-age SCs have eMSTO regions, which is in conflict with the expectations from SSPs [66]. Studies also show that for two SMC clusters, NGC 411 and NGC 419, their eMSTO regions are even consistent with an age spread of ∼700 Myr [67]. In addition, NGC 419 also displays a dual RCs, which again indicates an extended age distribution [68].

However, a series of objections to the eSFH scenario were proposed, based on very solid negative results. An analysis of LMC cluster NGC 1831, a ∼800 Myr cluster, have encountered an apparent conflict between the age spread derived from its eMSTO region and that implied by the compact RC [69]. Researches also extended to YMC candidates in local group galaxies other than LMC and SMC: a 570 Myr

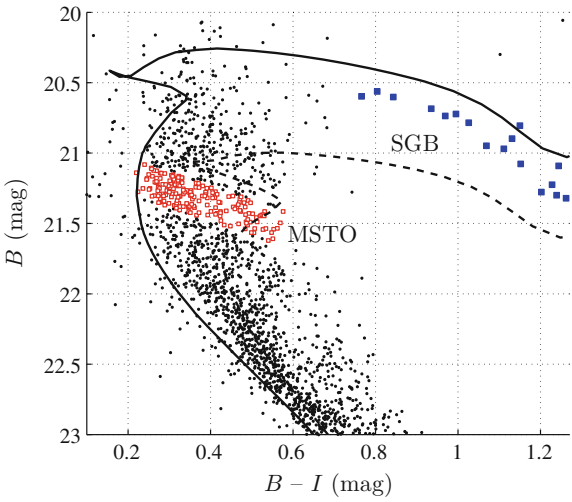

Fig. 2.2 The CMD of NGC 411 with best fitting isochrones (*black dashed* and *solid lines*), which indicates an age spread of ∼800 Myr [75], the *blue* filled squares and *red* open squares represent the samples of SGB stars and eMSTO stars, respectively

unresolved YMC candidate, NGC7252-W3, shows no evidence of eSFH, although it has an escape velocity of 193 km s^{-1} [70]. A survey for residual gas in 13 LMC and SMC YMCs with ages ≤300 Myr also denies any presence of residual gas in those YMCs [22], thus confirms that most YMCs in LMC and SMC may not be able to accrete large gas reservoirs to support ongoing star formation. On the other hand, if the eMSTO stars in these LMC and SMC clusters represent the same feature of MSPs in GCs, their member stars should show the well-know Na-O anticorrelation, however, a study on NGC 1806 report a negative result: no evidence of Na–O anticorrelation was found in the member stars of NGC 1806 [71], which indeed stands in marked contrast to the chemical variations present in GCs.

Numerous debates also focus on whether other features in the CMDs of intermediate-age SCs would be consistent with an eSFH. Li et al. (2014) claimed that in the 1.7 Gyr-old cluster NGC 1651, its SGB morphology can only be reconciled with an age spread of ≤160 Myr, which is much smaller than that derived from its apparent eMSTO region–450 Myr [72]. Their conclusion was subsequently confirmed in clusters NGC 1806 and NGC 1846 [73]. But an objection have argued that the morphology of SGBs in these clusters are actually consistent with an age spread scenario, if adopt a significant level of stellar convective overshooting to these SGB stars [74]. The dispute is ongoing, Li et al. (2016) discovered a very tight SGB in NGC 411, which can only be explained by an SSP [75]. As NGC 411 was claimed to harbor an age spread of ∼700 Myr [67], which immediately produces an discrepancy with respect to the observed SGB. Figure 2.2 presents the CMD of NGC 411, which is already zoomed in the regions of eMSTO and SGB, two isochrones are required to describe the blue and red boundary of its eMSTO region, which indicates an age spread of ∼800 Myr. It can be found that although the MSTO stars in NGC 411 were fully filled the region covered by these isochrones, almost all its SGB stars are alined with a narrow track, which actually corresponds to a single-aged isochrone.

Old GCs seem represent a different type of SCs. MSPs are believed to be a ordinary feature of the Galactic GCs (GGCs). Early evidence can date back to 1980s, where a dispersion in the CN-band strengths was found among seven MS stars in the GC 47 Tucanae (47 Tuc) [76], indicating that a process leading to N enhancement must have occurred in those stars, however, these MS stars themselves lack the capacity of mixing N to their stellar surface, the only explanation to the CN variation in these stars is they originated from the N-enhanced materials after the formation of N-poor stellar populations. Similar features were also detected in other GCs, like NGC 362 [77], NGC 6171 [78], NGC 6838 [79], NGC 5272 [80] and NGC 6205 [81, 280]. N-enhanced stellar populations also exhibit a strong absorption line at ∼3400 Å, therefore affects their CMD morphologies in ultraviolet filters, producing a split in the RGB, this feature have been observed in a dozen GCs [82]. Other evidence of MSPs in GCs were reflected by the variations in light elements (Na, O, Mg, Al), as introduced, the Na-O anticorrelation is the most well-known relationship for GC stars. The Na–O anticorrelation in GCs is shown in both the MSTO, SGB, and RGB stars (e.g., [83–85]). The Na–O anticorrelation may caused by the processes of CNO circle ($\sim 20 \times 10^6$ K) and Na proton-capture process ($\sim 35 \times 10^6$ K), this anticorrelation seems unlikely the result of stellar evolution because the central temperatures of the stars in GCs ($\sim 0.85\ M_\odot$) is too low to trigger these processes [32]. It looks like that all GGCs have Na–O anticorrelations, in addition, light-element variations are also detected in some LMC GCs [86]. Beside the Na–O anticorrelation, another relationship of Mg–Al anticorrelation has also been found in GCs (e.g., [87, 88]).

The iron abundance ([Fe/H]) dispersion, once appear in a cluster, would indicate that its SFH survived multi-supernova explosions, because only the ejecta of massive, core-collapse supernovae are able to enhance the iron abundance of ISM. There are lines of evidence show that at least some GCs have their member stars with dispersions of [Fe/O], like NGC 6656 (M22, [89]) and NGC 7089 (M2, [90]). This strongly suggests that at least some GCs have experienced much more complex SFHs. Precise photometry provide more impressive evidence, stellar populations with different elemental abundances, also show different properties in the CMDs: NGC 1851 was found to harbor dual SGBs in the CMD, different CNO contents were detected in stars belong to these two branches [92]. The GC NGC 2808 shows a triple MSs, indicating three stellar populations with helium-abundance of $Y = 0.248$, $Y = 0.30$, and $Y = 0.37$, respectively [93]. A recent study on NGC 7089 (M2) even reported seven stellar populations [94].

Because the photometric analyses usually involve stellar samples with much larger sizes than that explored by spectroscopic analyses, investigating the kinematics and dynamics of the different stellar populations becomes possible. Milone et al. [95] revealed dualities in the MS, SGB, and RGB of GC 47 Tuc, they explained these two stellar populations by a CN-weak, O-rich, Na-poor and normal helium abundances ($Y \sim 0.25$) stellar and a stellar generation with CN-strong, O-poor, Na-rich and enhanced helium abundances elemental abundances ($Y \sim 0.265$), they defined the former as first stellar population and the latter as secondary stellar population, respectively. They found that the secondary stellar population is more concentrated

than their first stellar population counterpart. Their conclusion is cemented through near-infrared observations [96, 201]. Similar results were also found in NGC 362 [97] and other GCs [98]

2.2 Proposed Scenarios

2.2.1 The Extended Main Sequence Turn-Off Regions in Star Clusters

As repeatedly mentioned, the most straightforward explanation to eMSTOs that observed in lots of LMC and SMC SCs is to assume they have experienced much longer initial SFHs, usually last for *at least* 300 Myr [66]. Goudfrooij et al. (2014) [100] proposed a scenario involves a prolonged round of SFH for massive clusters: the central escape velocities of the star clusters were high enough to accrete a large amount of pristine gas during the gas expulsion stage or to retain the ejecta of intermediate mass AGB stars and massive binaries. Most of this gas reservoir would be accumulated in the central regions of the clusters and form secondary stellar populationss. This process may last several million years until all gas is exhausted by star formation or multiple supernova explosions. However, the discovery of no gas residual in YMCs invalidates this scenario [100]. Another possible solution to the suspected age spread in these LMC and SMC clusters invokes the merger, the merger between two clusters with different ages [64] or between a cluster and a star-forming GMC [101] would be able to explain the observed eMSTO in SCs, which may indicates that there was initially a large fraction of binary SCs in LMC and SMC, because of the fraction for SCs who harbor eMSTO regions is very high (70% [66]).

The age spread model strongly indicates that it is time to relinquish the SSP scenario for the formation of these relatively young SCs, however, there is another scenario directly denies the MSPs in these clusters, this scenario attributes the observed eMSTO regions to the results of stellar self-rotation. Stellar rotation can alter the morphology of MSTO regions in two channels: (i) the centrifugal force resulting from rotation reduces the stellar self-gravity, decreasing the surface effective temperature, that means a fast rotator should appears redder than its non- or slow-rotating counterpart (if they have the same mass). The reduced self-gravity also lead to a reduction of stellar luminosity as it reduces the stellar central nuclear reaction rate. Because the rotating mainly affect a star's equatorial region, which would make a rapidly rotating star look redder around its equatorial region than near its poles. This effect is defined as 'gravity darkening'; (ii) Rotation would enlarge the stellar convective cores, transporting hydrogen from the outer layers into the stellar center, replenishing the central fuel for hydrogen burning, which will thus prolong the stellar main-sequence lifetime. Once the massive, fast-rotating stars have comparable MS lifetime to less massive stars, a mass spread in the turn-off region of a stellar

population appears, resulting a luminosity dispersion in its turn-off region. This is called 'rotational mixing.'

The less massive stars ($\leq 1.2 M_{\odot}$) are not expected to become fast rotators owning to a mechanism called 'magnetic braking' [102, 103], i.e., the stellar magnetic field will lead the angular momentum steadily transfer away from the star through exerting a torque on the ejected matter during a star's evolution. It has been confirmed that stars earlier than F0-type can easily reach an average rotational velocity of 100–200 km s^{-1}, while the G0-type stars' typical rotational velocity is only 12 km s^{-1} [104]. A study of a large number of B–F-type solar-neighborhood stars has confirmed that most of these stars are fast rotators [105].

In 2009, Bastian and de Mink [106] had proposed a scenario that rapid stellar rotation of F-type stars may lead to the misconception that intermediate-age SCs harbor dramatic age spreads. But their scenario has only considered the gravity darkening as the effect that is responsible for the extent of the eMSTO region. However, Girardi et al. [107] showed that rotational mixing will mitigate the broadening caused by gravity darkening, eventually leading to a narrow MSTO, therefore stellar rotation cannot be the (only) solution of the eMSTO. However, their conclusion was pointed out to has adopted an unrealistic convective mixing efficiency, it was found that the collective effects of gravity darkening and rotational mixing with a moderate mixing efficiency could produce the eMSTO region for 1–2 Gyr-old clusters [108]. A corollary of their results is that the MSTO area in a cluster would depend on its actual age, Fig. 2.3 presents the correlation between the FWHM of the clusters' age spreads and their typical ages for coeval stellar populations, based on the Fig. 8f of Yang et al. [108].

If the age spreads of several hundred million years are valid for YMCs ($\leq$300 Myr), a fraction of pre-main-sequence stars should appear in YMC CMDs, this is because their age distributions of member stars would scatter to zero age. However, as shown in Fig. 2.3, the internal age spreads of YMCs derived from their MSTO regions only occupy small fractions of their ages, this supports the stellar rotation scenario again, as it will partially broaden the MSTO region.

The relative importance of gravity darkening and rotational mixing in SCs is unclear because of the lack of direct observational evidence. To distinguish between these two effects, one promising approach is to study the loci of the rapidly rotating population on the CMD. Gravity darkening will produce an eMSTO where most fast rotators lie to the red side of the MSTO, while rotational mixing will lead most fast rotators to reside toward the blue side of the MSTO region. Another important feature that may shed light on this issue is the SGB. Because gravity darkening does not produce a mass spread among MSTO stars, once the MSTO stars have evolved off the main sequence, they will decelerate due to the conservation of angular momentum, the coeval MSTO population characterized by different stellar rotation rates will subsequently converge into a narrow SGB. On the other hand, the rotational mixing effect would produce a mass spread among evolved stars, broadening both the MSTO and SGB regions. If a fast rotating population is dominated by rotational mixing effect, it may display a broadened MSTO region and a SGB that largely dispersed in luminosity as well.

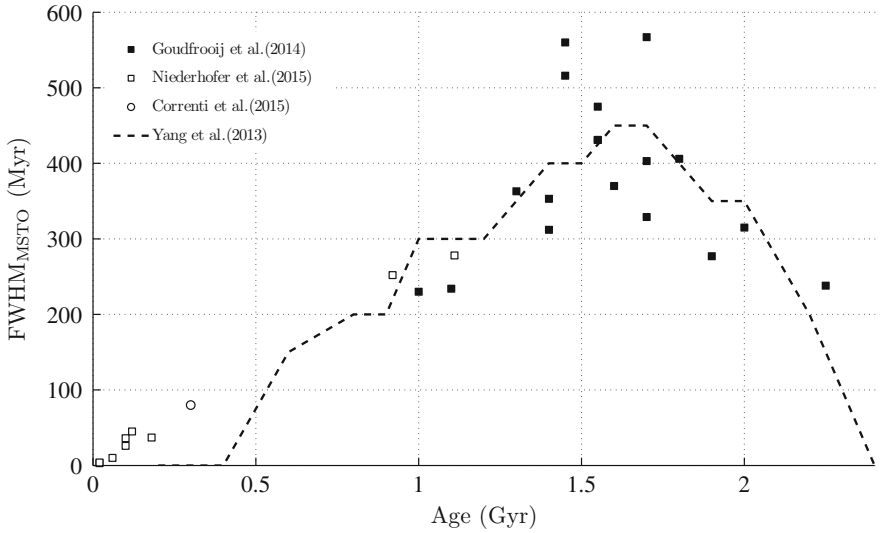

Fig. 2.3 Widths of implied cluster age spreads as a function of their isochronal age. *Black dashed line* Predicted FWHM of cluster age spreads that would be derived from their eMSTO regions as a function of cluster age. *Filled squares*, *open squares*, and an *open circle* are the data from [99, 109, 110], respectively

Stars with different rotational rates would be mainly affected by different effects, a stellar population composed of extremely fast rotators may be mainly affected by gravity darkening, while a stellar population only contains relatively moderate rotators may more prefer to be affected by rotational mixing. In stellar evolutionary model, the stellar rotational rate can be described by $\Omega/\Omega_{\rm crit}$, where Ω is the stellar angular rotation rate and $\Omega_{\rm crit}$ is the critical, 'break-up' value. To illustrate this difference, in Fig. 2.4 we present synthetic HRD of SSPs with $\Omega/\Omega_{\rm crit} \leq 0.5$ (left panel) and $\Omega/\Omega_{\rm crit} \geq 0.5$ (right panel) for an age of 1 Gyr and a metallicity of $Z = 0.006$, which is roughly the typical value of most intermediate-age LMC and SMC star clusters. Figure 2.4 shows that for stars with their rotational rates span from $\Omega/\Omega_{\rm crit} = 0$ to 0.95, the SGB also spans in a large range of magnitude; while for those extremely fast-rotating stars (left panel, $\Omega/\Omega_{\rm crit} \geq 0.5$), the SGB is well populated with very small magnitude dispersions.

Analyses on the SGBs of SCs who harbor eMSTO were carried out recently. As introduced, so far there were already four SCs, NGC 411 [75], NGC 1651 [72], NGC 1806 and NGC 1846 [73], seem harbor their SGBs that are inconsistent with an dramatic age spread (however, see [74]). A more exciting result appears soon, Wu et al. [112] found for SMC cluster NGC 419, its CMD shows apparent 'converging' in the SGB, i.e., the SGB seems wide in blue range while narrow in red range, the only explanation to this feature is these SGB stars are slowing down, i.e., the more evolved SGB stars have lower rotational rates than these less evolved SGB stars. All these results may suggest that the gravity darkening in these clusters is more important than

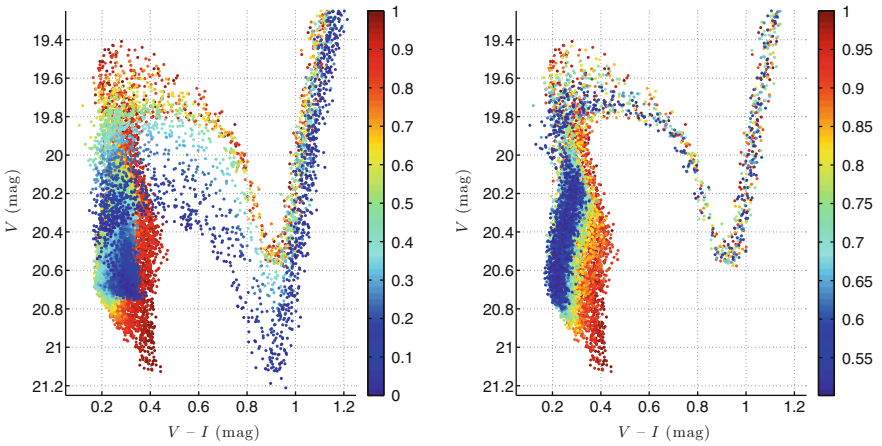

Fig. 2.4 Synthetic $(V, V-I)$ CMD for a coeval stellar population with an age of 1 Gyr and a metallicity of $Z = 0.006$, for stars with initial rotation rates of (*left*) $\Omega/\Omega_{\rm crit} \leq 0.95$ and (*right*) $\Omega/\Omega_{\rm crit} \geq 0.5$. The color bars indicate the initial stellar rotation rates. Calculated through Geneva stellar evolutionary model [111]

rotational mixing effect, based on Fig. 2.4, if the Geneva stellar evolutionary model is correct, then it may further indicate that most stars in these SCs are extremely fast rotators.

The discovery of eMSTOs in YMCs seems confirm this speculation: the eMSTO of NGC 1856, a 150 Myr-old YMC in LMC, suggests a possibly ∼80 Myr age spread, if assume this eMSTO is produced by stellar fast rotating rather than an age spread, then its stellar population should be composed by a combination of two-third rapidly rotating stars and one-third slowly/non-rotating stars [110]. Same conclusion was also reached in another YMC NGC 1755, which displays a split main sequence that favors the variable stellar rotation scenario rather than an age spread [113]

In summary, the apparent eMSTO regions in intermediate-age SCs and YMCs in the LMC and SMC can be explained by either an age spread scenario or rapid stellar rotation scenario. The discussions on the origin of eMSTO regions are still ongoing.

2.2.2 *Multiple Stellar Populations in Old Globular Clusters*

The presence of MSPs in old GCs is undoubted, but their origin remains unclear, so far almost all proposed scenarios that aim to explain the formation of MSPs in GCs can be classified into two categories. The first type of hypothesis suggests a primordial origin, in the sense that GCs may have been born with chemical inhomogeneities. The second type of scenario insists the SSP origin for GCs, which claims that the MSPs in GCs are the result of stellar evolution [114].

Most primordial scenarios invoke self-pollution of intra-cluster gas during the early stages of cluster evolution, possible polluters during that stage include the ejecta of rapidly rotating massive stars [32], massive binaries [115], or evolved post-giant-branch stars [116]. Another scenario divides GCs into three populations, GCs with initial masses $\geq 10^9 M_\odot$ can retain the ejecta of all types of massive stars, including those of their core-collapse supernovae. The relatively less massive GCs, with masses of several $10^8 M_\odot$ would only be able to keep a fraction of the fast winds from massive stars. The least massive GCs would not be able to capture any gas ejected by massive stars, they could only form new stars from the slow winds of intermediate-mass stars of the first stellar population [117]. A more recent scenario suggests that a temporal sequence of AGB populations may be able to explain the observed MSPs in GCs: such a pollution process occurs after the period of Type II supernovae, lasting until the third dredge-up associated with the AGB population. In this scenario, the cluster-to-cluster abundance variations is ascribed to the differences of many processes and gas sources which were involved in the formation of the secondary generation [118]. If this scenario was on the right track, then a GC should be able to keep its mass that is 100 times more massive then its current mass after the Type II supernovae epoch ($\sim$20 Myr), otherwise the self-pollution scenario would be failed to explain the high fraction of the observed secondary stellar populations in most GCs. However, another study have revealed an intrinsic problem among all self-enrichment scenarios that they are unable to produce consistent abundance trends among He, Na and O [119]. While all these self-cycle scenarios have predicted a extremely massive origin for GCs who have MSPs, however, current investigations have shown that clusters are almost gas-free at a very early stage (2–3 Myr), independent of their mass [120, 121], which indeed show that clusters may not be able to retain their initial gas during the initial gas-expulsion phase, but this does not prevent a cluster from accreting external gas onto its central region when moving through a background medium [122].

Another primordial formation scenario invokes the cluster merger, an advantage of this hierarchical formation scenario is that it does not require a extremely massive origin for individual clusters, thus solves the 'initial exhaustion' problem. Cluster members in crowded environments are easy to frequently collide and merge [123], resulting a stellar system contains more than one stellar populations. However, this scenario may preferentially favors clusters in crowded environments (e.g., cluster pairs in the Antennae interacting system [124]), while most GCs in our Milky Way are located in the Galactic halo, where frequent mergers are not expected to occur.

The evolutionary scenario treat the star-to-star abundance variations in GCs as the result of dredge-up of material that has been processed through the CNO cycle in the stars themselves. Because the observed elemental chemical dispersions in GC stars only reflect variations in their surface abundances, any process that would change the chemical compositions of stellar surfaces would produce a star-by-star variation in their elemental abundances. Lots of mechanisms that may affect the mixing of stellar material have been proposed. Some of them seem auspicious indeed, for example, a study had had shown that the significance of Na–O anticorrelation of GGCs is depend on their RGB luminosity [125], indicating this correlation may be affected by internal deep mixing of evolved stars during their ascent of the RGB, thus partially

support the evolutionary scenario. Another possible mechanism that may lead stars to undergo deep mixing invokes the stellar magnetic fields: Nucci and Buso [126] proposed a scenario involving the advection of thermonuclear ashes by magnetized domains emerging near the H shell to explain AGB-star abundances, confirming that the stellar-envelope crossing times are able to facilitate chemical dispersion in a huge convective shell, the stellar deep mixing induced by the magnetic advection may explain the observed abundance anomalies in GCs.

However, a key problem of the evolutionary scenario is that stars in GCs are usually late-G- or K-type stars, their central temperatures are not sufficient high to produce the observed Na–O anticorrelation. A possible solution to this problem invokes the binary merger, as binary stars usually occupy a considerable fraction in a stellar population, their mergers will produce a large number of zero-age massive stars, the BSSs. BSSs may be initially fast rotators, they may experience sufficient convective mixing, thus produce a star-to-star surface chemical dispersion once evolve to RGB phase. Such a model based on fast rotators that are produced by binary mergers or interactions have been confirmed to be able to produce a Na–O anticorrelation with high significance [127]. Clearly, this scenario strongly depend on the binary fraction of SCs, actually, it depends on how many binaries can be eventually evolve to interactive phases. It seems that more than half of objects in YMCs are actually binaries (at least for stars that earlier than F-type) ([69, 128, 129], also will be introduced in Chap. 3), this seems also hold for some OCs, Mathieu and Geller (2009) [130] have found that the population of BSSs in OC NGC 188 contains 76% binary systems, which confirms the close relationship between binary stars and BSSs. To test the evolutionary scenario, a promising approach is to study the elemental dispersion of BSSs in SCs, which may improve our understanding of the origin of MSPs in GCs.

Part II
Researches on Stellar Populations in Massive Star Clusters

Chapter 3
Binary Fraction in Young Massive Star Clusters

3.1 Introduction

Lots of researches have indicated that the majority of stars are belong to binary systems [131–135]. As mentioned in Sect. 1.1, stars are preferentially stayed in SCs, investigating the binary fractions in SCs is thus of fundamental importance for understanding many astrophysics of SCs. The dynamics of binaries in a SC thus plays an important role on both the formation and evolution of the SC. Because binaries are on average more massive than single stars, in SCs these systems are usually thought to be good tracers of (dynamical) mass segregation, that is, the two-body relaxation will cause the most massive objects (including both massive stars and binaries) to sink to the cluster center, while the relatively less massive objects remain in or migrate to orbits at greater radii [136–138]. However, it is also suggested that the generally wide binary systems, or the so-called 'soft' binary systems, will suffered external encounters, leading them to be disrupted [129, 139–143]. Because this process depends on the local stellar density, it would occur more frequently in a cluster's central region than in its periphery, which may mask the effects of mass segregation. If there are intermediate-mass black holes in cluster cores, this dynamical process will proceed more rapidly [144].

Since old GCs have already experienced significant evolution, their member stars will likely have reached a dynamical state of energy equipartition. In order to study the early dynamical mass segregation and binary disruption, more studies based on YMCs are required. Although the Milky Way hosts a small number of YMCs ($\sim 10^5$ $M_\odot$), like Westerlund 1, however, because the extreme reddening associated with these YMCs near the Galactic center prevents us from sampling significant numbers of their member stars in sufficient detail, these objects are not suitable to explore the properties of binaries in detail. Exploring the YMCs in the LMC thus becomes an alternative way. However, because the binary systems in dense SCs at the distance stage of LMC cannot be resolved with current instruments, binary fractions in distance YMCs have not yet been studied as thoroughly.

C. Li, *Not-So-Simple Stellar Populations in Star Clusters*, Springer Theses,
DOI 10.1007/978-981-10-5681-9_3

A promising method to study the binary fractions in dense SCs is to study their color-magnitude distribution. Because an unresolved binary system would looks like a single source with the total flux of its two components, it will therefore be found on the brighter and redder side of the single star MS. Their importance can be quantified through careful Monte-Carlo simulations. The advantage of this method is its high efficiency, since it only depends on a single set of observations. In principle, one does not need to assume many physics, because this approach is only depend on our understanding of stellar evolution. This also allows us to simulate artificial observations for comparison without too many physical considerations like the period distribution of the binaries or their orbital inclinations [145–149]. But for almost all SCs which have been analyzed based on this method are old GCs, where dynamical evolution is expected to have altered the initial binary population. Efforts have recently begun to address this issue in the context of YMCs in the LMC [128, 129, 150].

In this chapter, we introduce our analysis of the binary fraction properties of two YMCs in the LMC, NGC 1805 and NGC 1818, previous studies have revealed significant mass-segregation in these clusters [136–138]. It is also reported that the massive binary systems in this cluster are also segregated [150], but the dynamics of relatively less massive, F-type binary systems in these clusters is still not fully studied. We will introduce our studies of the number ratio of binary stars to the total stellar sample in the same magnitude range, based on analyzing their apparent "binary sequences" in the CMDs. We have also developed a more accurate approach based on χ^2 minimization using Monte-Carlo simulations. The results show that both methods consistent mutually for the same cluster.

This chapter is organized as follows, the data reduction is discussed in Sect. 3.2. The details of the isochrone-fitting and χ^2-minimization methods are present in Sects. 3.3 and 3.4. The discussions of detailed physical implications of our results are in Sect. 3.5. The Sect. 3.6 gives our conclusions of this work.

3.2 Data Reduction

Our datasets of clusters NGC 1805 and NGC 1818 belong to the *HST* programme GO-7303 (PI Gilmore). The complete data set for each cluster is composed of a combination of three WFPC2 images in the F555W and F814W filters, which roughly correspond to the Johnson–Cousins V and I bands, respectively. The total exposure times for V and I bands are 2935 and 3460s. All the data sets consist of long- and short-exposure images in which the Planetary Camera (PC) chip was centered on the cluster central region, with a third, longer-exposure image centered on the cluster's half-light radius to the cluster center. Images with total exposure time of 1200 and 800s for V and I bands of a nearby field region were also used to statistically correct the background contamination [128]. Figure 3.1 show the spatial distributions of all objects associated with the NGC 1805 (left) and NGC 1818 (right) cluster field, respectively.

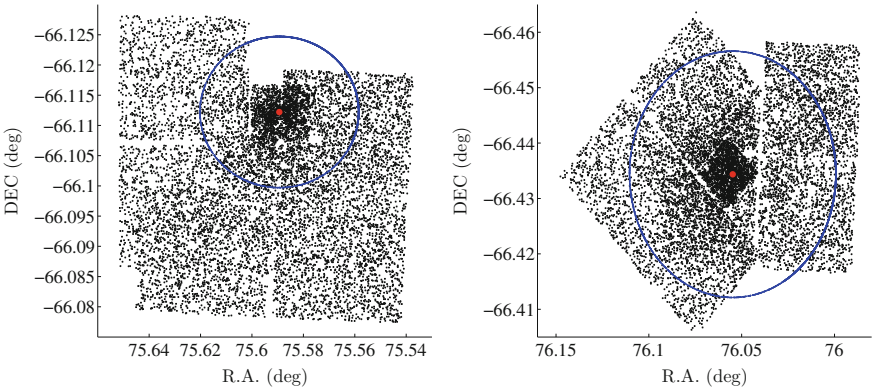

Fig. 3.1 Spatial distribution of the stars in the NGC 1805 (*left*) and NGC 1818 (*right*). *Blue circles* indicate the adopted cluster region in this work, which are 45 arcsec for NGC 1805 and 80 arcsec for NGC 1818, respectively. The *solid red circles* represent their cluster *centre*

Our photometry was performed with the package HSTPHOT [151], which is a specialized photometry package for analysis of *HST*/WFPC2 datasets. HSTPHOT. For each cluster, we use the point-spread function (PSF) photometry for their raw images, which thus resulted in three distinct stellar catalogues. Because bright stars are usually saturated in observations with long exposure times and faint stars will be merged into background skylight in short exposure images, we combined catalogues with different exposure times into a complete master data set through cross sections: If a given star appeared more than once in our catalogues (based on examine their relative positions), we adopted its magnitude and photometric uncertainty based on the deeper observation.

The best method to decontaminate the background stars from a SC is separate field stars from cluster members using stellar proper motions. However, the large distance of the LMC makes deriving proper motions challenging. Fortunately, because of the small size of the analyzed WFPC2 field of view, one can simply assume that the distribution of field stars is homogeneous, thus enable us to statistically reduce the field stars through comparing the color-magnitude distributions of a nearby field region with that of the cluster. The photometry of the nearby field region was processed by the same procedures. Once obtain the stellar catalogue of the field region, we then statistically reduced field stars from the cluster stellar catalogue through comparing their CMDs: we divided both the cluster and the field CMDs into a carefully considered number of grids and counted the number of stars in each (we have corrected the area difference for field sample). For our target clusters, the color and magnitude range for both the field and the cluster CMDs is about 3 mag and 10 mag, respectively. We divided the cluster and field CMDs into 50 cells in color and 100 cells in magnitude, that means the size of each cell is 0.1×0.15 mag. We adopted these cell sizes because of the comparable color difference between the MS of single stars and the binary sequence. We confirmed that small changes in cell size will not affect

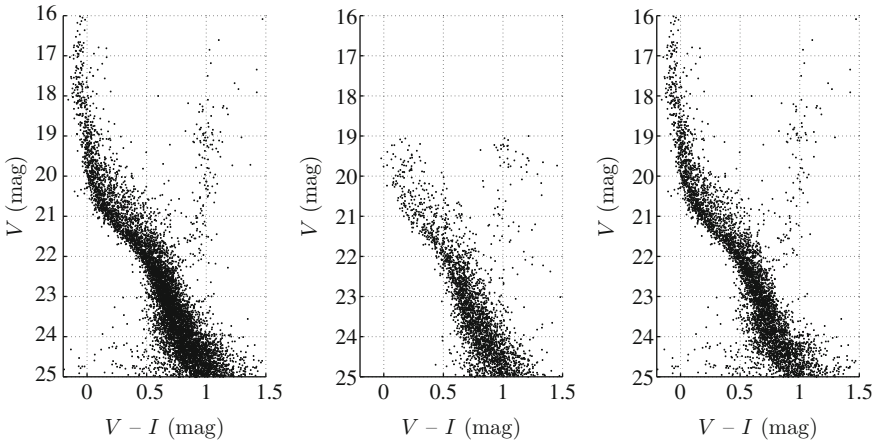

Fig. 3.2 (*left*) Raw CMD of NGC 1805. (*middle*) CMD of the nearby field region. (*right*) Decontaminated CMD of NGC 1805

our decontamination efficiency. Finally we randomly removed a number of stars corresponding to that in the area-corrected field star CMD from the cluster CMD. In Fig. 3.2 we present the performance of our decontamination for cluster NGC 1805, as an example.

3.3 Isochrone Fitting

Distant binaries in compact LMC clusters cannot be resolved into individual components with current facilities. The fluxes of the individual binary components will be returned as a single object, the photometric measurement of a unresolved binary will give a resulted magnitude below:

$$m_{\mathrm{b}} = -2.5 \log(10^{-0.4m_1} + 10^{-0.4m_2}), \tag{3.1}$$

where m_1 and m_2 are the magnitudes of the individual components. This means that the binary system will appear as a single object with a brighter magnitude than that of the MS of single stars, thus be biased towards the brighter envelope of the MS.

We used the Padova isochrones [24] to describe the decontaminated CMDs. Since photometric uncertainties also cause the MS to broaden, which thus renders a robust distinction between single stars and low mass-ratio binaries difficult, determining the photometric uncertainties as a function of magnitude thus become necessary before we take any further analyses. The relationship between the photometric magnitudes and their corresponding uncertainties can be described by an exponential function of the form $\sigma(m) = \exp(am + b) + c$ [128], where σ represents the photometric

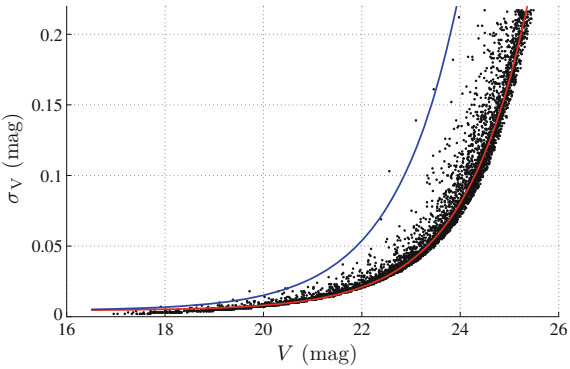

Fig. 3.3 The correlation between the photometric uncertainties (σ_V) and V band magnitude for the NGC 1805 data set. The *red solid line* is the best-fitting *curve* to the distribution's *ridge-line*, while the *blue solid line* represents the 3σ range

uncertainty and m is the corresponding magnitude; a, b and c are the fit parameters. Again, we take NGC 1805 as an example, Fig. 3.3 shows the functional form of this curve is applied to our observations.

We summarize the basic physical parameters for our analyzed clusters. Based on isochrone fitting, we obtained a distance modulus of $(m-M)_0 = 18.50\,(18.54)$ mag for NGC 1805(NGC 1818). With the fixed distance moduli, the ages of NGC 1805 and NGC 1818 derived by us are $\log(t/\mathrm{yr}) = 7.65$ and 7.25, respectively. Compare with previous works, our derived age for NGC 1805 is identical to that of Liu et al. [152], while the age for NGC 1818 is younger than their estimate, but fully consistent with that quoted in de Grijs et al. [136]. We note that this is because of the young age of NGC 1818 have made the age determination based on isochrone fitting very uncertain, since Liu et al. [152] determined their age based on the faint end of the cluster's MS, it is likely that their age estimate is an upper limit. After determined their ages and distance modulus, the best-fitting extinction values for NGC 1805 and NGC 1818 are estimated as $E(B-V) = 0.09$ and $E(B-V) = 0.07$, respectively. Finally, we adopted metallicities of $Z = 0.008$ and 0.015 for NGC 1805 and NGC 1818. These parameters are close to previous works [153–155]. The basic cluster parameters adopted in this work are present in Table 3.1.

Table 3.1 Basic parameters of NGC 1805 and NGC 1818

Parameter	NGC 1805	NGC 1818
$\log(t/\mathrm{yr})$	7.65 ± 0.10	7.25 ± 0.10
Z	0.008	0.015
$E(B-V)$ (mag)	0.09 ± 0.01	0.07 ± 0.01
$(m-M)_0$ (mag)	18.50 ± 0.02	18.54 ± 0.02
α_{J2000}	$05^{\mathrm{h}}02^{\mathrm{m}}21.9^{\mathrm{s}}$	$05^{\mathrm{h}}04^{\mathrm{m}}13.2^{\mathrm{s}}$
δ_{J2000}	$-66°06'43.9''$	$-66°26'03.9''$
R_{field} (arcsec)	45.0 ± 0.3	72.7 ± 0.3

3.3.1 Detect Binary Stars in the CMD

We then adopt the MS ridge-line and the region defined by the 3σ photometric uncertainties on each side of the best-fitting isochrone as the region that dominated by single stars. Stars that brighter or redder than this limit are defined as unresolved binary or multiple stellar systems. Binaries with different mass ratios, $q = M_s/M_p \leq 1$ (where M_p and M_s are the masses of the primary and secondary binary components), will lead them to attain magnitudes in the 'binary region'. We then predict where binary systems characterized by different mass ratios are located in the CMD. For the upper limit of the binary region, we adopt the fiducial equal-mass binary isochrone, i.e., $q = 1$ binary sequence that is about 0.752 mag brighter than the single isochrone. We have also chosen to adopt an upper limit to the binary region to exclude some odd objects with extremely red colors. These extremely red objects may be the residual of field contamination or possible triple or multiple stellar systems. Although this type of stellar system may be rare in regular OCs, they maybe observable if they are associated with very bright stars in massive clusters.

The multiplicity frequency involving triple and higher-order multiple systems in YMCs is poorly studied. In the solar neighborhood, the multiplicity frequency is about $4.5 \pm 2\%$ (9 of 164 solar-type primary stars, see [131]), while the simulation have predicted an $18 \pm 10\%$ multiplicity frequency in SCs [156]. We hence speculate that the 'odd' objects that located beyond the binary region may contain numerous multiple stellar systems, also some may be caused by occasional multiple blends. Our subsequent analyses will show that the blending fraction of two single stars is about of order 10% in the cluster inner region (see Sect. 3.3.3), indicating that the probability of triple or higher-order blending should only reach fractions of 1%.

In this work, we only focus on stars in the range from $V = 20.5$ (20) to $V = 22$ (22) mag for NGC 1805 (NGC 1818), roughly corresponding to F-type stars. The reason that we only focus on this magnitude range is because the effects of binaries are most significant in this magnitude range of $(V, V - I)$ CMD, because the MS slope is shallowest. At brighter magnitudes, the slopes of both the single-star MS and equal-mass binary sequence are so steep that they lie very close to one another. Also the spread in color at the bright stellar sequences (including MS and binary sequence) may be contaminated by BSSs [154], increasing the difficulties associated with investigating binaries at brighter magnitude. For stars fainter than $V \sim 22$ mag, the photometric errors begun to dominate the morphology of the stellar distribution, causing a significant broadening of the MS. The combination of these reasons have explained why the magnitude range of $V = 20.5$ (20) to $V = 22$ (22) mag for NGC 1805 (NGC 1818) are the only suitable range for exploring binary properties. In Fig. 3.4 we present the CMDs of NGC 1805 (left) and NGC 1818 (right), as well as their best fitting isochrones.

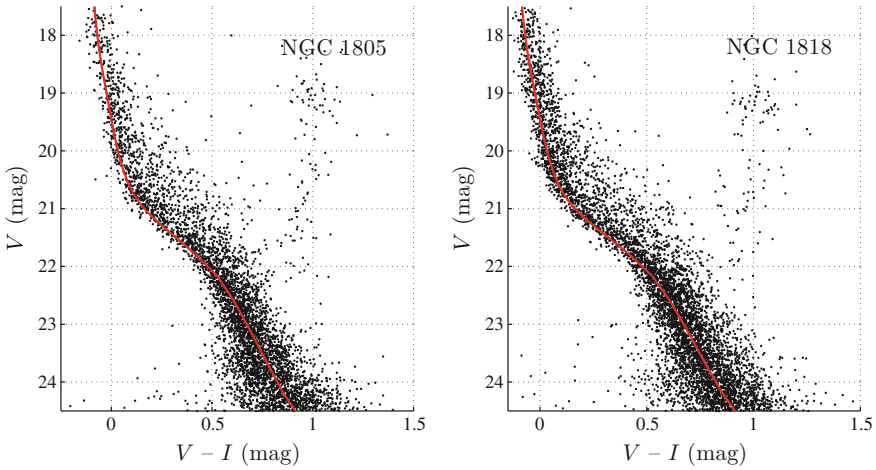

Fig. 3.4 The CMDs of NGC 1805 (*left*) and NGC 1818, *red solid lines* corresponding to their best fitting isochrones

3.3.2 Determine the Coordinates of Cluster Center

In order to explore the binaries' radial behaviors, accurate cluster center coordinates are essential. We divided the stellar spatial distribution into 20 cells in both right ascension (α_{J2000}) and declination (δ_{J2000}). We then count the number distributions of stars along with coordinate directions. A Gaussian function was found to provide a best-fitting profile to these distributions; the two-dimensional peak of the adopted Gaussian function thus indicates the center coordinate. The resulting coordinates are $\alpha_{J2000} = 05^h02^m21.9^s$, $\delta_{J2000} = -66°06'43.9''$ for NGC 1805 and $\alpha_{J2000} = 05^h04^m13.2^s$, $\delta_{J2000} = -66°26'03.9''$ for NGC 1818.

Once we obtained the position of cluster center, we then calculated the azimuthally averaged number-density profiles of both clusters, then we adopted the distances where the clusters' monotonically decreasing number-density profiles reach the average field level as the typical cluster radii. For NGC 1805, we found it subjects to a cluster radius of $R_{field} = 45.0 \pm 0.3$, while for NGC 1818, this value is $R_{field} = 72.7 \pm 0.3$, we thus adopted the analyzed regions for NGC 1805 and NGC 1818 as 45 arcsec and 80 arcsec, respectively. Mackey and Gilmore (2003) have determined radii for NGC 1805 and NGC 1818 as 69 and 76 arcsec based on *HST*/WFPC2 observations [157], but their results are based on surface brightness distribution, so it is reasonable that our results are not exactly the same. Figure 3.5 shows the number-density profiles of NGC 1805 (top) and NGC 1818 (bottom). We have also included the cluster sizes and their center coordinates in Table 3.1. At the LMC's distance, for a canonical distance modulus of $(m - M)_0 = 18.50$ mag, 1 arcsec is roughly equal to 0.24 pc.

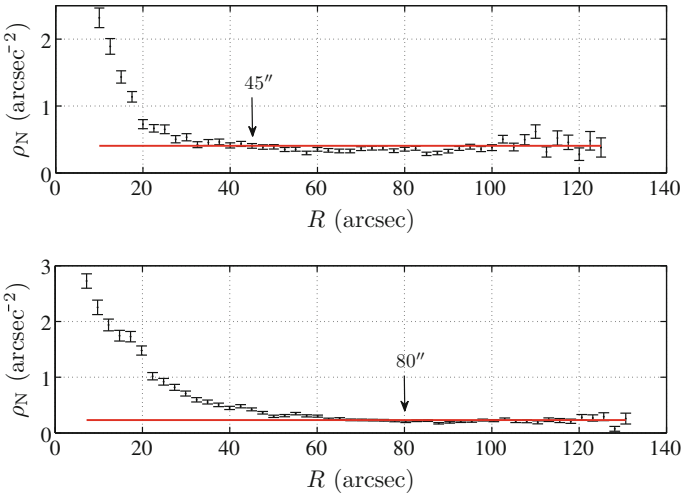

Fig. 3.5 Number-density profiles of (*top*) NGC 1805 and (*bottom*) NGC 1818. The *red solid lines* indicate the field density levels, while the arrays indicate the distances adopted clusters' radii in this work

3.3.3 Artificial-Star Tests

An important effect that will broaden the MS is the stellar line-of-sight blending because the observed clusters are actually the 2D projections of their member stars' real spatial distribution. This causes a similar observational signature as that owing to the presence of binary systems. To avoid overestimates of the binary fraction caused by stellar blends, one need to evaluate the blending ratio at different radii using artificial-star (AS) tests. The adopted approach in this work is based on the conclusion of Hu et al. [128], who found that two objects which are separated by fewer than 2 pixels in the CCD of *HST*/WFPC2 camera will failed to be resolved. We adopted their approach to obtain the blending fractions at different radii, we have also taken into account of the blending between single stars and cosmic rays or extended objects.

We added more than 640,000 ASs to the observed, decontaminated stellar catalogues, subsequently we compared their positions with all observed objects (including stars, extended objects and residual of cosmic rays), stars which are blended with extended sources will be detected as extended sources as well, only stars that actually blend with other stars may produce a 'blending binary' (also depend on their relative brightness), which will lead to a systematic offset of the binary fractions' radial profiles. We imposed that the ASs obey a luminosity function (LF) derived from a Salpeter-like stellar mass function [158], then we examined every single AS to check whether it would blend with any observed object, that means there is at least one single star located within 2 pixels to their positions. We adopted a minimum distance of 2 pixels between artificial and observed stars as the blending criterion, if this

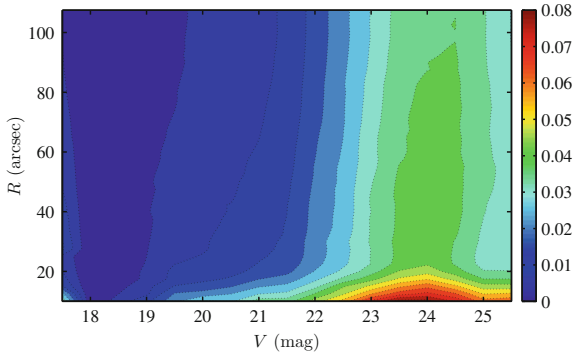

Fig. 3.6 2D contour of blending fraction (indicated by different colors) as a function of radius and magnitude for NGC 1805

criterion was met, we assumed that the fainter of the two objects would be dominated by its brighter counterpart, we call these blending pairs as 'optical pairs'. We then calculated the ratio of the number of optical pairs to the total number of stars in the sample of ASs, $f_{\rm opt} = N_{\rm blend}/N_{\rm tot}$, where $N_{\rm blend}$ and $N_{\rm tot}$ represent the number of relevant objects, we found that the $f_{\rm opt}$ is a function of magnitude. Figure 3.6 present the 2D contour figure of $f_{\rm opt}$ as a function of radius and V band magnitude for NGC 1805.

We have also consider the effect of sampling incompleteness, to determine the data sets' completeness curves, we generated ASs again, but this time we add this ASs into the reduced science images. We subsequently recovered the ASs using the same photometric approach as employed to obtain our main stellar databases. We used HSTPHOT to generate ASs covering the magnitude range of 19 mag $\leq V \leq$ 26 mag and $0.0 \leq (V - I) \leq 1.8$ mag, which fully covers the magnitude range of interest in this work. We have totally generated about 16,0000 ASs into the NGC 1818 and NGC 1805 *HST* fields, to aviod self blending between ASs and increases of the background brightness level, each time we only added 70–80 stars to an individual image. All ASs were randomly distributed across the chips, we repeated these processes 4000 times to reduce statistical dispersions. Finally we have confirmed that the sampling completeness for the magnitude ranges of our interest is between 85 and 90%. In addition, the sampling completeness should not significantly affect our results, because the binary fraction that we want to measure for each cluster is a number ratio between two stellar samples within the same magnitude range (see next paragraph).

We then calculated binary fraction at different radii for all stars in the magnitude range of our interest, the binary fraction is calculated as the number of stars in the single-star region of the CMD divided by that found in the binary region, corrected for the corresponding blending fraction of optical pairs, $f_{\rm opt}$,

$$f_{\rm bin} = \frac{N_{\rm b}}{(N_{\rm b} + N_{\rm s})} - f_{\rm opt}, \tag{3.2}$$

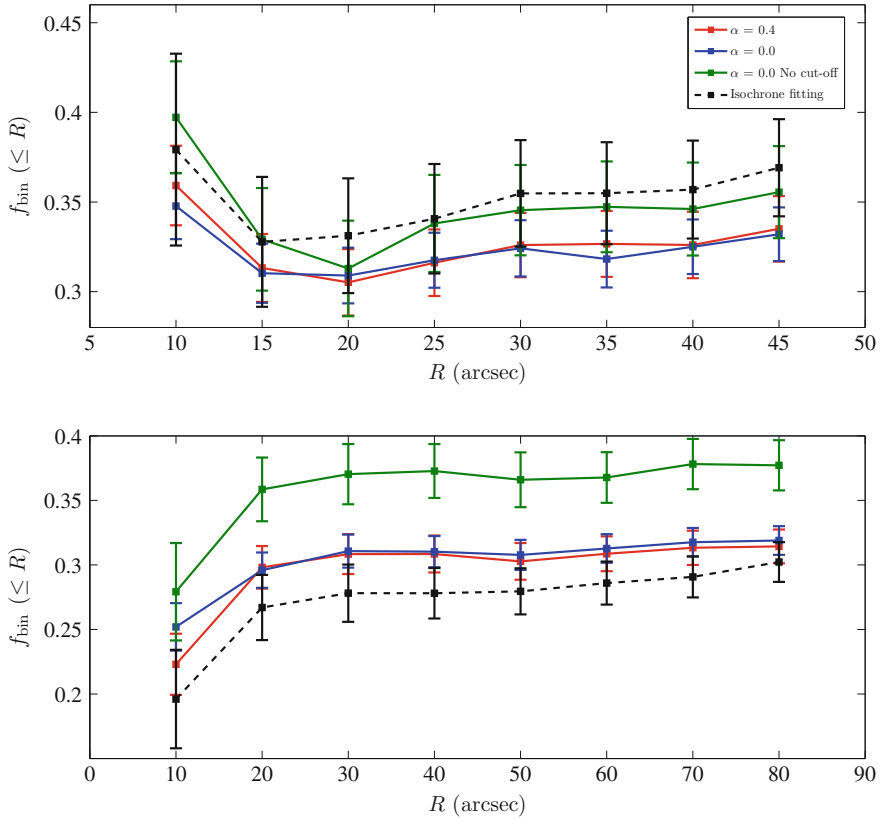

Fig. 3.7 Cumulative binary fraction radial profiles of (*top*) NGC 1805 and (*bottom*) NGC 1818 based on the results from χ^2 tests and isochrone fitting. The *blue* and *red solid lines* represent the results from χ^2 minimization for flat and power-law mass-ratio distribution ($\alpha = 0.0$ and 0.4) with a $q \geq 0.55$ cut-off, respectively; the *green solid lines* are for $\alpha = 0.0$ and no mass-ratio cut-off. The *black dashed lines* are the results based on isochrone fits

where $N_{\rm b}$ and $N_{\rm s}$ represent the numbers of stars located in the binary and single-star regions, respectively. In order to reduce statistical uncertainties, we calculated the resulting cumulative binary fractions for radii from $R \leq 10$ to $R \leq 45$ arcsec ($R \leq 10$ to $R \leq 80$ arcsec) for NGC 1805 (NGC 1818), the adopted uncertainties are Possionian uncertainties.

Figure 3.7 shows the cumulative binary fractions' radial profiles for NGC 1805 and NGC 1818 (the black dashed lines). In the inner regions of both clusters, opposite trends are found. In NGC 1805, the binary fraction first sharply decreases with increasing radius in the central region, followed by a gradually increasing trend to the cluster's outskirts, until it reaches a roughly constant level of the field's binary fraction. Meanwhile, NGC 1818 displays a almost monotonically increasing trend with radius, especially in the innermost regions.

3.4 Results Based on χ^2 Minimization

We also developed another independent, physically better justified approach, based on Monte-Carlo simulations and χ^2 minimization. We use this method to test whether the isochrone-fitting results obtained in the previous section are robust. Using the best-fitting isochrons, for each WFPC2 chip, we simulate a stellar catalogue representing a CMD that is similar to that of the observations. We generate millions of ASs that randomly distributed in each chip across an 800×800 pixel coordinate system. The ASs were again drawn from a Salpeter-like mass function [158], and their corresponding magnitude were obtained from interpolation of the isochrones. Gaussian noise was added to all ASs according to the best-fitting relation based on Fig. 3.3.

After we transferred the (x, y) pixel coordinates for all stars to $(\alpha_{\rm J2000}, \delta_{\rm J2000})$ values, for each observed stars, we first selected the nearest 20 ASs as possible counterparts, then we adopted the AS characterized by the most similar magnitudes in each bands as representative counterpart of the observed star of interest. For stars that located in the binary region, we firstly estimate their mass-ratios (based on the assumption that they are binaries) through comparing their positions with different mass-ratio binary sequences, then we calculate their primary stars' mass and magnitude and find the ASs with the most similar magnitude to that inferred for these primary stars. Figure 3.8 shows the theoretical ridge-lines of single stars and of unresolved binary systems characterized by different mass ratios (the black dashed line connects binaries whose primary stars have the same initial masses, we only show a 1.4 $M_\odot$ stellar mass as an example). Finally we have generated a stellar population with all ASs corresponding to single stars or primary stars of binaries in each cluster, they thus can represent the CMD of single stars in each cluster, Fig. 3.9 (top) shows the CMD of simulated cluster, without inclusion of any binaries or optical pairs. Because each AS that represent the observed star was selected from its most nearest 20 ASs, the sample of ASs hence have a similar spatial distribution to the observed cluster as well.

The remaining free parameters which will change the morphology of the CMD of the simulated cluster are the relevant mass-ratio distribution of the clusters' binary components and the binary fraction. For binaries in SCs, the most appropriate mass-ratio spectrum is still unknown. Hu et al. (2010) used to adopt a flat spectrum (they described it by a power-law, with a index of $\alpha = 0$) for NGC 1818 [128]. Studies also suggested that a power-law spectrum with an index of $\alpha = 0$ (i.e., low mass-ratio dominated) appears suitable for binaries in low-density environment [134, 159, 160]. Therefore, we adopted fixed power-law spectra for the binary mass-ratio distribution with indices of $\alpha = 0$ and 0.4 in subsequent simulations.

For the analysis of NGC 1805 (NGC 1818), we added artificial binaries with binary fractions spanning from 5 to 90% to the selection of observed stars. However, the photometric uncertainties will mix single stars with binaries with $q \leq 0.55$, we thus first adopted a lower mass-ratio cut-off of $q = 0.55$, binaries with $q \geq 0.55$ will appreciably broaden the MS of the simulated CMD towards brighter (and redder)

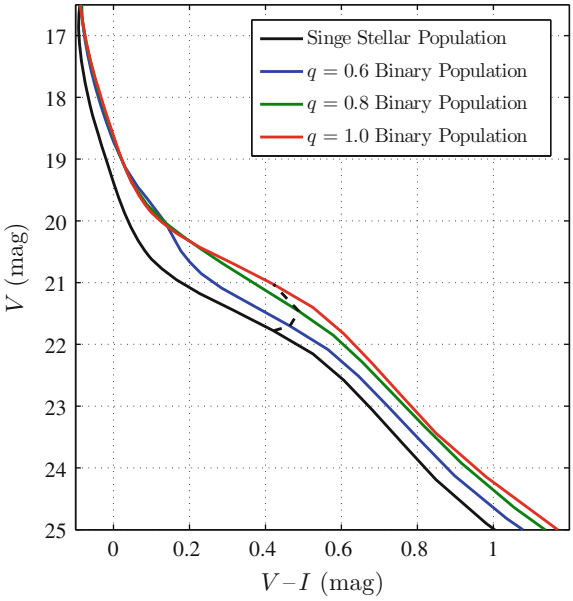

Fig. 3.8 Ridge *lines* for NGC 1805 of single and binary stellar populations with different mass ratios, the *black dashed line* indicate binaries whose primary stars have the stellar masses of 14 $M_\odot$

photometric measurements. Again, all stellar photometry (including binaries) follows the empirical uncertainties that shown in Fig. 3.3, the bottom panels of Fig. 3.9 show an example of simulated CMD with binary fraction of 50% and a flat-mass ratio spectrum (bottom left), as well as the observed CMD of NGC 1805 (bottom right).

We perform the same method in the isochrone fitting approach again to divide the simulated CMD into single-star and binary regions. For different input binary fractions, we count the number of ASs that are located in the single-star region, N_s, and in the binary region, N_b. The number of observed stars in the single-star region and binary region derived from our isochrone-fitting approach are denoted N'_s and N'_b (all treated as binaries). We then perform χ^2 minimization:

$$\chi^2 = \left(\frac{N'_s - N_s}{\sigma_{N_s}}\right)^2 + \left(\frac{N'_b - N_b}{\sigma_{N_b}}\right)^2, \tag{3.3}$$

where σ_{N_s} and σ_{N_b} are the statistical uncertainties associated with the numbers of ASs, so that

$$\chi^2 = \frac{(N'_s - N_s)^2}{N_s} + \frac{(N'_b - N_b)^2}{N_b}. \tag{3.4}$$

The χ^2 value represents the similarity between the simulated and observed CMDs. We vary f_{bin} from 5 to 90% and determine the minimum χ^2 value for each input binary fraction. The resulted $\chi^2(f_{bin})$ distribution was fitted by a quadratic function, which will provide both the global minimum χ^2 value (thus indicates the best-fitting binary fraction) and its 1σ uncertainty, the latter corresponds to the difference between χ^2_{min}

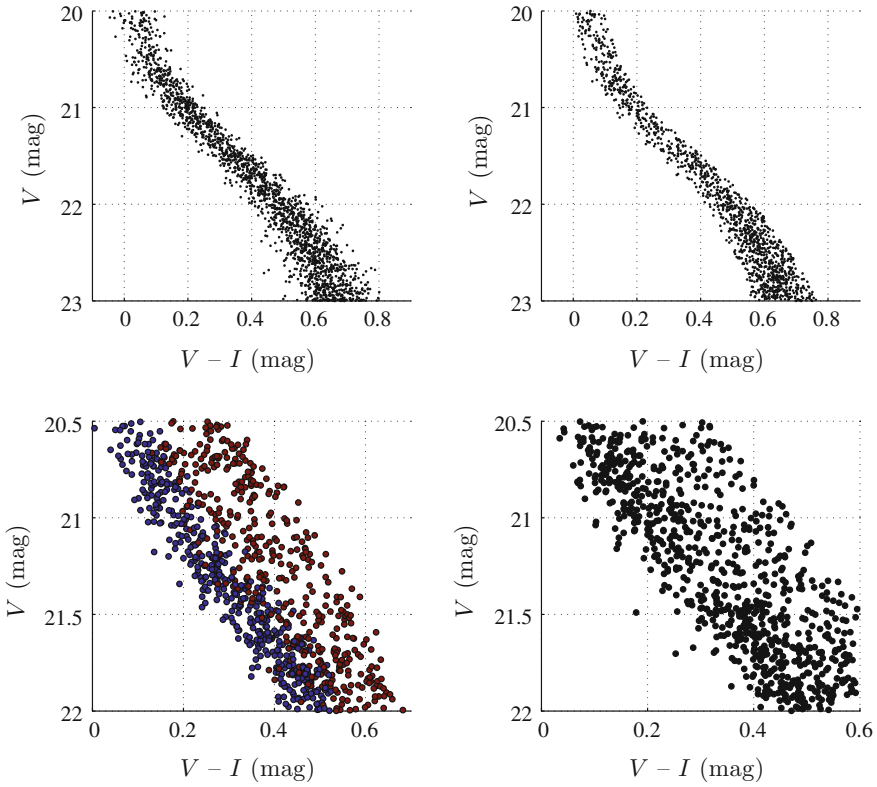

Fig. 3.9 (*top left*) CMD of the simulated cluster, without any binaries or optical pairs. (*top right*) The single stars region of observed CMD (i.e., data points found within $\pm 3\sigma$ of the MS ridgeline) of NGC 1805. (*bottom left*) Simulated cluster CMD, characterized by 50% binaries and a flat mass-ratio distribution, the *dark blue circle* and *dark red circle* represent single stars and binaries, respectively. (*bottom right*) CMD of NGC 1805 in same magnitude range

and $\chi^2_{\rm min} + 1$ [161]. Figure 3.10 shows an example of typical $\chi^2(f_{\rm bin})$ distribution and its corresponding 1σ uncertainty. For each radius, we derive $\chi^2_R(f_{\rm bin})$ using 10 independent generalizations to smooth fluctuations of random scatter. Once we have obtained the best-fitting binary fraction, we then correct the blending based on the results that shown in Fig. 3.6.

The $f_{\rm bin}(\leq R)$ distribution with blending corrected hence indicates the cumulative binary fraction's radial profile based on χ^2 minimization. These results for NGC 1805 and NGC 1818 are present in Fig. 3.7 (blue and red solid lines for different mass-ratio distribution assuming, $\alpha = 0.0$ and 0.4, respectively. Comparing the results from χ^2 minimization with that based on isochrone-fitting approach (black dashed line), we found both methods agree mutually in each cluster, which thus supports that both the general behavior and the actual levels of the radial profiles of the clusters' cumulative binary fractions derived are robust. The imposition of a mass-ratio cut-off at $q = 0.55$

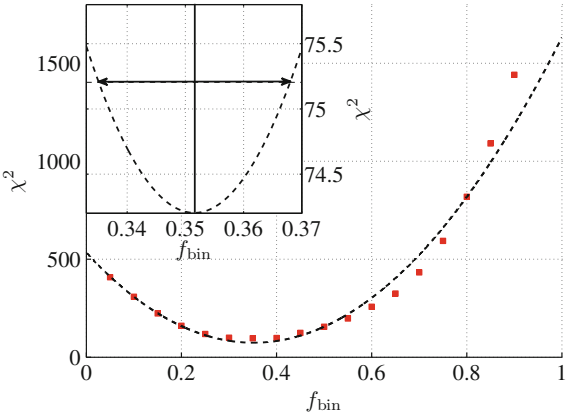

Fig. 3.10 A example of $\chi^2(f_{\rm bin})$ distribution, the *red* squares are the calculated values of χ^2. The *black dashed line* is the best-fitting quadratic *curve*, the double *arrow* indicates the 1σ uncertainty and the *vertical black line* represents the best-fitting $f_{\rm bin}$

is not strictly necessary to reach this agreement, we adopted this limit just because we want to properly compare the results from both methods. We have also checked the results based on χ^2 minimization but with this restriction released, for simplicity, we have assumed that for all q the mass-ratio distribution is represented by a flat spectrum, that is, $\alpha = 0.0$. The result (shown by the solid blue lines) again shows the same trend of binary fractions versus radius as found from previous results.

As shown in Fig. 3.7, different mass-ratio distributions of $\alpha = 0.0$ and 0.4 show a good agreement about their general trends of binary fraction's radial profile. We have also checked whether the resulting binary fractions will depend on other values of α, we confirmed that the choice of α does not affect the main trend of the binary fractions' radial profiles. For both clusters, the main trend of binary fraction's radial profile appears stable and robust for $\alpha \leq 0.5$, which hence proves that our choice of $0.0 \leq \alpha \leq 0.4$ is reasonable.

We now compare the actual binary fraction determined here with other results in previous work for different stellar systems. Sollima et al. (2010) analyzed the binary fractions in five Galactic OCs through using a similar approach as that adopted in this work [148], their results show that the core binary fractions in these five OCs span from 11.9 to 34.1%, with a mass-ratio cut-offs of $q \geq 0.48$ to $q \geq 0.55$. They also evaluate a complete binary fraction (without imposing a mass-ratio cut-off), and find their values are between 35.9 and 70.2%. Clearly, the binary fraction of NGC 1818 falls within their range of values if assume a core radius of roughly 10 arcsec [157], the core binary fraction of NGC 1805 maybe higher than any of the values reported by Sollima et al. [148]: Mackey and Gilmore (2003) derive a cluster core radius for NGC 1805 of 5.47 ± 0.23 arcsec, whereas we only explored the binary fraction for radii in excess of 10 arcsec in this work owning to the statistically smaller number of stars in the core of NGC 1805.

The binary fraction in GGCs seems significantly smaller than the values we derived for NGC 1805 and NGC 1818, based on the results of Milone et al. (2012), the maximum core binary fraction among 59 GCCs is only roughly 17%, for a

mass-ratio cut-off of $q = 0.5$. The fact that our results yield systematically higher binary fractions than those for GCs is expected. In old GCs, the cluster cores will have undergone sufficient dynamical evolution, leading to a significant fractions of binaries being destructed, while the binaries in YMCs NGC 1805 and NGC 1818 are still in the early stage of their dynamical evolution. We will discuss the evolution of binary systems in dense star clusters and the relevant time-scales in Sect. 3.5.

3.5 Physical Implications

3.5.1 Binary Segregation

The cumulative binary fraction's radial profile in NGC 1805 shows an apparent decreasing trend for the innermost two radial bins ($R \leq 15$ arcsec), followed by a gradual increase to the field's binary fraction. This result can be explained by mass segregation, since binaries are more massive than single stars of similar spectral types on average, it is reasonable to conclude that mass segregation is responsible for the observed behavior of the radial profile of binary fraction in NGC 1805.

de Grijs et al. (2002b) reported a clear signature of mass segregation in NGC 1805 [137], although these authors ignored the observational effects caused by unresolved binaries and assumed that all stars in their sample were single stars. They pointed out that it is not straightforward to correct the observed LF owing to the presence of binaries, in addition, measuring binary fraction as a function of brightness is difficult. Note that, despite significant improvements that developed in this work, we still can only determine the binary fraction for cluster MS stars spanning a narrow mass range (roughly equal to a mass range from 1.3 $M_\odot$ to 1.9 $M_\odot$, corresponding to F-type primary stars).

To understand the radial behavior of the binary fraction of F-type stars in NGC 1805, one need to compare the timescale of early dynamical mass segregation with the cluster's age. de Grijs et al. (2002b) concluded that the core of NGC 1805 is 3–4 crossing times old, although the age of NGC 1805 was $\log(t/\mathrm{yr}) = 7.0^{+0.3}_{-0.1}$ in their work [137]. The adopted age for NGC 1805 in our work is older, implies that the cluster age of 3–4 crossing time in their work is probably a lower limit. We estimate that the core of NGC 1805 may be already 8–10 crossing times based on the adopted age of $\log(t/\mathrm{yr}) = 7.65 \pm 0.10$ in this work. In addition, clusters may form clumpy rather than as spherically homogeneous Plummer spheres [42, 162], they will undergo early dynamical mass segregation more rapidly, usually on time-scales of 1–2 Myr for the most massive stars in the cores. In view of these time-scale arguments and compared with the cluster's chronological age, its binary population should also have been modified by the dynamical interactions.

On the other hand, binary systems can be formed through both three-body encounters ('3b') and tidal capture (Spitzer (1987) [9]), i.e.,

$$\left(\frac{\mathrm{d}n_{\mathrm{b}}}{\mathrm{d}t}\right)_{\mathrm{tot}} = \left(\frac{\mathrm{d}n_{\mathrm{b}}}{\mathrm{d}t}\right)_{\mathrm{3b}} + \left(\frac{\mathrm{d}n_{\mathrm{b}}}{\mathrm{d}t}\right)_{\mathrm{tc}}. \tag{3.5}$$

a useful numerical approximation to the formation rate of binaries through three-body encounters can be calculated through the formula below,

$$\begin{aligned}\left(\frac{\mathrm{d}n_{\mathrm{b}}}{\mathrm{d}t}\right)_{\mathrm{3b}} &= 1.97\times10^{-13}\left(\frac{n}{10^4\ \mathrm{pc}^{-3}}\right)^3\left(\frac{m_*}{\mathrm{M}_\odot}\right)^5 \\ &\times\left(\frac{10\ \mathrm{km\ s}^{-1}}{\sigma_{m_*}}\right)^9 \mathrm{pc}^{-3}\mathrm{yr}^{-1},\end{aligned} \tag{3.6}$$

where n and σ_{m_*} are the stellar density and 3D velocity dispersion of single stars, respectively. The rate of binary formation through tidal capture can be calculated through:

$$\begin{aligned}\left(\frac{\mathrm{d}n_{\mathrm{b}}}{\mathrm{d}t}\right)_{\mathrm{tc}} &= 10^{-8}\kappa\left(\frac{n}{10^4\ \mathrm{pc}^{-3}}\right)^2\left(\frac{m_*}{\mathrm{M}_\odot}\right)^{1+\mu/2} \\ &\times\left(\frac{R_{\mathrm{s}}}{\mathrm{R}_\odot}\right)^{1-\mu/2}\left(\frac{10\ \mathrm{km\ s}^{-1}}{\sigma_{m_*}}\right)^{1+\mu}\mathrm{pc}^{-3}\mathrm{yr}^{-1}.\end{aligned} \tag{3.7}$$

Here, $(\kappa, \mu) = (1.52, 0.18)$ and (2.1,0.12) for the polytropes $n = 3$ (based on the Eddington standard model of stellar structure for MS stars) and 1.5 (relevant to degenerate stellar cores, white dwarfs and less massive bodies), respectively, and R_{s} is the stellar radius.

We now estimate the number of binaries that may have formed through tidal capture during the evolutionary history of NGC 1805. Mackey and Gilmore (2003) determined the central density of $\log \rho_0[\mathrm{M}_\odot\ \mathrm{pc}^{-3}] = 1.75 \pm 0.06$ and a total mass of $\log(M_{\mathrm{cl}}[\mathrm{M}_\odot]) = 3.45^{+0.10}_{-0.11}$ for NGC 1805. In this work, we have detected about 3500 stars within a radius of 45″, which roughly represents the size of NGC 1805. This number, after the incompleteness corrected, then assume a Kroupa-like LF down to the hydrogen-burning limit at 0.1 $\mathrm{M}_\odot$ to the sample [163], indicates a total number of stars that in NGC 1805 of approximately 10,000. The average stellar mass in the cluster is thus of order of 0.28 $\mathrm{M}_\odot$, corresponding to a central number density of $\rho = 70$ stars pc^{-3} based on the assumption that the average mass of stars for $20.5 \leq V \leq 22.0$ mag is 1.6 $\mathrm{M}_\odot$. MS stars in this mass range would have radii of about 1.3 $\mathrm{R}_\odot$, the cluster's stellar velocity dispersion is still unknown for NGC 1805, but de Grijs et al. (2002b) estimated that the velocity of NGC 1805 should be at least 10 times smaller than that of NGC 1818 [137], while Elson et al. (1987) estimated a velocity dispersion for NGC 1818 of $\geq 6.8\,\mathrm{km\ s}^{-1}$. We thus conservatively assume a velocity dispersion for NGC 1805 of $\sim 0.7\ \mathrm{km\ s}^{-1}$. If adopt 5 arcsec as the projected

core size of NGC 1805, then the physical core size of this cluster should be ∼1.3 pc (at the distance of the LMC). With all of these considerations being taken into account, we calculated out that only 5.6 and 0.2 binaries are expected to have formed in the cluster core through three-body interactions and tidal capture, at the current age of NGC 1805.

Based on the core radius of 5.47 ± 0.23 arcsec [157], NGC 1805 exhibits a significantly decreasing binary fraction out to 3 core radii. We do not explore the binary fraction in the innermost 5 arcsec owning to the large uncertainties associated with the small number of stars. However, it is still reasonable to conclude that the enhanced binary fraction in the cluster's inner region is most likely caused by the effects of early dynamical mass segregation [42, 162]. After all, binaries are more massive than the single stars on average, so that binary systems are subject to a more significant degree of dynamical friction, hence, mass segregation.

In addition, as the more massive objects sink towards the cluster center, the dynamical evolution accelerates as well [165], thus producing dense cores very quickly, where stellar encounters occur very frequently, leading to a very effective binary formation [164, 166]. Actually, the presence of binary stars may accelerate the early stage of dynamical mass segregation significantly, since two-body encounters are very efficient at this stage [142, 150, 167–169]

3.5.2 Binary Dynamical Disruption

Since NGC 1818 has a similar age as NGC 1805, its opposite radial behavior of the binaries should possibly indicate additional dynamical effects that have played important roles. This apparent deficit of binaries in the NGC 1818 core may be the observational signature of the dynamical disruption of soft binary systems. An similar conclusion has been made earlier for NGC 1818 [129], although with less significance. In massive clusters, hard binaries get harder and soft binaries become softer [139], the timescale of the disruption of soft binary systems is always significantly shorter than the local relaxation timescale. This implies that binary disruption should have proceeded efficiently if there are sufficient number of soft binaries and the host cluster has undergone evolution for longer than its half-mass relaxation time.

The age of NGC 1818s core in crossing time compares favorably with the age estimate of the NGC 1805 core (also in units of crossing times), previously work show that it is already ≥ 5–30 crossing times old [137]. Both clusters have similar chronological ages, however their binary fractions' radial profile are markedly different, which takes us a conundrum immediately: what causes this apparent diversity? Disruption of binaries is caused by kinetic-energy transfer from a cluster's bulk stars to their components, once the kinetic-energy of the binary components are much lower than the average kinetic-energy of the bulk stellar population, such a binary star can be treated as soft. The 'watershed' energy of soft binaries is $-m\sigma^2$, where σ

is the local velocity dispersion of the environment in which the binaries reside [170]. Since the mass ranges of the binaries we analyzed in NGC 1805 and NGC 1818 are similar, the key factor which determines if a binary system is soft or not is its velocity dispersion. As mentioned before, the velocity dispersion in the core of NGC 1818 is roughly 10 times greater than that of the core of NGC 1805 [137], many more binaries in NGC 1818 hence can be thought as soft binaries, i.e., they are more easily disrupted in the dense core of NGC 1818, while such binary systems are likely more easy to survive in NGC 1805. In addition, NGC 1818 also harbor a relatively denser core compared with NGC 1805. Sollima (2008) derived a relationship between the survival probability of binary systems and the density and velocity dispersion of their host clusters, which shows that binaries survive frequency is much lower in environments characterized by relatively high densities and velocity dispersions [171]. We speculate that these differences in physical conditions are the main factors that caused the significantly different radial binary fraction profiles observed for these two YMCs.

We then adopt velocity dispersions for NGC 1805 and NGC 1818 of 7 and 0.7 km s^{-1}, respectively, and total masses of $\log(M_{\rm cl}[{\rm M}_\odot]) = 3.45^{+0.10}_{-0.11}$ and 4.01 ± 0.10 [157]. Again we estimate the total number of stars that associated with NGC 1805 as 10,000 (see Sect. 3.5); for NGC 1818 we estimate a total number of member stars within 73.7 arcsec as 14,500, this allows us to derive an average stellar mass of $\bar{m} = 0.28^{+0.07}_{-0.06}(0.71^{+0.18}_{-0.15})$ $M_\odot$ for NGC 1805 (NGC 1818). We then estimate the typical semi-major axis length of the binary systems in both clusters through:

$$a = \frac{G\bar{m}}{2\sigma^2} \tag{3.8}$$

where G is the gravitational constant and σ is the cluster's velocity dispersion. Based on this formula, the binaries that are able to survive for a significant period of time in the cluster center of NGC 1805, should harbor their semi-major axis of order 250 AU, while that for NGC 1818 is only ~6 AU. Duquennoy et al. (1991) explored the properties of the binaries in the solar neighborhood, found for nearby field binary systems, their typical semi-major axes peaks at 30 AU [131]. If the same solar neighborhood conditions also apply to the LMC field, then it may indicate a medium value for the semi-major axes of surviving binaries.

These arguments thus support that relatively wide binaries are more easily disrupted in the environment of the NGC 1818 central region, which also corroborates the idea that dynamical evolution is likely to have acted on stars in the core of NGC 1818 and NGC 1805 (although to a lesser degree). For the core of NGC 1818, because of its severe conditions for binaries to survive, most binaries may be disrupted before they sink towards the cluster central region, leading to a avoidance region of binary fractions in the innermost region of NGC 1818.

3.6 Summary on This Work

We give a brief summary on all of the results and their indications in this work: we have used isochrone fitting and χ^2 minimization to investigate the binary fraction radial profile in the YMCs NGC 1805 and NGC 1818, These two independent methods all give a consistent result in each cluster. Our scientific results exhibit opposite trends of the radial behavior of binary fractions in the inner regions of both clusters: for NGC 1805, a significant decrease in the binary fraction from the central to periphery is detected, while for NGC 1818, we found a monotonic increase of the binary fraction with radius. We conclude that while dynamical mass segregation and the disruption of soft binaries should compete with each other for both clusters, timescale arguments imply that early dynamical mass segregation may already dominates the dynamical processes of the core of NGC 1805, however, in NGC 1818, its core is probably dominated by disruption of soft binary systems. We suggest that this may be owning to the higher velocity dispersion in the NGC 1818 core, which creates a more severe environment for binaries' survival compare with that of the NGC 1805 core.

As we have introduced in Chap. 2, binary properties are important for understanding the stellar populations in SCs. Some primordial scenarios have suggested binary population maybe the source that is responsible for abundance anomalies that observed in most GCs [115, 127], it is thus important to know how many binaries will have the potential to impact on stellar populations in SCs through long timescale. Based on this work, we know at least for some YMCs, a fraction of binaries will be disrupted rapidly during very early stage of a SC, depend on its interior environment. That means not all binaries will be able to contribute the enhancement of abundances to their subsequent stellar populations. In Chap. 4, we will introduce another work that focuses on the products of binaries in GCs, BSSs.

Chapter 4
The Formation and Evolution of Blue Straggler Stars in Globular Cluster

4.1 Introduction

In a SSP, in view of its CMD, single stars that are more massive than the MSTO stars are expected to evolve off the MS. This is based on the assumption that all member stars in a stellar system were to evolve in isolation and without undergoing any dynamical interactions. Clearly, this assumption is not applied to SCs, as stellar interaction of SCs is usually very frequently, especially for GCs, because of their old age, stars that are sufficiently evolved in dynamics may have undergone many dynamical interactions to other stars or stellar systems. As introduced in Chap. 3, soft binaries will be quickly disrupted in the very early stage of a SC, the remaining hard binaries will continually interact with bulk stellar populations, leading them become more and more compact and merge finally, the products of binary's merger are BSSs. In reality, if some of these binary products are more massive than the MSTO stars in a SC, they will occupy the bright MS extension [174, 175], this is why people call these objects "Blue Stragglers". Except for the coalescence of close binary companions [34, 35, 176–179], another scenario involves direct stellar collisions was also thought as a formation channel for BSS formation [36, 37, 178, 179].

The relative importance of these two formation channels is still poorly studied. Knigge et al. (2009) reported a strong correlation between the number of BSSs in cores of GGC and the associated core mass, however, only a weak correlation with the predicted number of BSSs formed through collisions was detected [180], however, this correlation may only be found in extremely dense GGCs. In addition, Piotto et al. (2004) tried to find significant correlation between the global BSS frequency and the collision rate in their sample clusters, however, no positive result was detected, but they found that the LF of BSS is significantly different in clusters brighter and fainter than $M_V = -8.8$ mag. On the other hand, simulations indicates that the relative importance of stellar collision and binary mass transfer would vary as a cluster evolves [182].

C. Li, *Not-So-Simple Stellar Populations in Star Clusters*, Springer Theses,
DOI 10.1007/978-981-10-5681-9_4

The morphology of radial profile of the relative BSS frequency,[1] may be treated as a dynamical clock to a cluster's evolution [183]. The dynamically young GCs may have roughly flat redial profiles of relative BSS frequency (e.g., ω Cen, Palomar 14, and NGC 2419 [183]), in those clusters, BSSs formed through binary mass transfer [182, 184]. On the other hand, GCs with intermediate dynamical age will have the BSS frequency's radial profile displays a 'bimodality' [182–185]. In this case, stellar collisions dominate the cluster central region, while binary mass transfer dominates the clusters' outer regions (e.g., 47 Tucanae, M3, and NGC 6752 [183]). The dynamically old GCs (e.g., M30, M75, M79, and M80 [183]) will even exhibit clear signature of collisional formation, Ferraro et al. (2009) [186] discovered two distinct BSS sequences in the CMD of GC M30, they found these two sequences ideally trace the theoretical single-age stellar-collision and mass-transfer tracks, because the collisional BSSs may not be chemically homogeneous, they will be bluer and brighter than their fully chemically mixed counterparts (i.e., binary merger BSSs) [187, 188].

A straightforward expectation is that for both dynamically intermediate-age and old GCs, in the absence of any clear substructures, collisionally induced BSSs should be preferentially located in a GC's inner region compared with BSSs formed through binary mass transfer. If BSSs of different origins will occupy different parts of CMD, the distribution of the different BSS types in the CMD will thus depend on their spatial positions. However, because the BSSs in a given GC would not form simultaneously, the theoretically expected single-age BSS sequences would be broadened [177–179], leading both BSS types to partially overlap in CMD. However, provided that both populations may not be fully mixed yet, it is possible to detect two subgroups in the CMD of a GC.

There are only few studies of extragalactic BSSs, Shara et al. (1998) detected 42 BSS candidates in the SMC cluster NGC 121, they finally confirmed 23 stars as BSSs [189]. In the LMC clusters NGC 1466 and NGC 2257, there are 73 and 67 BSSs are detected, respectively [190]. Mackey et al. (2006) analyzed the LMC cluster ESO121-SC03, they found 32 BSSs [191].

Here we use the high-resolution *HST*/WFPC2 observations again, to investigate the radial dependence of the BSS frequency in the LMC GC Hodge 11. We detect a significant number of BSSs, whose radial profile of BSS frequency shows clear bimodality in morphology. We will show that the BSSs in the inner region are bluer and fainter on average, compare with the peripheral BSSs, which are relatively redder and brighter, their relative distribution is consistent with the position of theoretical 'collision sequence' and 'binary region'. This result offers unprecedented evidence in support of the theoretical predictions, which also allows us to study the evolution of the cluster's collisionally BSS population.

[1]The number of BSSs normalized to that of HB or RGB stars.

4.2 Data Reduction

The datasets of Hodge 11 were obtained with the instrument of *HST*/WFPC2, filtered in F555W (hereafter V) and F814W (hereafter I) bands [136]. The total exposure times of the observational data were 435 s and 960 s in the V and I bands, respectively. The PSF fitting photometry based on the package HSTPHOT was applied to the scientific images [151]. The cluster center was determined as described in Sect. 3.4. A stellar catalogue of nearby field region have been also obtained to statistically reduce the background contamination [192]. The raw, field and decontaminated CMDs of Hodge 11 are present in Fig. 4.1. The number of objected in the BSS region of the raw CMD is 338; after decontamination, 176 stars are removed, finally the decontaminated CMD contains 162 stars in the same region. This latter sample forms the bases of our subsequent analysis. Because BSSs are bright, the photometric catalog have completeness of >95% in their relevant magnitude range, even in the cluster central region. The left panel of Fig. 4.2 displays the spatial distribution of all observed stars in the Hodge 11 and its BSS population.

We divided the MS and RGB regions in the Hodge 11 CMD into 32 grids, with their magnitude span from $V = 18.3$ to 27.0 mag with bin size of ∼0.30 mag. In each magnitude range, we determined the peak and corresponding 3σ spread of all stars' color distribution, based on a Gaussion function fitting. Hodge 11 is a metal-poor GC with [Fe/H] = -2.1 ± 0.2 dex [193, 194] to -1.86 dex [195]. Adopting a metallicity $Z = 0.0002$ ([Fe/H] ≈ -1.98 dex, which between the latter two values of Hodge 11's metallicity), and using the ridgeline, we thus obtained the best-fitting isochrone from the Padova stellar evolutionary models [24] and calculated the MSTO locus. The adopted best fitting cluster age is $\log(t\,\mathrm{yr}^{-1}) = 10.07 \pm 0.01$ ($11.7^{+0.2}_{-0.1}$ Gyr [190]), and the extinction is $E(B-V) = 0.09 \pm 0.01$ mag. We adopted the canonical LMC distance modulus, $(m-M)_0 = 18.50$ mag, which indicates that $1'' \equiv 0.24$ pc. In Hodge 11, many of HB stars are located in the extreme blue HB,

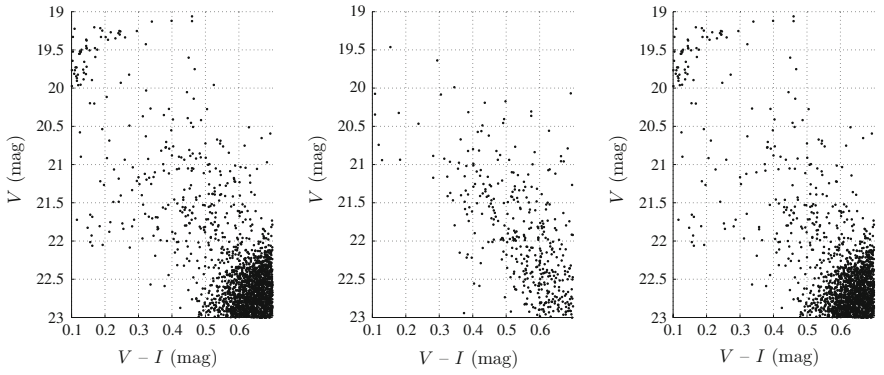

Fig. 4.1 The CMD zooms focusing on the BSS-dominated region. (*left*) Original CMD; (*middle*) CMD of corresponding nearby field region; (*right*) The decontaminated CMD

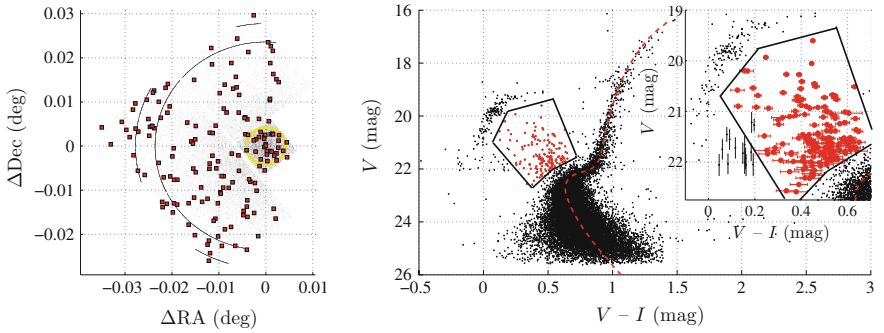

Fig. 4.2 (*left*) Spatial distribution of stars in the Hodge 11 area. *Red circles* BSSs. *Yellow* and *black* (partial) concentric circles indicate radii of $R = 15, 85$, and $100''$. (*right*) Corresponding CMD, including the best-fitting isochrone (*red dashed lines*) [41]. *Red points* represent BSSs; the *inset* shows the photometric uncertainties for all BSS candidates. *Black points* with *error bars* have photometric errors $\Delta V > 0.1$ mag (color uncertainties have been omitted for clarity). *Thick solid lines* delineate the BSS region adopted

we have confirmed that our sample BSSs can easily be distinguished from HB stars by adopting a minimum HB–BS difference in color and magnitude of 0.3 mag, as a result, the HB stars and BSSs are clearly separated in the CMD (see right panel of Fig. 4.2), as the absolute photometric errors for their magnitude range are significantly smaller than 0.3 mag.

Finally stars meet all of the following criteria will be identified as a BSSs:

1. It is bluer and brighter than the MSTO region.
2. Its distance in CMD from the MSTO and MS ridgeline is $>3\sigma$ (σ refers to the spread in MS color distribution at the relevant magnitude range).
3. Its photometric uncertainty is <0.1 mag in both V and I bands.

The right panel of Fig. 4.2 shows the CMD of Hodge 11, where the inset focuses on the region dominated by BSSs. The red points represent BSSs candidates (after field decontamination process). The small black points with error bars are objects with photometric errors that are larger than 0.1 mag. These data with high uncertainties may comes from the short exposure time observations, or caused by effect of instrumental artefacts. We thus discarded these objects from our BSS sample.

4.3 Analysis and Results

The top panels of Fig. 4.3 shows the cluster's stellar number density radial profile for all stars with $V \leq 25$ mag. The black dashed line indicates the field's average density value based on the catalogue of the nearby field region. The distance where the cluster's monotonically decreasing number-density profile reaches the field density has been determined as the cluster region, which is $R = 102.3^{+2.7}_{-2.3}$ arcsec (indicated

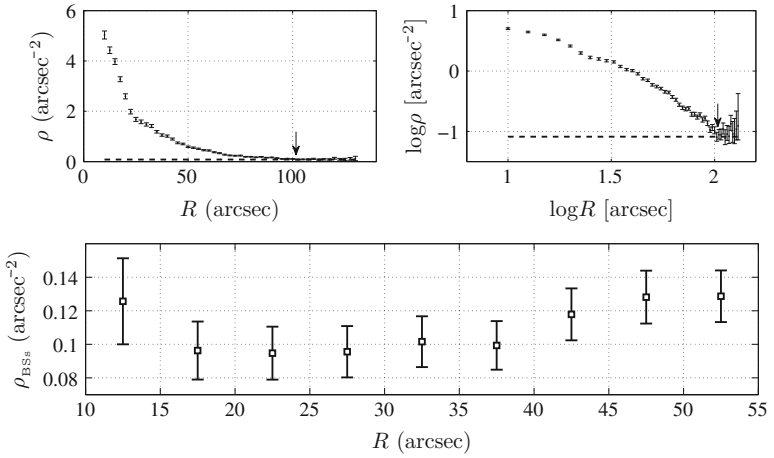

Fig. 4.3 (*Top left*) Hodge 11 number-density profile. The *black dashed line* indicates the average field density, implying a cluster size of $R = 102.3^{+2.7}_{-2.3}$ arcsec, indicated by *black arrow*. (*Top right*) Corresponding logarithmic number-density profile. (*Bottom*) BSS-frequency profile (normalized to the number of RGB stars) of Hodge 11, including Poissonian uncertainties

by black arrows). In addition to the sample of BSSs, we selected a sample containing RGB stars in the magnitude range from $V = 19.60$ to 22.05 mag, which roughly equal to the BSSs' typical magnitude range. We normalized the number of BSSs to the number of selected RGB stars: $f_{\rm BSSs} = N_{\rm BSSs}/N_{\rm RGB}$, where $N_{\rm BSSs}$ and $N_{\rm RGB}$ are the number of BSSs and RGB stars, respectively. We then determined the radial dependence of the BSS frequency, $f_{\rm BSSs}$, which is present in the bottom panel of Fig. 4.3. The resulted BSS-frequency profile is very similar to the equivalent radial profile in GCs 47 Tuc, M3 and NGC 6752 [184].

The number of BSSs that determined in Hodge 11 is extremely large. Ferraro et al. (1995) summarized the number of BSSs in 26 GGCs, their results show that the number of BSSs in GGCs span from four (NGC 5024) to 137 (NGC 5272) [196]. In Hodge 11, we detected totoally 150 BSSs within $R = 100''$, the total number of BSSs on all four chips of Hodge 11 observations even reaches 162. The BSSs distribution associated with Hodge 11 is very extended, the number of BSSs located in our outer subsample, $R \in [85'', 100'']$, is 27, this large number of BSSs strengthens the statistical robust of our conclusions.

Mackey et al. (2003) determined the core radius of $R_{\rm core} = 12.14 \pm 0.66$ arcsec for Hodge 11 [157]. Our number-density profile of Hodge 11 also shows a relatively sharp radial decline to $R \sim 15$–$20''$. Therefore, we defined an inner BSS subsample covering the cluster core at $R \leq 15''$ (Fig. 4.4, left). The open red and blue squares in the CMD of Fig. 4.4 (left) are the inner ($R \leq 15''$) and outer ($R \in [85'', 100'']$) subsamples. We constrained the out subsample contains the same number of BSSs to inner subsample, both them contain 27 BSSs. A distinct difference is seen between their distribution in CMD. We also attached the separation between the two BSS

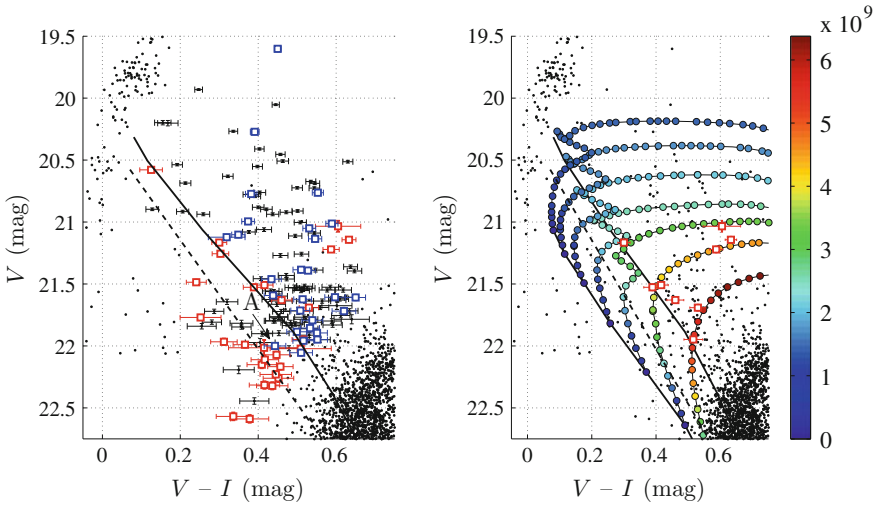

Fig. 4.4 (*left*) CMD of BSs in Hodge 11. *Red open squares*: BSs at $R \leq 15''$; *blue open squares*: BSs at $R \in [85'', 100'']$. The *black dashed line* is the critical line separating the two BSS sequences in M30 [186]; the *black solid line* indicates the predicted ZAMS adjusted by -0.75 mag. (*right*) Evolutionary tracks of stars with masses from 1.0 to 1.6 $M_\odot$ (*bottom* to *top* [41]) for $Z = 0.0004$ (closest available metallicity). Different colors indicate the evolutionary timescales for stars to evolve from the ZAMS to their current positions. *Red open squares* indicate inner-sample BSs ($R \leq 15''$) located above the locus of equal-mass binary sequence

subpopulations in M30 that detected by Ferraro et al. (2009) (dashed line [186]). They suggested that BSSs below this 'critical' line might preferential result from stellar collisions, while BSSs that above line may more prefer to have formed through binary mass transfer.

However, because M30 and Hodge 11 have different evolutionary histories and environments, it is not surprise that the relative distribution of our two subsamples are not appropriately divided by the 'critical' line. Indeed, if we shift the zero-age main sequence (ZAMS) upward in the CMD by 0.75 mag—roughly equal to the locus of equal-mass binary sequence—we found that this provides an excellent separation between these two subsamples. This result thus support the claims of Ferraro et al. (2009) for GC M30 [186]. We also found one outer-sample BSS is located in the 'bottom region' (star 'A' in Fig. 4.4 left panel), except for the only exception, all other 26 outer sample BSSs are all located above the locus of equal-mass binary sequence. In contrast, the inner sample BSSs only have four BSSs are unambiguously located in this CMD region, given the photometric errors.

4.4 Physical Implications

Because the central region of GC Hodge 11 is very crowded, the BSSs in this region may be more likely the result of stellar collisions. On the other hand, the low number density of cluster peripheral region reners a high frequency of stellar collisions unlikely, the BSSs in the cluster's periphery may more prefer to originate from mass transfer bbetween individual components in binary systems. Based on the adopted locus of equal-mass binary sequence, the mixture of the two BSSs subsamples in the CMD seems 'unbalanced': only few out-sample BSSs are found in the bottom region, however, the inner-sample BSSs frequently penetrate to the top region. We speculate three possible explanations for this observation:

1. The spatial distribution of the BSSs in Hodge 11 is a two-dimensional projection of a 3D spatial distribution. Some BSSs that looks like in the central region may not be genuine inner-sample members, but could be the result of projection of outer-sample BSSs that close to the cluster center in the line-of-sight direction. However, a projected outer-sample BSSs must truly far away from the center. Based on this geometry considerations, assuming a uniform BSS distribution in the outer annulus, $R \in [85'', 100'']$ would suggest that 4 ± 2 (Poissonian uncertainty) outer-sample BS be projected along the line-of-sight through the cluster with radii $R \leq 15''$.
2. BSSs would evolve in the CMD. Although without any new dynamical interactions, the BSSs in the bottom region will move upward, but the BSSs in the top area will never move back (downward). To estimate the approximate time necessary for BSSs to evolve from the ZAMS to the region above the locus of equal-mass binary sequence, in Fig. 4.4 (right) we show evolutionary tracks for stars of different masses [41]. We select those inner-sample BSSs that are located above the locus of equal-mass binary sequence (red open squares) and compare their position to the tracks for stars with masses from 1.0 to 1.6 $M_{\odot}$ (bottom to top; 1.6 $M_{\odot}$ is roughly equal to 2 M_{MSTO}). The colorbar indicates different evolutionary timescales for stars to evolve from the ZAMS to their observed positions.
3. Although the relative frequency is small, there may still be some BSSs resulted from binary mass transfer channel, these type of BSSs will be located in the top region.

The object 'A' in Fig. 4.4 is found in the CMD's bottom region, but its belong to outer sample BSS. The photometric color spread also cannot explain its locus. This star, however, could either be a projected foreground star or a collisionally formed BSS that may have been ejected from the cluster central region [197]. Such ejected BSSs will subsequently sink toward the cluster center again through dynamical mass segregation. Compared with the other BSSs, this star may have a relatively low mass due to its low luminosity, so that this process is likely still underway.

The radial distance bias of BSSs in the Hodge 11 CMD is significant, suggesting that our result is robust. In addition, compared with M30, the number of *field* BSSs located beyond the typical region of Hodge 11 is very large. There are totally 12 BSSs are detected in the partially observed annulus $R \in [100'', 130'']$, considering that the *HST*-based coverage is only 9.3% complete (for comparison, our coverage of the actual cluster area, $R \leq 100''$, is 50.2% complete), this indicates that there are at least 130 BSSs would located in this region. If we adopt an outer boundary to the peripheral BSS population such that all observed BSSs are included and compare their CMD with that of the inner BSS population, the distinction between the two samples is still significant.

Based on the assumption that all selected objects are genuine cluster BSSs, the locus of the most massive BSS—which should originally have been located in the 'bottom region' of the CMD but is actually distributed above the locus of equal-mass binary sequence—probably reflects its stellar evolution. Geometry considerations indicate that 4 ± 2 stars may be seen in projection, however, nine inner-sample BSSs have been found crossed the locus of equal-mass binary sequence. This means that about 5 objects could be actually evolved BSSs. If confirm, this may allow us to evaluate their time of birth at 4–5 Gyr ago. The BSSs characterized by magnitude between $V = 21.0$ and 21.5 mag may also be evolved stars. However, for BSSs that are fainter than $V = 21.5$ mag, the time required to evolve to their current position in the CMD is so long that their loci in the CMD may be caused by 2D projection of the cluster's 3D spatial distribution.

4.5 Conclusion

In this Chapter, we analyzed the position of BSSs in GC Hodge 11, based on the prediction of stellar evolutionary models, BSSs resulting from stellar collisions and from binary mass transfer should be located along two distinct sequences. However, two well-populated sequences can only be detected if all BSSs formed in a starburst mode in a given cluster, that is, they are all short-lived, close to their locus of ZAMS. Long-term, continuous BSS formation will render their expected boundary less distinct. However, BSSs formed through either of these two scenarios should show the signature of a clustercentric radial dependence in their color–magnitude space. Based on the analysis of *HST*/WFPC2 observations of GC Hodge 11, we found a clear signature of such a spatial dependence. The average luminosity of inner region BSSs is relatively lower, while BSSs in the outer region are brighter. Even when considering the impacts of 2D projection and stellar evolution, this difference is significant. This result hence offers strong evidence in support of the theoretical prediction of dual-mode BSS formation and allowed us to estimate their evolutionary timescales.

Looking back to Chap. 3, we know that the initial binary disruption is very efficiency for YMCs, but this dynamical process also make the survived binary systems gradually tighter as their host cluster evolve, making the formation of mass transfer BSSs possible. However, the number of BSSs in GCs is usually small, in Hodge 11, we only detected hundreds of BSSs, in Fig. 4.3, we know the fraction between the number of BSSs to RGB stars is around 10%, which already represents a relatively high BSS fraction when compare that to GGCs. Although some scenarios suggest that binary interaction may be a solution to the ubiquitous secondary stellar populations in GCs, the small fraction of BSSs may suggest that binary merger cannot fully explain the high fraction of secondary stellar populations in GCs. In Chap. 5, we take a GGC, 47 Tuc., as an example, we will see that it harbors a high fraction of secondary stellar populations in its RGB sample, which also exhibits an apparent dynamical difference between the second population stars and first population stars.

Chapter 5
Multiple Stellar Populations in the Giant Branches of Galactic Globular Clusters

5.1 Introduction

As introduced in Chap. 2, stars in a given SC are usually assumed to have originated from a coeval SSP with similar metallicity (at least within a narrow range determined by the metallicity of their progenitor molecular cloud). Although this scenario has led to numerous very successful SC analyses, the obvious populations anomalies that appear in both their photometric and spectroscopic properties in intermediate-age SCs and GCs have strongly challenge the applicability of the SSP scenario [64, 65, 93, 96, 198–203].

The breakdown of the SSP model is particularly convincing for GCs, the apparent MSPs that discovered in GCs show obvious differences in their chemical abundances [204, 205]. Based on photometry, the MSPs in GCs are found to harbor apparent dynamical difference: Milone et al. (2012a) found two distinct MSs in GC 47 Tuc, they explained these two sequences as a CN-weak/O-rich/Na-poor population and a CN-strong/O-poor/Na-rich population, where the latter population is the remnant of the first stellar generation, which is more centrally concentrated [95]. Similar results are also confirmed in GC M3 (NGC 5272), which harbors two RGBs that are well separated in the CMD, which again can be explained by a N-poor/Na-poor first stellar populations and a N-rich/Na-rich second stellar population, the letter shows apparent higher concentration than the first stellar population [206]. More comprehensive results was made by Lardo et al. (2011), who found for 9 GCs, their ultraviolet red (UV-red) RGBs, which generally identified with the second stellar populations, are more concentrated than their UV-blue counterparts, which are presumed as first generation stars [98].

In this Chapter, I present our analysis on the stellar populations in GC 47 Tuc, we will show that our result cements the conclusions made by Milone et al. (2012a) [95], with a higher significance. 47 Tuc is a cluster which displays apparent MSP features across its entire CMD. It was reported to have a clear nitrogen (N) dichotomy [207–209]. Despite its two distinct MSs, it has been found to possess a broadening of the SGB or multiple SGBs [95, 210], as well as double or multiple RGBs

C. Li, *Not-So-Simple Stellar Populations in Star Clusters*, Springer Theses,
DOI 10.1007/978-981-10-5681-9_5

[95, 211]. In addition, its RGB-bump and HB stars also display radial gradients, indicates a helium-enriched second stellar population [212]. Its member stars also harbors the well-known Na–O anticorrelation [213], indicating contamination by products of the proton-capture process [214]. All these evidence strongly imply the presence of more than one stellar population in 47 Tuc.

Different scenarios have been proposed to explain the secondary stellar populations; As introduced in Chap. 2, they mainly invoke scenarios involving the ejecta of rapidly rotating massive stars [32], massive binaries [115], or evolved AGB stars [116]. Previous studies have also shown the dynamical difference between the second stellar population stars and their first generation counterparts, where the second generation stars are generally more centrally concentrated [30, 215, 216]. Indeed, the results of Milone et al. (2012a) have shown that the second-population stars in 47 Tuc gradually start to dominate at increasing smaller radii based on their analysis of RGB and HB stars [95], their conclusion was supported by Cordero et al. (2014) through analyzing their chemical abundances [213]. The broadening of SGB stars in 47 Tuc also supports the presence of multiple stellar populations [210], but the radial behavior of these SGB stars is not explored yet owning to the constraints inherent to sample selection.

In this Chapter, we present a deep, large-area, near-infrared (NIR) CMD of 47 Tuc, based on the observation of 4 m Visible and Infrared Survey Telescope for Astronomy (VISTA). The SGB and RGB of 47 Tuc in the NIR CMD are significantly broadened, which cannot be explained by the combination of photometric uncertainties and differential extinction. Compare with the results of Milone et al. (2012a) [95], we find a more obvious color bias in the RGB's radial behavior, the average color of the RGB stars at large radii is significantly bluer than their innermost sample, which strongly indicates that the two RGB populations contain significantly different fractions of second population stars. We also find that the SGB stars in the periphery are systematically brighter than their innermost counterparts. The combination of these features is striking, which can even be seen based on a single glance at the global CMD. Our NIR observations of 47 Tuc covers a very large field, which reaches a maximum distance to the cluster center of $4000''$, thus enable us to well characterize the effects of background contamination. This Chapter is organized as follows, in Sect. 5.2, we introduce the data reduction approach. Section 5.3 contains our main results, the discussion to these results are present in Sect. 5.4. In Sect. 5.4, I summarize all possible things that we can learn from these chapter.

5.2 Data Reduction and Analysis

The dataset that analyzed in this work was obtained from the VISTA NIR Y, J, K_s survey of Magellanic System (VMC[1]; PI M.-R. L. Cioni: see [218]). The time range of this survey last 5 yr, and it started in November 2009. The main goals of this

[1] http://star.herts.ac.uk/mcioni/vmc.

survey and its first data are also included in Cioni et al. (2011) [218]. The GC 47 Tuc is fortuitously located in front of the SMC, on VMC tile "SMC 5_2". The VMC images were reduced by the Cambridge Astronomy Survey Unit based on the pipeline of VISTA Data Flow System (VDFS) [219]. Our photometry is based on PSF technique, starting from the raw VMC images. We selected epochs with limited seeing inhomogeneities for both three filters (Y, J, K_s). The reduced data, containing two epochs in Y and J and nine in K_s, are PSF-homogenized and combined to obtain a deep tile image. We performed PSF photometry on the deep image of tile SMC 5_2 based on the IRAF DAOPHOT package. The PSF and ALLSTAR tasks were used to generate PSF models and perform the photometry. The aperture corrections have been performed based on catalogs retrieved from the VISTA Science Archive [220] for the bulk of the observed stars.

In this work, we focus on the (Y, $Y - K_s$) CMD of 47 Tuc, because the features of interest are most apparent in this CMD. We have also confirmed that our conclusions also hold based on the analysis of the (Y, $Y - J$) and (J, $J - K_s$) CMDs, although with less significance. The observations cover an area of roughly 1.2×5 deg^2, the bulk of GC 47 Tuc stars are located toward the southwest of the observed image, providing the opposite corner of the field as a suitable region for statistically background decontamination. 47 Tuc is extremely large and crowded, our observed data contains more than 300,000 stars with $Y \in [11.0, 25.5]$ mag. Almost all of the more massive ($m_* \geq 0.88 M_\odot$), bright ($Y \leq 13$ mag) cluster stars are contained within the central region owing to the effects of mass segregation [136–138]. These segregated bright stars dramatically increase the background magnitude in the cluster core region, making almost all stars fainter than $Y \sim 13$–15 mag fade into the background. Because of this, we only use 3071 stars brighter than $Y = 13.0$ mag to determine the cluster center, the approach we used to determine cluster center is similar to that described in Sect. 3.2, the resulting center coordinates are $\alpha_{J2000} = 00^h24^m04.80^s(6.020°$; statistical uncertainty $0.007° \equiv 25'')$, $\delta_{J2000} = -72°04'48''(-72.080° \pm 0.006° \equiv 20')$. As we only select the top bright stars to explore their geometric center in spatial, we confirmed that this adoption will introduce negligible biases, because the member stars of old GCs should all have adapted their kinematics to be in equilibrium, thus presuming both the bright stars and fainter stars would experience the same gravitational potential is reasonable. Our results is also consistent with previous studies [221–223].

We then selected a circle region centered at $\alpha_{J2000} = 00^h31^m59.00^s(8.00°)$, $\delta_{J2000} = -71°42'00''(-71.70°)$, with a radius of $600''$, to calculate the background stellar number density, we again constrain our sample with stars that are brighter than $Y = 13.0$ mag. Most of stars in this region are foreground MW and background SMC stars. Based on the assessment of the cluster's extended radial profile, we estimate that the contamination by 47 Tuc member at these large radii is $\ll 15\%$, this thus supports that the adopted field region is a suitable choice for background decontamination. In addition, the center of the field is located more than $2400''$ from the cluster center, this distance is close to the cluster's tidal radius ($r_t = 56$ pc $\equiv 2500''$ [224, 225]), indicating this region should be mainly dominated by background stars rather than cluster member stars. We cannot rule out the presence of extratidal stars from 47

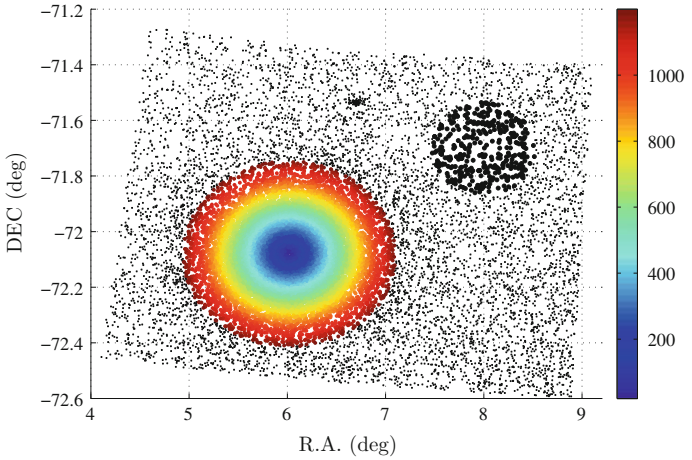

Fig. 5.1 Spatial distribution of 47 Tuc stars that are brighter than $Y = 17.0$ mag. Cluster stars are indicated by *color circles*, with their color represent corresponding distance to the cluster *center*, the maximum distance of cluster stars reaches $1200''$, the filled *black circles* represent stars in the adopted field region, with a radius of $600''$

Tuc, previous work have predicted that 47 Tuc may exhibit at least one extratidal tail that cross from the northwest to the southeast of the observed filed in this work [225]. Indeed, we do found that the stellar number density in the southeast region is higher than that in the northeast. The comparison between the cluster's stellar number density and that of the background field reports that at the radius of $R_{\rm f} = 1220 \pm 20''$, the cluster's stellar number density becomes indistinguishable from the background level. We thus adopted a cluster "size" of $1200''$ for further study, this value is equal to approximately 50% of its tidal radius. This choice is kind of conservative, because we excluded the brightest stars from our analysis. The dynamical mass segregation will cause an underestimation of the "bright" cluster size compared with its homogeneous stellar sample. Figure 5.1 shows the stellar spatial distribution of stars with $Y \leq 17$ mag. Stars in the adopted field region are highlighted by black filled circles, while the cluster stars are indicated by color circles, where the color also represent their relative distance to cluster center.

We next adopted the most suitable isochrone to describe the resulted CMD, using the PGPUC stellar evolution code[2] [17, 226]. We adopted a typical age for 47 Tuc of 12.5 Gyr ($\log(t\ {\rm yr}^{-1}) = 10.10$ [221, 227–229]), the derived best fitting metallicity is $Z = 0.0042$ or [Fe/H] $= -0.55$ dex, which is consistent with the determination of Natef et al. (2011) [212]. The average extinction is $E(B-V) = 0.04$ mag, based on the fixed age and metallicity [210, 213, 224]. Another parameter that requested by PGPUC model is the [α/Fe] ratio, Carretta et al. (2009) have determined [α/Fe] = 0.40 dex for 47 Tuc, we thus adopted the maximum available value of [α/Fe] = 0.30

[2] http://www2.astro.puc.cl/pgpuc/iso.php, PGPUC model assumes $Z_{\odot} = 0.0152$.

dex, to generate the most representative isochrone for 47 Tuc; we confirmed that this offset will not introduce significant fitting problems. Based on all these input parameters, the best-fitting distance modulus to 47 Tuc is $(m - M)_0 = 13.40 \pm 0.10$ mag [224, 227, 229].

As illustrated in Fig. 5.1, we selected stars from a suitably chosen nearby region as field reference to statistically correct background contamination. The field region is a circular area with a radius of 600″, which corresponds to one quarter of the adopted cluster area. We compared the CMD of field region with that of the cluster, for each star in the CMD of the field region, we removed the closest four counterparts in the corresponding cluster CMD. Because we mainly focus on SGB and RGB region, which are relatively bright compare to the typical magnitude of field stars, we found only very few of field stars in the region adopted for decontamination are this bright.

Figure 5.2 presents the decontaminated cluster's CMD, as well as the best fitting isochrone derived from the PGPUC model. The color scale indicates the distance to the cluster center (in arcsec). In this figure, even at a quick glance, one will immediately found a systematic difference between the cluster stars in the central region and in the outskirt. Even if we ignore the MS stars with lower accuracy owning to the low completeness at cluster's core region (see Fig. 5.3), the SGB and RGB stars still display a clear difference as a function of radius in their color-magnitude distribution. SGB stars with large radii are systematically brighter than

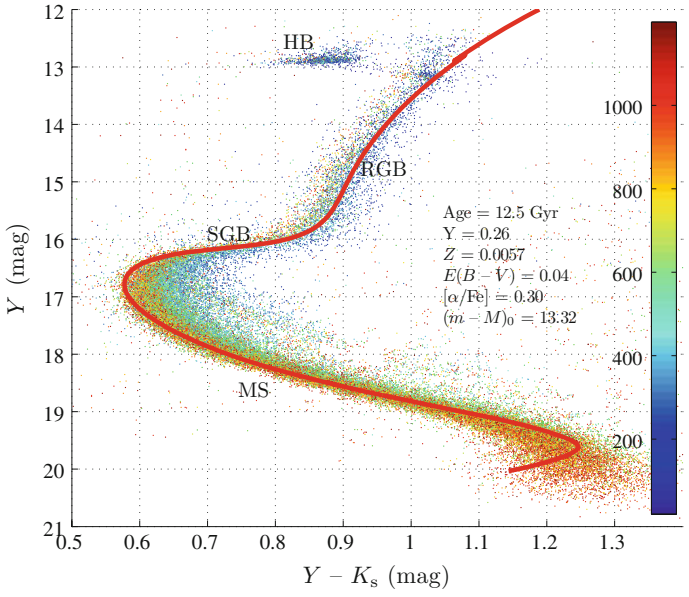

Fig. 5.2 The decontaminated CMD of 47 Tuc, showing only stars with photometric uncertainties of ≤0.02 mag. The color bar represents the distance to the cluster *center* (in arcsec). The *red solid line* represents the best-fitting isochrone

inner SGB stars (with small radii); they also join the RGB at clearly bluer colors compared with the color range of the central RGB stars, indicating higher surface temperatures for these outer sample objects. We have constrained all stars shown in Fig. 5.2 have photometric uncertainties not higher than 0.02 mag. It is thus clear that the observed broadening morphology of both the SGB and the RGB are not owning to the photometric dispersions.

Given that both the significant mass segregation and stellar blending due to crowding effects will dramatically complicate the physical conditions pf 47 Tuc observations, most faint stars have large photometric uncertainties, while some brightest stars (in particular for those with $K_s \leq 11.5$ mag) are partially saturated. We therefore removed stars that have photometric uncertainties exceed 0.02 mag in all three filters. This finally selected out sample that contained the ∼30% of stars with the highest-accuracy photometry in the corresponding magnitude range. The crowding will also make centrally located stars have larger errors, in order to quantify the possible bias that may be caused by crowding, we used AS tests to explore the systematic effects of crowding on the photometric uncertainties in the resulting PSF photometry. We added 7.2×10^6 ASs to the raw image, then we measured these ASs in the same manner as our sample of real stars. The number of ASs that we input to the raw image is roughly 20 times larger than the number of real stars. To avoid a situation in which the ASs affect the background level and crowding, each time we only add 3500 stars to the raw image. We confirmed that the effects of ASs blending with other ASs are negligible. For ASs, their spatial distribution as well as distribution in the CMD is similar to the real distribution. The resulting AS catalog contains the input and output magnitudes, and corresponding photometric errors computed as output—input magnitudes. Based on the AS tests, we found that the positions in the CMD of the SGB and RGB stars are negligibly affected, but it indeed becomes

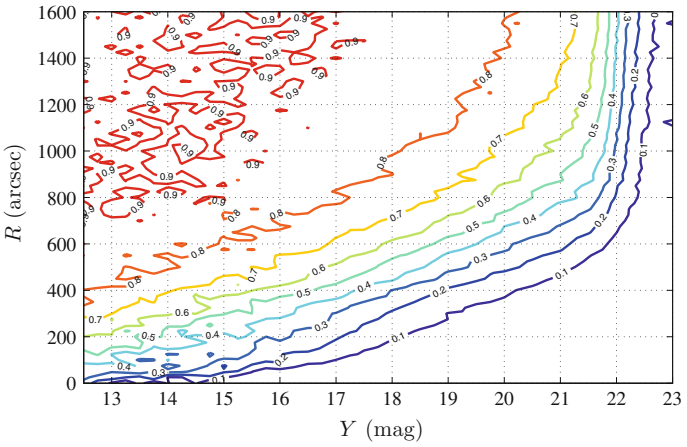

Fig. 5.3 2D completeness contour figure as a function of radius and Y magnitude

important for stars that are fainter than the MSTO. Our results hence confirm that the spread in the SGB/RGB is caused by physical reality rather than the effect of blending.

The AS tests also provide us the photometric completeness of stellar catalog. In this case, we generated artificial stars that were homogeneously distributed across the entire region of observations. Those output ASs with no photometric magnitude or with output magnitude that are significantly different to their input magnitude with more than five times their photometric uncertainties were counted as not be recovered, thus contributing the incompleteness. Figure 5.3 shows the cumulative 2D completeness contour figure as a function of both radius and Y band magnitude.

5.3 Main Results

5.3.1 Sub-giant Branch Stars

We firstly take our analysis on the region occupied by the SGB stars. We select a box delineated by $Y \in [15.5, 16.7]$ mag and $0.70 \leq (Y - K_s) \leq 0.85$ mag. The selection of this region is quite arbitrary, we only ensure that the region contains most SGB stars. We further impose a maximum photometric uncertainty of 0.015 mag for the select SGB sample owning to their more accurate nature than the faint MS stars. This constraint finally leaves us with the ∼30% of stars with the highest-accuracy photometry in the total sample.

We subsequently adopt the cluster-wide ridge line as standard model, the ridge line of the SGB is the loci of the maximum stellar number density as a function of color. After that we calculate the magnitude deviation with respect to the ridge line for all selected SGB stars, $\Delta Y = Y_{\rm SGB} - Y_{\rm iso}$. The resulting magnitude distribution is described by a Gaussian function with $\sigma_{\Delta Y} \sim 0.18$ mag. We rule out stars that were found beyond $3\sigma_{\Delta Y} = 0.54$ mag of the ridge line, this finally result in a sample contains 1389 stars: see Fig. 5.4.

In Fig. 5.4, one can see that the SGB stars in the cluster's outskirt are systematically found above the ridge line, indicates that they are brighter compared with their more centrally located counterparts. We subsequently divide the SGB sample into five rings as a function of radius to explore whether their magnitude dispersion varies with radius. The four boundaries between these five annuli were set at 340″, 450″, 590″, and 800″, which resulted in stellar numbers per radial bin span from 269 to 283. For each radial bin, we calculate the distribution of their magnitude dispersion, normalized to the total number of stars in that bin. This is actually the probability distribution of ΔY in each radial bin, as shown in Fig. 5.5.

Figure 5.5 shows that the SGB stars in the innermost radial bin (top panel) are systematically fainter ($\Delta Y > 0$ mag) than their peripheral SGB sample (bottom panel). The average magnitude of the bulk of the SGB stars becomes gradually brighter ($\Delta Y < 0$ mag) as a function of increasing radius. The magnitude dispersion of cen-

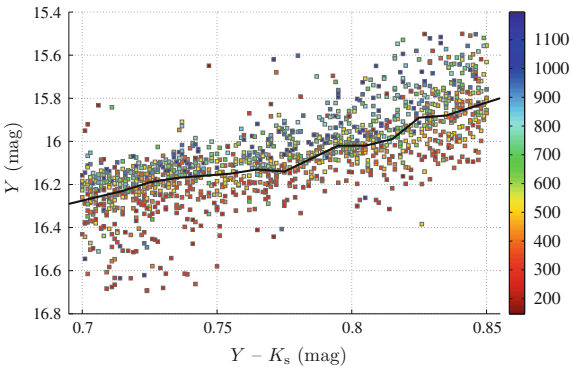

Fig. 5.4 CMD of the adopted SGB stars. The colorbar indicates their distance to the cluster *center* (in arcsec). The minimum radius attainable is $\sim 150''$ owning to sampling incompleteness in the cluster core. All stars have magnitudes within $3\sigma_{\Delta Y} = 0.54$ mag of the SGB *ridge line*

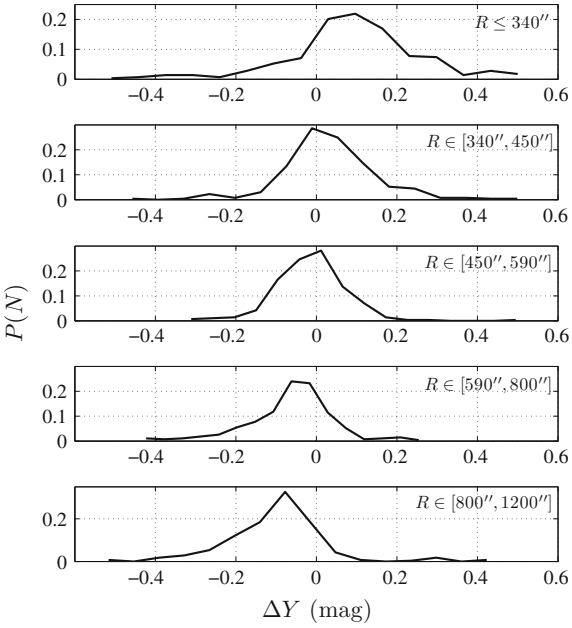

Fig. 5.5 Probability distribution of ΔY as a function of radius for SGB stars in 47 Tuc. The radial bins from the cluster's inner regions to its outskirts are labeled

tral sample is also larger than that of the peripheral SGB sample. This is not surprise, as the observed stellar distribution in 47 Tuc is a 2D projection onto the plane of the sky: the stars in the peripheral sample are located far from the cluster center, but the innermost stars will be significantly contaminated by stars that are physically located at large radii. If the properties of SGB stars in the peripheral sample differ systematically from those in the central sample, the contaminated innermost sample will therefore display a large dispersion in magnitude distribution.

Blending of unresolved stars in the line-of-sight direction will also cause a dispersion of SGB stars to brighter magnitude. The blending frequency is expected higher in the cluster innermost regions than peripheral regions as the central region

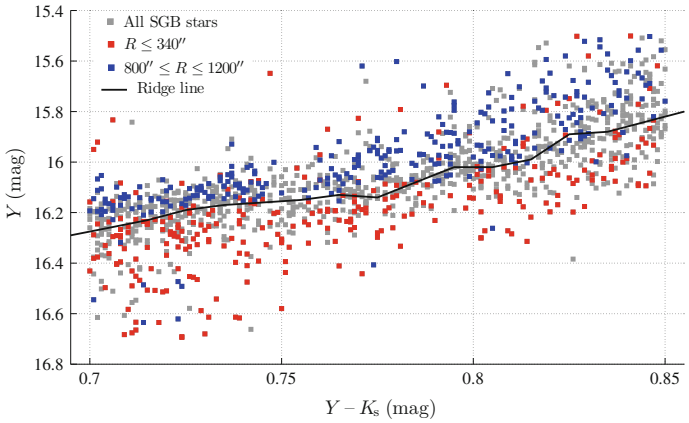

Fig. 5.6 CMD of the SGB stars at $R \leq 340''$ in 47 Tuc (*red solid squares*) and the outermost SGB stars ($R \in [800'', 1200'']$: *blue solid squares*). The *grey squares* represent all SGB stars in our sample

has higher stellar number density. Both of these effects will cause a bias to brighter magnitude for the innermost sample of SGB stars. Because of this, the observed magnitude distribution for the innermost SGB stars should have higher dispersion than their intrinsic distribution. In Fig. 5.6 we show the CMD of innermost SGB stars ($R \leq 340''$) and outermost SGB stars ($R \in [800'', 1200'']$). It is clear that the innermost SGB stars are more dispersed in their magnitude distribution than the outermost SGB stars, both samples are apparently different.

Using a Monte Carlo method, we estimate how many projected stars at large radii will contaminate the stellar sample drawn from the central regions. For example, if we want to calculate the contamination fraction of SGB stars in the ring defined by $R_1 \leq R \leq R_2$, we first calculate how many SGB stars are located at $R \geq R_2$, defined as $N = N(R \geq R_2)$. Then we assume that these N stars are located in a three-dimensional (3D) spherical shell at $R_2 \leq R \leq R_f$, where $R_f = 1200''$ is the cluster size. The stellar density at this spherical shell is

$$\rho = \frac{3N}{4\pi(R_f^3 - R_2^3)}. \tag{5.1}$$

We subsequently generate a 3D spherical cluster of R_f, which contains $N_{art} = (4\pi R_f^3/3) \times \rho$ fake stars. The fake stars are homogeneously distributed with density ρ, we then randomly select a direction to represent the line-of-sight direction, in this direction, the number of stars that located at $R \geq R_2$ that are projected at $R_1 \leq R_{proj} \leq R_2$ is referred to as N_{proj}. For each radial bin, we repeat this process 10 times to obtain the average N_{proj}, which thus represents an approximate projected number of stars in the radial annulus of interest.

Table 5.1 Contamination due to line-of-sight projection for SGB and RGB stars as a function of radius

SGB stars	$f_{\rm proj}$ (%)	RGB stars	$f_{\rm proj}$ (%)
$R \leq 340''$	36.40	$R \leq 260''$	29.00
$R \in [340'', 450'']$	20.82	$R \in [260'', 370'']$	20.55
$R \in [450'', 590'']$	20.42	$R \in [370'', 510'']$	19.46
$R \in [590'', 800'']$	15.87	$R \in [510'', 730'']$	16.26

Based on this method, we can quantify the resulting ratio of the projected contamination. For example, for the sample drawn from the (projected) innermost radii, $R \leq 340''$, 103 stars are actually physically located at $R > 340''$. While for the radial range $590'' \leq R \leq 800''$, only 43 stars are actually located beyond $R = 800''$ along the line-of-sight direction. After normalize the number of contaminated stars to the total number of stars in each projected radial bin, we find that the 2D projection contamination fraction decreases from 36% for innermost radii ($R \leq 340''$) to 16% for the penultimate radial range ($590'' \leq R \leq 800''$, we have assumed that for radii $800'' \leq R \leq 1200''$, the effects of projection are negligible). Clearly, as almost half of the central SGB stars are actually peripheral stars that have been projected along the line-of-sight, it is thus not strange that the innermost SGB stars have a larger magnitude dispersion than peripheral sample(s). Table 5.1 includes the details of projected contamination fraction that derived from our method.

A more intuitive 2D contour figure of the SGB stars' probability distribution, $P(\Delta Y, R)$, as a function of ΔY and radius, is present in Fig. 5.7. This figure strongly indicates that there are at least two SGB populations in 47 Tuc, where their relative fractions of which clearly display a gradual change in terms of their magnitude. One population may be mainly concentrated at radii between $R = 600''$ and $R = 900''$, while the other one peaks between $R = 400''$ and $R = 500''$. It is possible that there is a third peak that is associated with the innermost cluster regions, but the significant magnitude dispersion caused by 2D projected contamination and blending masks the significance of such a feature. It is also clear that the typical magnitude of the innermost and peripheral SGB stars are characterized by an offset of $\sim$0.2 mag.

5.3.2 Red-Giant Branch Stars

Another striking feature appears in 47 Tuc's RGB, which shows a trend between RGB color and radius. Bluer RGB stars are preferentially located in the cluster's outskirt while the innermost RGB stars are apparently redder. This trend is particularly apparent for stars located close to the bottom of the RGB. We defined a box that included most stars at the bottom of the RGB, covering the region of $14.3 \leq Y \leq 15.8$ mag and $0.7 \leq (Y - K_{\rm s}) \leq 1.2$ mag. We again confine all our analyzed sample stars have

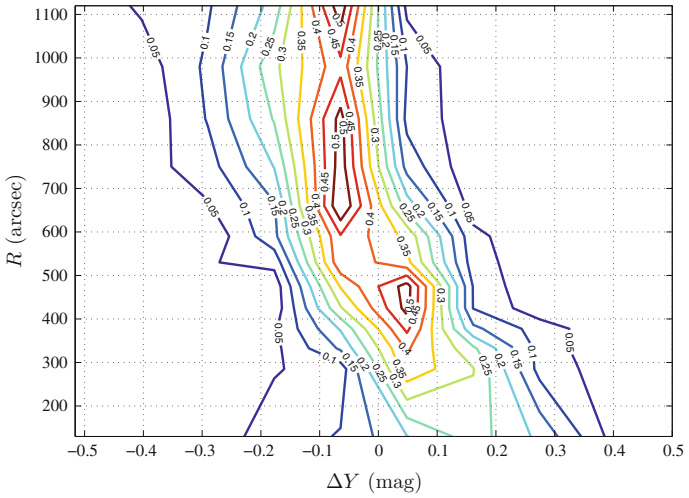

Fig. 5.7 2D contour figure of the SGB stars' probability distribution as a function of ΔY and radius, $P(\Delta Y, R)$

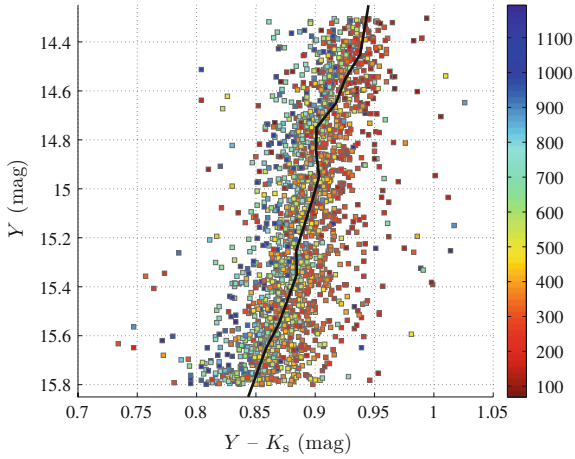

Fig. 5.8 CMD of the RGB region, showing only stars found within $3\sigma = 0.135$ mag of the isochrone's *ridge line*, where σ is the standard deviation of all RGB stars' color spread based on a Gaussian fitting function. The color scale again represents stars' distance to the cluster *center*. Stellar photometry is only robustly available for radii beyond $R \sim 70''$ owning to the high incompleteness of cluster core

their photometric errors smaller than 0.015 mag. Like what we have done for SGB stars, we adopted the cluster-wide ridge line and calculate the color deviation to this ridge line for the selected RGB stars, $\Delta(Y - K_s) = (Y - K_s)_{RGB} - (Y - K_s)_{iso}$. We again used a Gaussian function to fit the distribution of the color dispersion, characterized by a standard deviation of $\sigma_{\Delta(Y-K_s)} = 0.045$ mag. Finally we only consider 1850 RGB stars that are found within $3\sigma = 0.135$ mag of the ridge line. Figure 5.8 shows the zoomed-in CMD of the RGB region for 47 Tuc.

The next procedure is similar to what we have performed for SGB stars. We divided all RGB stars into five radial bins, with boundaries at $260''$, $370''$, $510''$, and

730″, the number of RGB stars in these bins span from 365 to 377. We subsequently calculated the $\Delta(Y - K_s)$ probability distributions, which is present in Fig. 5.9. Our result shows that the RGB gradually becomes bluer as a function of increasing radius, indicating that the peripheral RGB stars are systematically hotter than their innermost counterparts. Like SGB stars, the innermost RGB is quite dispersed compared with the RGB stars at larger radii. As we already explained, this is most likely due to contamination from projected RGB stars that are physically located at large(r) radii. The blending effect may also change the photometric colors of the RGB stars, but because the RGB is almost vertical, blending will most likely lead to a magnitude shift.

Figure 5.10 shows a comparison between the innermost RGB sample ($R \leq 260''$) and outermost RGB sample ($730'' \leq R \leq 1200''$) in their CMD. Similar to what we have observed in the SGB region, both RGB samples occupy apparently different loci in the CMD, with almost all peripheral RGB stars being bluer than the ridge line.

A 2D contour figure of the probability distribution of RGB stars, as a function of both $\Delta(Y - K_s)$ and radius, is present in Fig. 5.11. It is obvious that the average color and its corresponding dispersion gradually evolve from the cluster's outskirts to the central regions. The CMD of the RGB stars located at large radii is systematically narrower and bluer than that of their inner-sample counterparts. The probability distribution exhibits a continuous ridge from the cluster's outermost regions to $R \sim 500''$, followed by a peak between $R = 200''$ and $R = 400''$ and a increased color dispersion in the innermost regions. Such a large color dispersion cannot be solely caused by an intrinsic photometric dispersion, as we have already constrained the

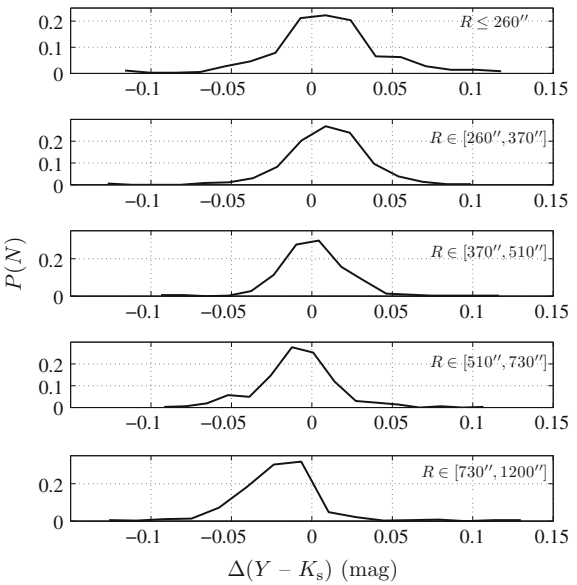

Fig. 5.9 Probability distribution of $\Delta(Y - K_s)$ as a function of radius for RGB stars. From *top* to *bottom*, the panels represent the corresponding distributions of $\Delta(Y - K_s)$ with increasing radial bins

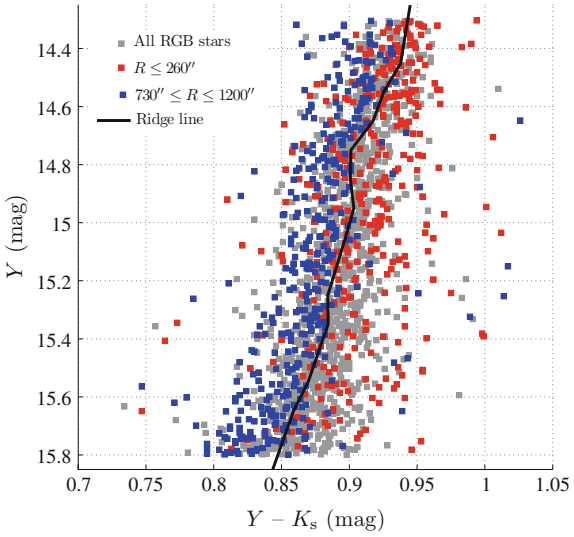

Fig. 5.10 A comparison between the CMD of the innermost RGB sample ($R \leq 260''$, *red solid squares*) with that drawn from the largest radii associated with the cluster ($730'' \leq R \leq 1200''$, *blue solid squares*). The *grey squares* represent the full RGB sample

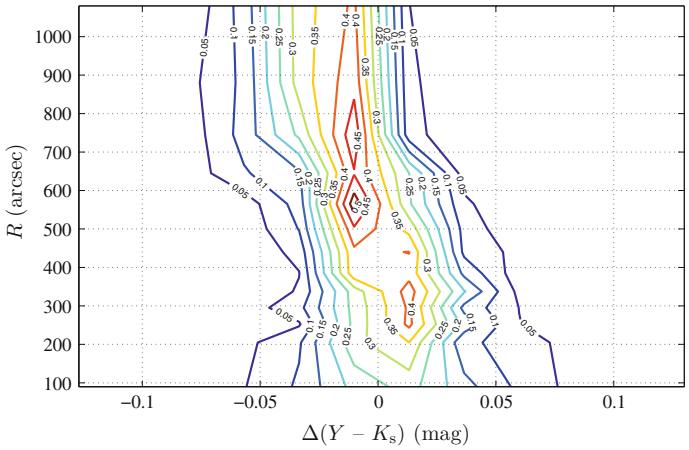

Fig. 5.11 As Fig. 5.7, but for RGB stars' probability distribution as a function of $\Delta(Y - K_s)$ and radius

photometric uncertainties of all sample stars to $\leq$0.015 mag. The observed spread of $\Delta(Y - K_s)$ is five times the allowed maximum photometric broadening. We again use the Monte Carlo method to calculate the contamination fraction due to projection at different radial ranges (see Table 5.1).

5.4 Physical Inplications

We first discuss if the differential reddening is the dominant cause of the observed trend for the SGB and RGB stars in 47 Tuc. We obtained the extinction map of the 47 Tuc area from the IRAS/DIRBE database based on the NASA/IPAC Infrared Science Archive [230–232]. Given that the native spatial resolution of the database is on the order of an arcminute, that means all details within the cluster region are smoothed. The radius of the cluster region that adopted in this work is about $20'$, while the radial bins that used for the analysis are smaller than $5'$, so we could still potentially resolve the dust substructures in the cluster. Also the spread on the lower RGB is larger than that higher up on the RGB, which cannot be explained by extinction effects. We measured the extinction distribution from the cluster innermost region to $R = 1200''$ in radial steps of $5'$. The extinction map reports that the average extinction in this region varies from $E(B - V) \simeq 0.027$ mag to 0.028 mag, clearly, this is negligible in the context of the observed broadening of both the SGB and RGB in the CMD of 47 Tuc. This is also supported by previous work [233].

In addition, it has been proved that RGB stars in 47 Tuc will not produce dust [235]. Also Bonatto et al. (2013) map the differential reddening in 66 GCs (including 47 Tuc), they conclude that the main source of differential reddening is interstellar rather than intracluster dust [236].

Milone et al. (2012a) attribute the double MS in 47 Tuc to helium and nitrogen enhancements, which indicates that the second stellar population formed from material that had been polluted by first population stars. This is also found in the GC NGC 6656 (M22), which was reported to contain N-rich but CO-depleted second-generation stars [237, 238]. Variations in C+N+O abundances may also cause a broadening of GC SGB features, as differences among CNO-group elements will change the relative strength of their compound absorption lines (e.g., OH, NH, CN and CH) [228]. Optical filters with central wavelengths between 3500 Å and 4500 Å are sensitive to these absorption lines [95]. Therefore the CNO variations may introduce an additional broadening of CMD features in optical range. However, our datasets were based on NIR Y and K_s bands observations, which are characterized by effective wavelengths peak at 1.02 and 2.15 μm, respectively. It is thus impossible to resolve CNO differences in SGB and RGB features in the 47 Tuc (Y, $Y - K_s$) CMD.

The ejecta of first population stars will contaminate the second generation stars, thus producing α enhancement. However, previous analyses have excluded any significant [α/Fe] dispersion in 47 Tuc [83]. We nevertheless explored the impacts of [α/Fe] variations. Based on PGPUC model, we adopted isochrones characterized by [α/Fe] = 0.0 − 0.3 dex for comparison, the result shows that there is no significantly change between the isochrone's morphology in either SGB or RGB phases. Because the effects of [α/Fe] differences is negligible, we thus adopt a fixed [α/Fe] = 0.30 dex.

As already suggested by Milone et al. (2012a) [95], the most straightforward explanation of the observed radial trends in the magnitude of SGB stars and colors of RGB stars in 47 Tuc, is the presence of MSPs. Indeed, they found the apparent

triple MSs in 47 Tuc can be explained by a significant helium dispersion, Y = 0.256 − 0.288, which is consistent with that of Nataf et al. (2011) [212]. Note that these authors did not base their conclusions on the cluster's SGB and RGB stars, which is explored in this work.

Another parameter that may affect the morphologies of SGB and RGB is the stellar metallicity. Lots of studies have explored this issue, going back to Brown and Wallerstein (1992), who studied four giant-branch stars in 47 Tuc, found the minimum and maximum [Fe/H] abundance of −0.88 and −0.69 dex, respectively, or Z ranging from ∼0.0020 to 0.0031 [239]. Subsequent spectroscopic observations of three 47 Tuc RGB stars report a mean [Fe/H] abundance of -0.70 ± 0.03 ($Z = 0.0028 - 0.0033$) [240]. Given that these studies only based on small numbers of stars, which cannot used to infer statistically robust results. More recent observations based on analysis of three dwarfs and nine subgiant stars confirmed an [Fe/H] range from −0.59 dex to −0.78 dex ($Z = 0.0026 - 0.0041$) [84]. Another study of eight RGB and one MSTO stars shows the most representative metallicity, [Fe/H] $= -0.76 \pm$ 0.05 dex, which is equivalent to a Z range from 0.0024 to 0.0030 [241].

The metallicity as well as its dispersion derived from photometric measurements is usually higher than that from spectroscopic studies. Salaris et al. (2007) used the BaSTI models to analyze their photometric observations of 47 Tuc, yielding a metallicity of $Z = 0.004 \pm 0.001$ [233]. Nataf et al. (2011) explored the 47 Tuc RGB bump stars and claimed that a model with [M/H] = −0.50 or −0.52 dex is the best fitting model (corresponding to [Fe/H] = −0.53 or −0.55 dex for [M/H] = 0.95 [Fe/H]) [212]. Anderson et al. (2009) investigated the spread among the SGB stars, they conclude that a metallicity dispersion of 0.10 dex is required if metallicity is the only driver of the observed spread. The differences between the metallicity derived from photometric studies and spectroscopic analyses may be owning to an inherent selection bias that predominantly affects spectroscopic observations, as the samples that used for spectroscopic analyses are usually located far from the cluster center to avoid the effect of crowding. For instance, Carretta et al. (2004) selected all their sample stars at distances greater than 800″ from the 47 Tuc center [83]. In this work, we adopt $Z = 0.0041$ from Carretta et al. (2004) as the typical 47 Tuc metallicity [83], but we assume that the metallicity dispersion is represented by that derived from the photometric analyses, $\Delta_{\rm [Fe/H]} \sim 0.10$ dex (corresponding to $Z = 0.0033 - 0.0051$).

Using a Monte Carlo method, we mimic the distribution in CMD of the observed SGB and RGB stars based on two suitable 'bracketing' isochrones. We follow the a reasonable assumption that the helium-rich stellar population should also be metallicity enriched. The adopted metallicity dispersion is based on the literature for our model isochrones, i.e., $Z = 0.0033 - 0.0051$ and Y = 0.25 − 0.28. The helium and metallicity abundances should be varies only between these two values. We also considered the presence of an age dispersion among the cluster's member stars. At the typical age of 47 Tuc, a very small fraction of age dispersion represents a long time span, which may be enough for the most massive first population stars to evolve to late evolutionary stages. Previous studies have suggested a possible age spread among 47 Tuc member stars of order 1 Gyr (∼12–13 Gyr [228]). Gratton et al.

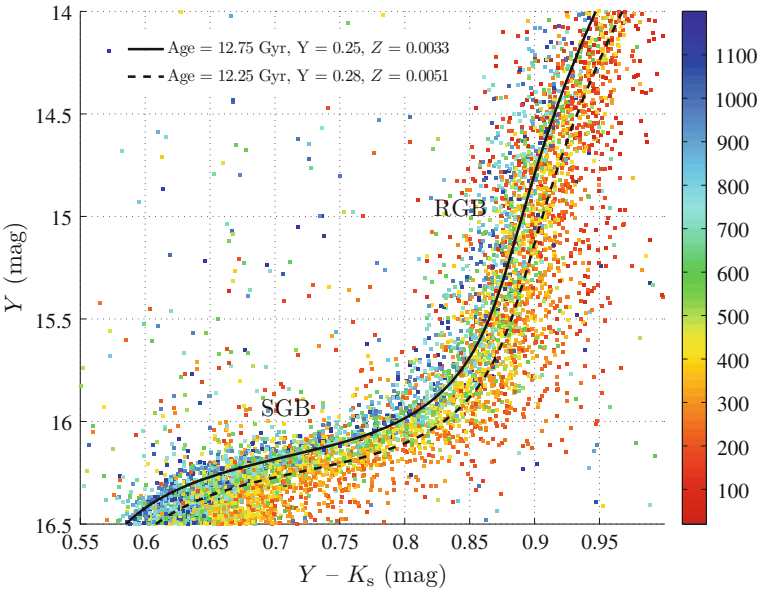

Fig. 5.12 Isochrone fits of a first stellar population (*black solid line*), described by a old age, normal helium and metal abundances, as well as a second stellar population, described by a young age, enriched helium and metal abundances (*black dashed line*). The color bar indicates the stars' distance to cluster center (in arcsec)

(2003) have determined a model-dependent age for 47 Tuc of either 11.2 ± 1.1 Gyr or 10.8 ± 1.1 Gyr [242]. Zoccali et al.(2001) determined an age of 13 ± 2.5 Gyr for 47 Tuc [227]. Recent papers have reported smaller age spreads, with a typical age span of 12.8 ± 0.6 Gyr [243], 12.75 ± 0.5 Gyr [244] and 11.75 ± 0.25 Gyr [245]. We therefore conservatively adopt a minimum age spread of 0.25 Gyr to our model, e.g., 12.50 ± 0.25 Gyr. We then generate an artificial 47 Tuc CMD defined by Y$= 0.25 - 0.28$, $Z = 0.0033 - 0.0051$, and an age range of 12.25–12.75 Gyr. We present the corresponding range in best-fitting isochrones in Fig. 5.12.

We found if we only mimic stars with photometric errors of up to 0.015 mag, we will failed to reproduce the observations. This again confirms that the observed SGB and RGB broadening is not solely owning to photometric errors but caused by a dispersion in stellar populations. Note that $1\sigma_{\Delta Y}$ and $1\sigma_{\Delta(Y-K_s)}$ dispersions of the SGB and RGB stars are 0.18 and 0.045 mag, which are dramatically larger than the dispersions derived from typical photometric uncertainties. The observed dramatic dispersion should be caused by the combination of photometric uncertainties and a dispersion in stellar-generation properties (age, helium abundance, and metallicity). In order to avoid complications associated with adopting a full age range, we assume that the bulk of the cluster stars are adequately resembled by two distinct populations of stars (but see below), but we relax their dispersions to cover $0.5\sigma_{\Delta Y} = 0.090$ mag and $0.5\sigma_{\Delta(Y-K_s)} = 0.022$ mag for the simulated SGB and RGB stars, respectively,

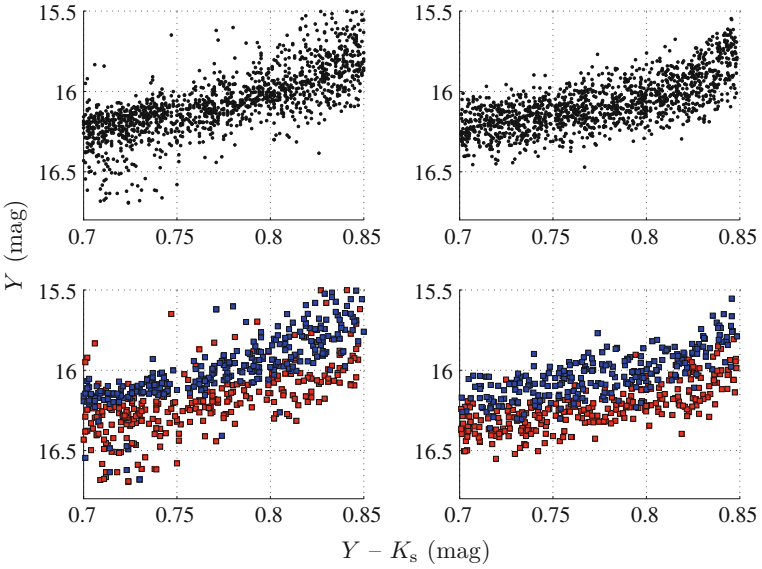

Fig. 5.13 *Top left* Observed CMD of overall SGB stars. *Top right* Simulated CMD of SGB stars. *Bottom left* CMDs of observed innermost SGB stars ($R \leq 340''$: *blue squares*) and outermost SGB stars ($R \in [730'', 1200'']$: *red squares*). *Bottom right* CMDs of simulated innermost SGB and outermost SGB stars

which still reproduces two apparent branches in the CMD. Figures 5.13 and 5.14 show the simulated CMDs for the SGB and RGB stars (right-hand panels) and observations (left-hand panels), respectively. The top two panels represent the overall comparison, while the bottom two panels only display the observed inner- and outermost samples, as well as their corresponding simulated counterparts. The simulated SGB and RGB samples have the same number of stars as the observations. We have adopted a flat magnitude distribution, as the magnitude range of the SGB stars is very narrow, and for the RGB stars we only concerned with their color distribution, thus any difference in their LF will not affect our analysis. We also confirmed that the observed LF of observed RGB stars is close to flat.

Instead of visual inspection, we quantify the similarity between the observations and simulations using χ^2 minimization. At a given radius, we assume that the simulated CMD is composed by a certain fraction of first-generation stars, $f_{\rm fg}$. The remainder of the stellar population at this radius then follows the second-generation isochrone, characterized by a fraction $f_{\rm sg} = 1 - f_{\rm fg}$. We then use the adopted ridge line (see Figs. 5.4 and 5.8) to calculate the probability distributions of ΔY and of $\Delta(Y - K_{\rm s})$ for the simulated SGB and RGB stars, respectively. As a function of radius, we then calculate the χ^2 value through the formula below,

$$\chi^2 = \sum_n \frac{(N' - N)^2}{N}, \tag{5.2}$$

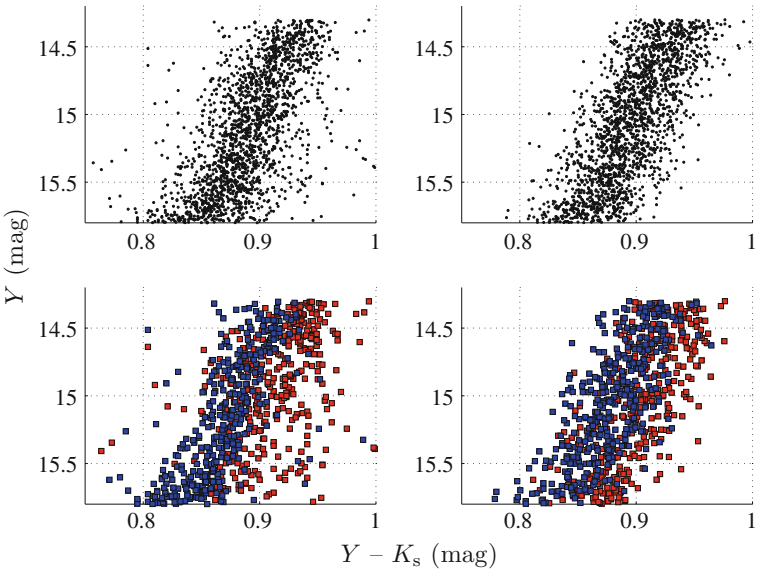

Fig. 5.14 As Fig. 5.13, but for RGB stars

Here N' and N indicates the simulated and observed number of stars in different ΔY or $\Delta(Y - K_s)$ bins (for SGB and RGB stars, respectively), and n is the number of bins. The χ^2 value represents the level of similarity between the simulated and observed CMDs. We adopt the f_{fg} range from 5 to 95% and find out the minimum χ^2 value. Using a parabolic function to describe the resulted $\chi^2(f_{fg})$ distribution, we thus determine the corresponding minimum χ^2 value and its 1σ uncertainty, which corresponds to the difference between χ^2_{min} and $\chi^2_{min} + 1$ (see Sect. 3.4). This procedure has been repeated 100 times for each radius to smooth the χ^2 curve as a function of f_{fg}.

Figures 5.15 and 5.16 show the calculated χ^2 distributions for different input fractions of f_{fg} at different radius, the best-fitting parabolic curves for the SGB and RGB samples are attached as well. From top to bottom, the panels show the results for the innermost to outermost samples; the arrows indicate the placement of the best-fitting best-fitting f_{fg} fractions. For both the SGB and RGB stars, the best-fitting f_{fg} fractions for the outmost samples are beyond 100%, based on the indication of χ^2 distributions, which indicates that at those radii, the composition of 47 Tuc is close to expected for a SSP. It is also apparent that for both the SGB and RGB samples, the first-generation stars only occupy a minor fraction in the inner region, but this fraction increases significantly toward the cluster's outskirts, reaching 100% at the adopted outer boundary, $R = 1200''$.

In Fig. 5.17 we show the radial profile of best-fitting f_{fg} fraction, for both the SGB stars (blue squares with black solid line) and RGB stars (red squares with black dashed line). The error bars are the 1σ statistical uncertainties, which are all

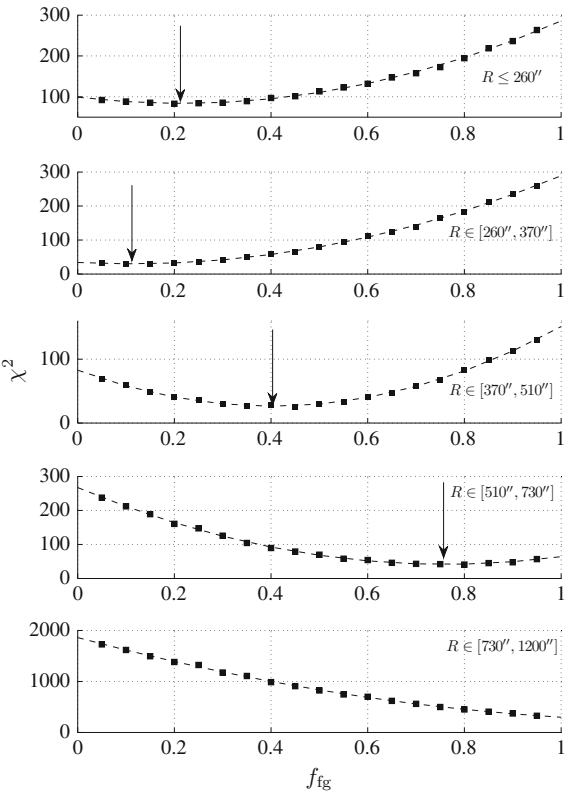

Fig. 5.15 χ^2 as a function of $f_{\rm fg}$ for the SGB stars. From *top* to *bottom*, panels represent the results from the innermost to outermost regions of the cluster. The *black dashed curve* represents the best-fitting parabolic function; arrows indicate the placements of $f_{\rm fg}$ which correspond to the minimum χ^2 value. The *bottom* panel has a best fitting $f_{\rm fg}$ of 100%

smaller than 5.5%. The innermost sample is only composed of a minor fraction of first-generation stars, while it appears that the outermost region is fully described by a SSP. In addition, both the SGB and RGB stars exhibit consistent trends in $f_{\rm fg}$ from $R \sim 400''$ to $R \sim 600''$, which strongly implies that they form intrinsically uniform samples. However, compared with the SGB stars, the RGB stars in the innermost region show a relatively large $f_{\rm fg}$ fraction, which may be owning to the large projected contamination and small completeness in the central region. We summarize all these statements quantitatively in Table 5.2.

In summary, the distribution of observed SGB and RGB stars in GC 47 Tuc CMD can be well explained if the cluster's SGB and RGB stars in the outer regions are normal in helium abundance and metallicity, while their more centrally located counterparts are helium and metallicity enriched.

Our results confirm the presence of second stellar population in 47 Tuc. Milone et al. (2012a) calculated the number fraction of red RGB stars (the "RGBb" component in their work), which increases from the cluster's periphery (RGBb/RGB $\sim$ 60%) to central region (RGBb/RGB $\sim$ 80%), but their analysis shows that the average RGB color and dispersion remain constant [95]. A similar result also shows that the

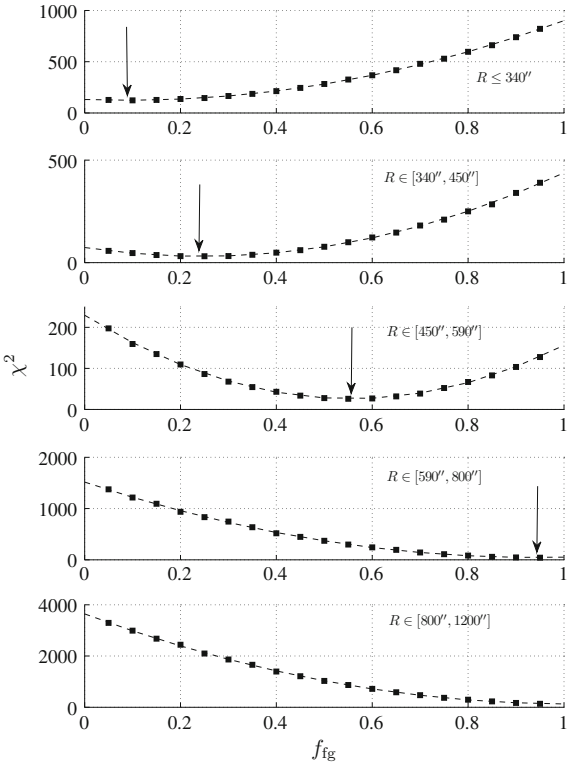

Fig. 5.16 As Fig. 5.16, but for the sample of RGB stars

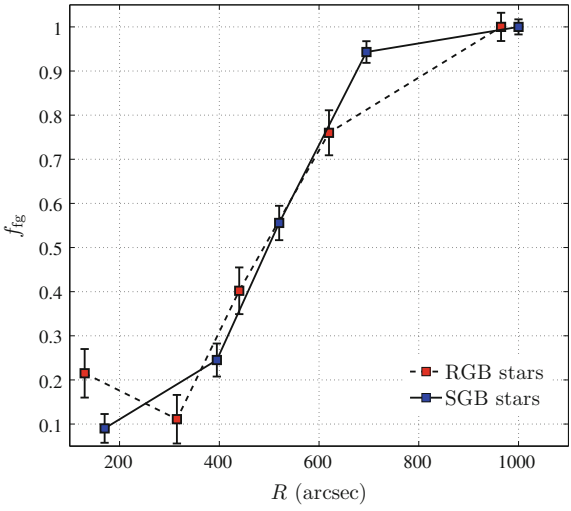

Fig. 5.17 The radial profile of best-fitting $f_{\rm fg}$ fraction for SGB stars (*blue squares* associated with *solid line*) and RGB stars (*red squares* associated with *dashed line*)

Table 5.2 Best-fitting $f_{\rm fg}$ fractions as a function of radius

SGB stars	$f_{\rm fg}$ (%)	RGB stars	$f_{\rm fg}$ (%)
$R \leq 340''$	9.02	$R \leq 260''$	21.50
$R \in [340'', 450'']$	24.50	$R \in [260'', 370'']$	11.10
$R \in [450'', 590'']$	55.57	$R \in [370'', 510'']$	40.20
$R \in [590'', 800'']$	94.31	$R \in [510'', 730'']$	76.00
$R \in [800'', 1200'']$	100	$R \in [730'', 1200'']$	100

fraction of RGBb stars increases from ∼40 to ∼90% from the cluster's outskirts to its central regions [213]. Based on the NIR CMD of 47 Tuc, our analysis yields a fraction of 5–10% in the outermost region to ∼90% in the cluster central region. This is even more significant trend as that reported by these previous works. Our result is also consistent with the predictions derived from N-body simulations [217].

This scenario is supported by the observed spatial distributions of the SGB and RGB stars. The second stellar population stars would preferentially form within the denser core region of a cluster, and their clearly difference in radial distributions suggest that the second stellar population stars may originally have been dominated (in terms of stellar numbers) by first-generation stars, but that these first population stars subsequently somehow evaporated from the cluster. This may be caused by expansion of the cluster triggered by either Type II supernovae [215, 216] or tidal stripping [95], which finally led to a stellar system with second stellar population stars dominated the cluster central regions.

Our analysis is the first investigation of the radial behavior of the MSPs of SGB stars in 47 Tuc, which suggests a helium abundance dispersion of $\Delta Y = 0.03$ (also see [210]). This helium enhancement may be most significant near $R \sim 500''$, as indicated by Fig. 5.7, where two clear peaks appear on either side of this radius. Our simulation results confirms this result as well: for both SGB and RGB stars, the $f_{\rm fg}$ fractions increase significantly from $R \sim 400''$ to $R \sim 600''$, well covering the positions of these two peaks. This strongly indicates that pollution by a second population stars becomes significant at these radii. The discovery of a helium-rich stellar population with higher centrally concentration is also consistent with previous analysis [30, 212, 246]. The derived enriched metallicity may indicate an origin related to the ejecta of massive stars [32, 115, 116, 213].

5.5 Conclusion

Based on the analysis of a deep, wide-area, NIR CMD of 47 Tuc obtained with the VISTA telescope. Apparent difference are found between SGB and RGB stars in cluster's outermost regions compared with its innermost regions. The peripheral

SGB stars are significantly brighter than the SGB stars in the cluster region. RGB stars in the cluster's outskirts are bluer than the corresponding innermost samples.

Following the adoption of isochrone defined by the cluster's overall physical properties as benchmark, we carefully explored the magnitude spread of the SGB stars as a function of radius. The resulting 2D probability distribution shows two apparent peaks between $R = 600''$ and $R = 900''$, and between $R = 400''$ and $R = 500''$. Similar approach have been also performed in analysis of the cluster's RGB stars, the corresponding probability distribution shows a continuous ridge from the cluster's outer edge to $R \sim 500''$, followed by a peak located between $R = 200''$ and $R = 400''$. Both SGB stars and RGB stars show clear difference in magnitude and color between the samples of large radius and small radius.

We adopted a Monte Carlo method to quantify the contamination of line-of-sight projection as a function of radius, we find that the innermost radial ranges are seriously contaminated by projected peripheral stars. This explains the larger dispersions of magnitude and color of innermost SGB and RGB stars, compared with their corresponding samples at larger radii. If we could properly reconstruct the 3D distribution of the observed stars, we expect that the inner stellar sample would most likely be more clearly different from the outer sample.

Using different models to fit the observations, with considerations of dispersions in helium abundance, [α/Fe], metallicity, and age. The most convincing explanation is that the observed SGB and RGB stars are characterized by variations in helium and metal abundance, with the outermost sample stars being both more helium-poor (Y $= 0.25$) and metal-poor ($Z = 0.0033$), while the more centrally concentrated stellar sample is helium-rich (Y $= 0.28$) and metal-rich ($Z = 0.0051$). The effect of [α/Fe] variations are not important in our NIR CMD. The helium-rich, metal-rich sample is consistent with a younger isochrone, with age of 12.25 Gyr, while the helium-poor, metal-poor sample follows a 12.75 Gyr isochrone, which indicates an possible age dispersion of $\sim$0.5 Gyr to match the morphologies of both the SGB and RGB stars. In this work, the helium abundance and metallicity dispersion invoked to explain the broadening of the CMD features would have originated from pollution by first population stars. We produce a series of simulated CMDs covering both the SGB and RGB stars, and use a minimal χ^2 test to quantify the best-fitting fraction of first stellar population. The result shows a apparent increasing trend from the cluster innermost region to its outskirts. This implies that only a very small fraction of first population stars is contained in the cluster central region, while the stellar population in the cluster outermost regions is close to a SSP. The χ^2-minimization results also show a good agreement between both the SGB and RGB stars in their radial profile of first population stars, indicating that the SGB and RGB stars are both belong to the same stellar population composition.

Based on the analysis presented in this article, we can see that 47 Tuc is indeed composed of more than one stellar population. The most straightforward interpretation of the origin of a second stellar population is that it formed by the remnant of the first population stars with enhanced helium abundance and metallicity, this strongly indicates that the material in 47 Tuc have already polluted by supernovae explosions, and, possibly, 47 Tuc was succeed to retain the material ejected by those explosions.

However, if this speculation is on the right track, that means 47 Tuc should much more massive at its early stage of multi-supernovae explosions, its may lost most of its materials after this epoch. Unfortunately, based on this scenario, the timescale of contamination caused by first population massive stars is extremely short ($\leq$10 Myr, see Sect. 2.1.1), such a small timescale cannot show any detectable feature in the CMD of 47 Tuc, because 47 Tuc is too old. This means people should try to find indirect hints from the "relatively young globulars", which we will introduce in the following Chapters.

Chapter 6
Do Intermediate-Age Star Clusters Have Extended Star Formation Histories?

6.1 Introduction

As introduced in Sect. 2.1.1, the star formation mode in a SC is thought as a particular starburst event, with a maximum age spread of only 1–3 Myr [247]. However, recently the discovery of the eMSTO regions in intermediate-age, 1–2 Gyr SCs (see Sect. 2.1.2) in the LMC and SMC has strongly challenged our thought of the validity of the SSP scenario for SCs [64–66, 99, 248, 249], as the areas of the TO regions in their CMDs are significantly larger than that would be expected for SSPs. The most straightforward explanation of these eMSTOs in intermediate-age SCs is their initial star forming processes have lost longer than several hundreds Myr [66], which has led to heavily debates as to whether SCs can harbor extended SFHs.

As we already see, most YMCs cannot retain their initial runaway gas at their early stage, indicating star clusters cannot continually build their mass at this stage. Lots of scenarios have been proposed to explain the possible eSFHs in these clusters, including those involving the presence of chemical inhomogeneities, internal age dispersions, rapid stellar rotation and possible select effects (see [250] for a discussion). Among these scenarios, there are two most popular, but mutually competing scenarios, they are the internal age dispersions model and stellar fast rotation model. Some authors have suggested that the initial dynamical interactions between two star clusters, or star clusters and star-forming GMCs may be able to explain the age dispersions in these clusters [64, 101]. But these scenarios cannot explain why such dynamical processes might have acted in a global manner and affected many intermediate-age LMC clusters. D'Ercole et al. (2008) and Goudfrooij et al. (2009) proposed that the ejecta of first-generation AGB stars might be the polluters [216, 251]. In addition, Goudfrooij et al. (2014) proposed a scenario that invokes two distinct rounds of SFH in massive clusters to explain the observed wide TO regions [99], in their model, the first star-formation episode is a star burst mode, subsequently there is a 10–100 Myr period with no star formation. In turn, this quiescent period is then followed by a second star-formation episode, which lasts a few hundred million yeas, this star-formation episode is responsible for the observed eM-

C. Li, *Not-So-Simple Stellar Populations in Star Clusters*, Springer Theses,
DOI 10.1007/978-981-10-5681-9_6

STO in intermediate-age SCs. The evidence that they claim to support this scenario is the width of the eMSTO of intermediate-age SCs seems to correlate their central escape velocity, v_{sec}. However, critiques of many aspects of this scenario have been presented [70, 73, 109, 252], as YMCs do not show any evidence of significant age spreads of several hundred million years [20, 98, 100, 109].

As already introduced in Sect. 2.2.1, the stellar fast rotation has been determined as a parameter that may affect the area of the MSTO region at the same time. This is caused by the reduction in self-gravity owning to the effect of centrifugal force, which leads to a reduction in the stellar luminosity and surface temperature (the gravity darkening effect [106, 225]). But this channel has been argued, because the effect of a prolonged stellar MS lifetime caused by rotational mixing would mask the broadening of MSTO regions produced by the gravity darkening [107, 253], conspire to retain a narrow TO region for a SSP. However, this conclusion has been criticized that it is only based on very high mixing efficiency, if one adopt reasonable significance for the effects of this prolonged stellar lifetime, rapid stellar rotation could still be able to explain the eMSTO regions [108, 109, 254]. The stellar rotation scenario was further supported by a more recent discovery from YMC NGC1755 in the LMC, which shows a split MSs that could be ideally explained by stellar rotation, and not by adopting an age spread [113].

In order to distinguish between the age spread scenario and the stellar fast rotation scenario, a promising method is to study the SGB in these SCs who already show apparent eMSTO regions. Because sub-giant phase happens immediately after the star departs the MS, it should smoothly joint to the eMSTO region. If the eMSTO region is caused by an internal age difference, then the SGB should also show apparent broadening in its morphology, because stars in this phase have still not experienced significant mass loss. On the other hand, if the eMSTO is caused by stellar fast rotation, because SGB stars will quickly slow down owning to the conservation of angular momentum, the morphology of the SGB will thus deviate to the prediction of age spread scenario. In this Chapter, I present our latest research on the SGBs in three intermediate-age SCs, NGC1651, NGC411 and NGC419, we found although both these three SCs show apparent eMSTO regions, the morphology of their SGB are inconsistent with the age range derived from their eMSTO, suggesting that an eMSTO region may not necessarily imply a significant internal age spread.

6.2 Data Reduction

The datasets of NGC1651 and NGC411 were obtained from archival *HST*/WFC3 observations, while the datasets of NGC419 were based on the archival images of *HST* ACS/WFC. For NGC1651 and NGC411, their datasets are both composed of a combination of science images in the F475W and F814W filters, roughly correspond to the Johnson-Cousin B and I bands, respectively. The NGC419 datasets are in the F555W and F814W filters, corresponding to Johnson-Cousin V and I bands. The total exposure times for NGC1651 are 1440 s and 1430 s in B and I bands,

respectively; for NGC411, the total exposure times in these two bands are 1520 s and 1980 s; while for NGC419, it is 1984 s and 1896 s in V and I bands in total. We used two independent software packages, *DAOPHOT* [255] and *DOLPHOT* [256, 257], to perform photometry on the scientific images.

Similar to what we did in Sect. 3.2, we divided the stellar spatial distribution into serval tens bins along both the right ascension (α_{J2000}) and declination (δ_{J2000}) axes. We subsequently use a Gaussion function to find out the position where the stellar density reach its maximum value, thus the closest coincidence of both Gaussion peaks represent the cluster center. For NGC1651, we determined its center coordinate as $\alpha_{J2000} = 04^h37^m32.16^s$ and $\delta_{J2000} = -70°35'08.88''$; For NGC411, the results are: $\alpha_{J2000} = 01^h07^m56.22^s$ and $\delta_{J2000} = -71°46'04.40''$; For NGC419, they are: $\alpha_{J2000} = 01^h08^m17.02^s$ and $\delta_{J2000} = -72°53'03.12''$. After determined the coordinates of clusters' centers, we then check all these clusters' stellar number density radial profiles, again, similar to the approaches that are illustrated by Figs. 3.5 and 4.3, we select 75 arcsec, 50 arcsec and 75 arcsec as the typical cluster regions for NGC1651, NGC411 and NGC419, respectively.

The method that used to reduce the field contamination is identical to those introduced in Sects. 3.2, 4.2 and 5.2. Because this time the focused features are SGBs in three relatively young SCs, we have confirm that compare with the CMDs of their nearby region field stars, the background contamination level is negligible because the SGB regions are very bright. In addition, a well-populated SGB cannot be explained by field stars with different ages and metallicities. For NGC1651 and NGC411, the reference of field regions are directly selected from the images which contain the bulk of cluster stars, as at the distance of LMC and SMC, our scientific images are large enough to contain both the cluster regions and field regions. For NGC1651, stars that are further than 85 arcsec to cluster center have been determined as field stars, while for NGC411, we directly select a square with Y coordinate smaller than 800 pixels in the CCD as the field region. For NGC419, we have another images that at some 230 arcsec from the cluster center, observed as part of the same *HST* program with the same instrumental setup. We thus select the whole area of separated image to represent the reference field.

6.3 Main Results

6.3.1 NGC1651

The CMD of NGC1651 is present in Fig. 6.1, to take a simplistic approach, we obtain best fits to the blue and red boundaries of the eMSTO by matching the best set of stellar isochrones [89]. The ages of these two isochrones correspond to the blue and red edge are $\log(t/\mathrm{yr}) = 9.24$ (1.73 Gyr) and 9.34 (2.18 Gyr), respectively.

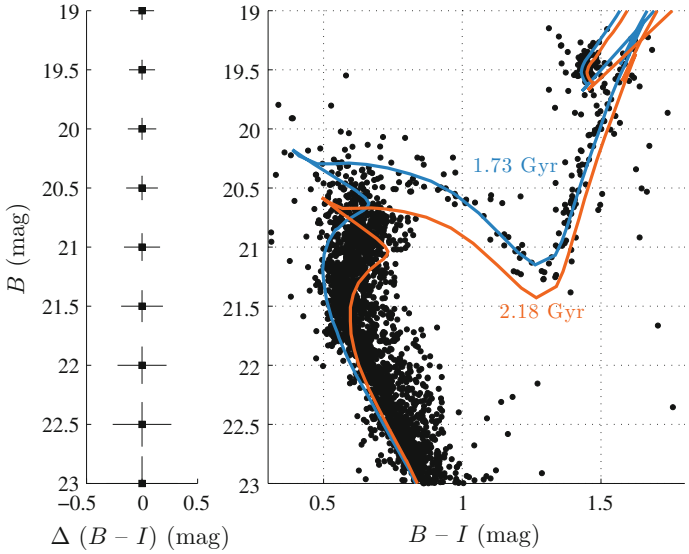

Fig. 6.1 The CMD of NGC1651 as well as the best fitting isochrones correspond to the *blue* (*light blue line*, 1.73 Gyr) and *red* edge (*orange line*, 2.18 Gyr) of its eMSTO, the *left* panel shows typical 3σ photometric uncertainties

Both these two isochrones have the metallicity of [Fe/H]$= -0.52$ dex ($Z = 0.006$[1]), extinction of $E(B-V) = 0.11$ mag and distance modulus of $(m-M)_0 = 18.46$ mag [258, 259]. From Fig. 6.1, one can see although the eMSTO region is well described by adoption an age dispersion of approximately 450 Myr, the SGB stars of NGC1651 are predominantly confined to the $\log(t/\mathrm{yr}) = 9.24$ isochrone. If we only focus the SGB stars located in the core region (20 arcsec[2]), they are even confined to an narrower distribution associated with the youngest isochrone, despite their TO counterparts strongly indicate a dramatic age spread.

To evaluate the association of SGB stars with either the youngest or the oldest isochrone, we adopt the $\log(t/\mathrm{yr}) = 9.24$ isochrone as the baseline and calculate the magnitude deviations, ΔB, to this isochrone for all selected SGB stars. Then we set the $\log(t/\mathrm{yr}) = 9.34$ isochrone as fiducial locus, to estimate the typical region for SGB stars with this age, assuming a typical 3σ magnitude dispersion of $\Delta B \approx 0.12$ mag. Based on this simple analysis, we found 30 of 38 stars are actually associated with the youngest isochrone, only one exception is located outside this region and associated with the region defined by the oldest isochrone. This result is more apparent for the core sample, there are 14 of 15 stars are located in the ΔB region defined by the youngest isochrone, none of them have been found to have a ΔB that is consistent with the prediction of the oldest isochrone. If we directly use

[1] The Marigo et al.(2009) stellar evolutionary model have set the solar metallicity as $Z = 0.019$ [89].

[2] We use a EFF function to fit the brightness profile of NGC1651, finding that its core size will have a radius of 17.11 arcsec (4.45 pc) [260].

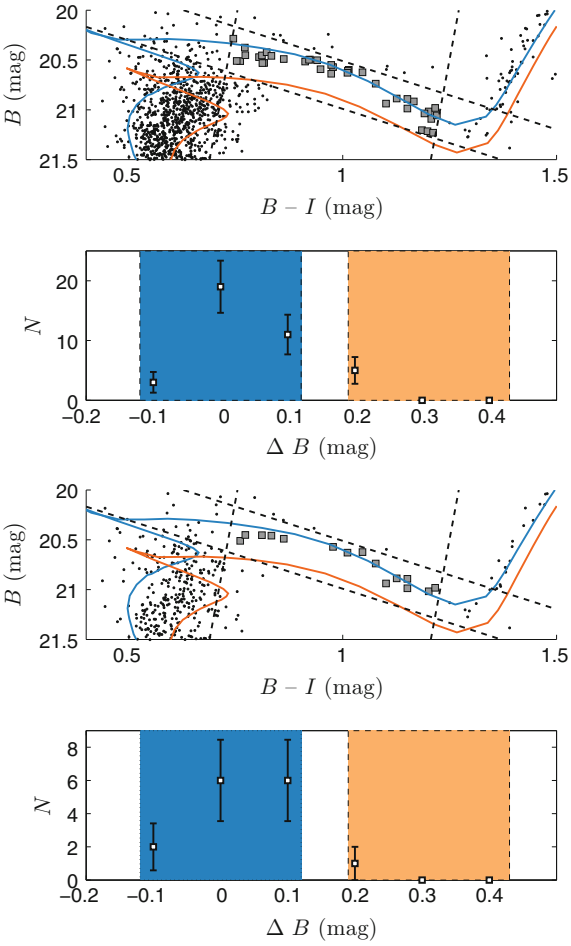

Fig. 6.2 The *top* two panels, CMD covering the eMSTO and SGB regions (indicated by *black dashed lines*. *Grey squares* represent SGB stars); Number distribution of SGB stars as a function of the deviation in magnitude, ΔB, with the adoption that the youngest isochrone is the zero deviation ridge line. If SGB stars have an age spread from 1.73 to 2.18 Gyr, it should disperse from the *light blue* background to the *orange* background. *Bottom* two panels, the same as the *top* two panels, but for the samples located at radii of ≤20 arcsec

the magnitude dispersion of these stars in the CMD to estimate a maximum likely age spread, Δt, then all these SGB stars should have an age spread of $\Delta t \leq 160$ Myr, for the core sample, this age spread can be further constraint to $\Delta t \leq 160$ Myr. In Fig. 6.2, we present the comparison of the observed stellar distribution with the expectation of a 450 Myr internal age spread in NGC1651 for the whole sample of 38 SGB stars as well as 15 SGB stars in the core region.

If the cluster's stellar population were characterized by an age dispersion of 450 Myr, this dramatic age spread should produce a broadened SGB. In order to compare the difference of age dispersion between TO stars and SGB stars, we quantitatively assess the probability of the presence of a genuine internal age dispersion for these two stellar samples. We calculate the number density distribution of the bulk stars located in eMSTO and SGB regions (correspond to blue squares and orange circles, which are indicated by solid and dashed boxes in Fig. 6.3), adopting isochrones with

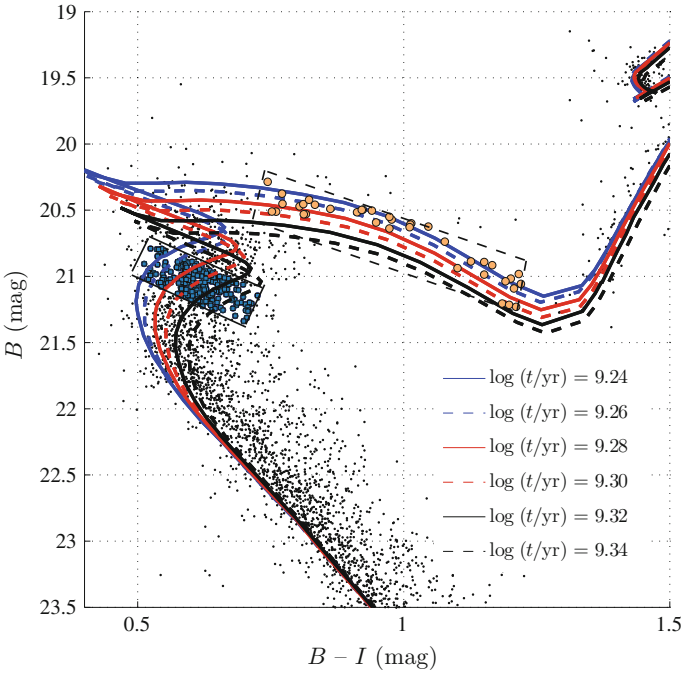

Fig. 6.3 Comparison of the number of stars of NGC1651 at selected evolutionary stages, the *blue squares* represent typical TO stars used as basis of the comparison, the *orange circles* are the selected SGB stars. Isochrones of different ages are attached

different ages. The resulting distribution of eMSTO and SGB stars are significant different, as shown in Fig. 6.4. Whereas the eMSTO stars exhibit a spread from $\log(t/\mathrm{yr}) = 9.24$ to $\log(t/\mathrm{yr}) = 9.34$, the SGB stars are systematically younger than these distributions, with most of them are associated with the youngest isochrone, this indicates the lack of a genuine age dispersion in NGC1651.

6.3.2 NGC411

Compare with NGC1651, the number of SGB stars in NGC411 is smaller, but it also shows a tight, well-populated SGB with even higher significance than NGC1651. Figure 6.5 shows the CMD of NGC411 and its apparent eMSTO region with magnitude range of $20 \leq B \leq 22$ mag, where the average 1σ magnitude uncertainties are 0.04 mag in both bands, which cannot explain the large area of the MSTO region. In addition, NGC411 also exhibit a well-populated RC, which can be further used to constrain its internal age spread. Based on the Padova stellar evolutionary model [24], we adopted a series of isochrones with ages span from 1.38 Gyr ($\log(t/\mathrm{yr}) = 9.14$)

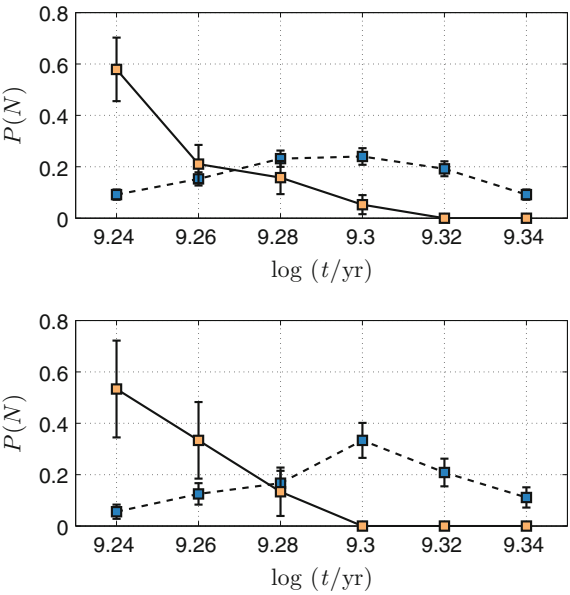

Fig. 6.4 The derived age distribution from the cluster's TO and SGB stars. *Top* panel, Number density distribution, $P(N)$ as a function of age. *Blue squares*, associated with *dashed line*, represents the age distribution of TO stars, *orange squares* and *solid line* represents that for SGB stars. *Bottom* panel, As the *top* panel, but for the sample within cluster core region

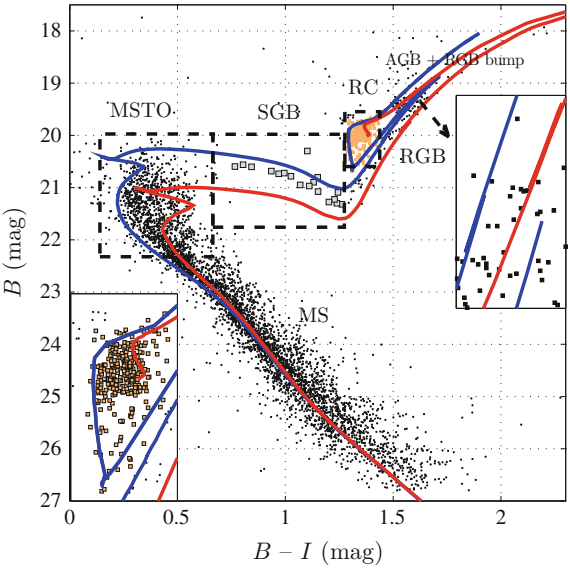

Fig. 6.5 A full view of the CMD of NGC411, showing isochrones for ages of 1.38 Gyr ($\log(t/\mathrm{yr}) = 9.14$, *blue solid line*) and 2.18 Gyr ($\log(t/\mathrm{yr}) = 9.34$, *red solid line*). *Grey* and *orange squares* are the SGB stars and RC stars. The *bottom left* sub-panel is the zoomed-in region focusing on the RC stars

to 2.18 Gyr ($\log(t/\mathrm{yr}) = 9.34$) to describe its entire eMSTO region. That means the eMSTO region may require at least ~800 Myr to explain this broadening if these TO stars are composed by multi-aged stellar populations. Previous studies also suggest a significant age spread from ~700 Myr to 1 Gyr for this cluster [67, 99]. Again, although we need isochrones with different age to describe the eMSTO region, all other parameters pertaining to these isochrones are the same, including a metallicity of $Z = 0.002$, extinction of $E(B-V) = 0.08$ mag and a distance modulus of $(m-M)_0 = 19.05$ mag. One will immediately find a extremely tight SGB, which can only be explained by a single isochrone, in contrast with its apparent eMSTO region, where the letter require at least 800 Myr age difference to explain its large area. We determined that the best-fitting age to the SGB is about 1.58 Gyr, equal to $\log(t/\mathrm{yr}) = 9.20$.

We then quantitatively analyze the distribution of SGB and RC stars to study their internal age distribution. Firstly, we define a parallelogram-shaped box, bounded by $19.7 \leq B \leq 21.8$ mag and $0.75 \leq (B-V) \leq 1.25$ mag. This region was defined to properly exclude possible contamination by eMSTO stars and at the bottom of the RGB. Stars located inside this box were determined as possible SGB stars. Because the magnitude range of this box is so large, which is more than 2 mag, any reasonable physical processes that may affect the brightness of SGB stars should be already considered in this magnitude range. For example, the maximum magnitude offset caused by unresolved binaries is ~0.75 mag (see Fig. 3.8); The enhancement in magnitude owning to stellar convective overshooting (adopting a strong overshooting ranging from $\Lambda_e = 0.35 - 0.50$), is less than 0.1 mag. In Fig. 6.6, we show the best fitting isochrones to the boundaries of the eMSTO (Blue dashed line and red solid line, corresponding to the youngest isochrone and oldest isochrone, respectively), tight SGB (Purple solid line) and the corresponding locus of unresolved binaries with mass ratio of $q = 1$ (the equal-mass binary systems, purple dashed line). It also shows only one exception (marked as star 'A' in Fig. 6.6) has significant high deviation to the best-fitting isochrone. But the luminosity of this star is also much brighter than the locus of the youngest isochrone (1.38 Gyr or $\log(t/\mathrm{yr}) = 9.14$), which indicates that it may be a bright foreground or background star. Another possible origin of star 'A' is it is actually a equal-mass unresolved binary system (that is, a SGB-SGB binary system), as its position is close to the locus of such a binary sequence. Both cases indicate that this star is not a genuine single SGB star. Because of this, we have excluded this star from our subsequent analysis, also a single exception will not change our statistical results. For the selection of RC stars, we first select stars located in the color and magnitude range defined by $1.28 \leq (B-I) \leq 1.45$ mag and $19.6 \leq B \leq 20.7$ mag. As the isochrones in the RC range trace open loops, we next select stars which close to the loop pertaining to the most extreme isochrone (normally is the 1.38 Gyr isochrone) as RC stars. For stars that not located in this loop, we also adopt those which are still located within the 2σ level uncertainties related to that isochrone. Finally, we made a cut across the MSTO region to define the MSTO stars, which is similar to the approaches that used in Fig. 6.3 and some previous works [73, 96, 99, 201].

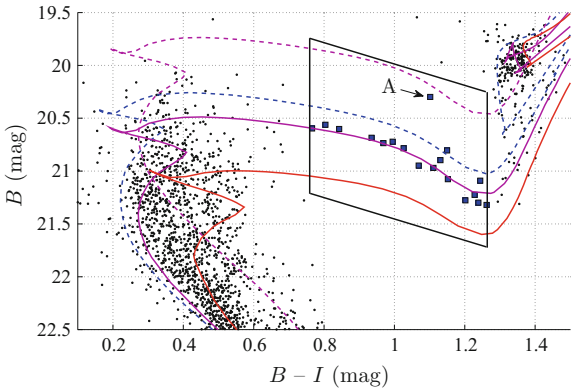

Fig. 6.6 This figure demonstrates our selection of SGB stars, the parallelogram-shaped box contains all selected SGB tars, which are marked with *blue squares*. The resulted best fitting isochrone to these SGB stars has an age of 1.58 Gyr (the *purple solid line*). The *purple dashed line* represents the corresponding locus of equal-mass binary systems. The *blue dashed line* and *red solid line* represent isochrones for 1.38 and 2.18 Gyr, respectively

After we have determined a relative complete sample of MSTO, SGB and RC stars, we then assign the age of the closest isochrone to each star, which enable us to obtain a comparison between the SFHs of these different stellar samples, we illustrate this approach in the top panel of Fig. 6.7. To test if their SFHs are consistent with SSPs, we have also generated a CMD of an SSP for an age of 1.58 Gyr as a comparison. In the simulated CMD, we have included the photometric uncertainties and unresolved binaries, the method that we used to determine the binary fraction is identical to that used in Chap. 3. We found the binary fraction with mass-ratio $q \geq 0.6$ is about 20%, indicating totally 50% MS-MS binary fraction if the mass-ratio distribution is flat [160]. A significant binary fraction may broaden the TO region. However, for evolved stars, only equal-mass binary systems (i.e. SGB-SGB or RGB-RGB binaries) will show apparent difference from single stars, because the numbers of these binary systems are very small.[3] Because of this, we did not assign binary status to any evolved star in our simulation. The simulated MS stars have the same LF to the observations, for evolved stars, we have assumed that they obey the Chabrier IMF, which is already built into the isochrones [261]. The bottom panel of Fig. 6.7 shows the simulated CMD for an SSP with an age of 1.58 Gyr. We then apply the identical approach we perform on the observed CMD to the simulated CMD.

We subsequently derive the SFHs of MSTO, SGB and RC stars and compare them with their corresponding SSP samples. The derived SFH for the eMSTO region is almost flat, spanning from 1.38 Gyr to 2.18 Gyr, indicating an dramatic age spread of

[3]One can assume that only binaries with $q \geq 0.95$ will exhibit significant difference to single SGB stars, that means only 5% of our SGB sample, thus 0.9 of 18 stars, will affect our analysis, this is consistent with our observation (only one exception of star 'A' has shown apparent difference to the bulk of SGB stars).

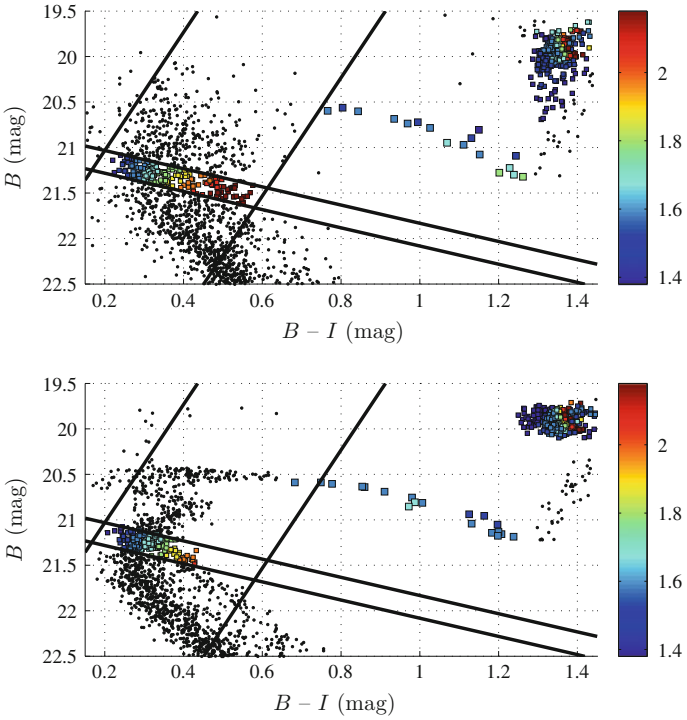

Fig. 6.7 *Top* panel CMDs of the NGC411 that zoomed into MSTO, SGB and RC regions, color bar indicates their best-fitting ages (in Gyr). *Bottom* panel the same as the *top* panel, but for an 1.58 Gyr SSP

800 Myr, which is consistent with previous result [67]. However, the SFHs resulting from oth the SGB and the RC stars are apparently different: all SGB stars and more than 80% of the RC stars are actually younger than 1.78 Gyr. Using the Kolmogorov–Smirnov (K–S) test,[4] we examine if the SFHs of MSTO, SGB and RC stars are consistent with SSPs. The K–S test reports that the distribution of both the observed SGB and RC stars are actually agree with SFHs derived from SSPs ($P = 0.87$ and 0.37, respectively), but it return a negative result for MSTO stars, that is, they are not an SSP: $(H, P) = (1, 6.8 \times 10^{-8})$.

Although the K–S test already reports quite positive results for both the observed SGB and RC stars when compare their distribution to the expectation of SSP, there is a clear secondary RC which extends to $B \sim 20.2$–20.5 mag (see Fig. 6.7). These secondary RC stars are more massive than normal RC stars, which may reflect some-

[4]The K–S test can quantify the similarity between distributions of two samples, it returns two values when evaluate this similarity, H and P. If H is returned as 0, it means that the two samples are drawn from the same distribution. P indicates the p value, which is the probability that these two samples are drawn from the same underlying distribution, normally when $P \geq 0.05$, the K–S test will return H as 0.

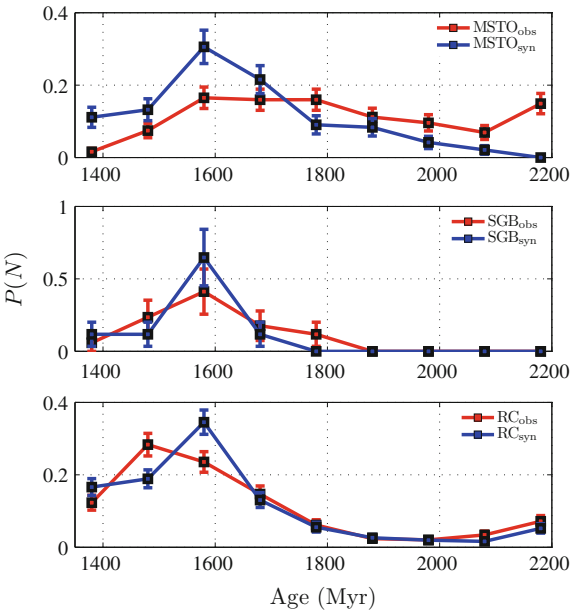

Fig. 6.8 Comparisons of the SFHs derived from the observed MSTO (*top* panel), SGB (*middle* panel) and RC stars (*bottom* panel), as well as their corresponding SFHs of synthetic samples

what eSFH or rapid stellar rotation [262, 263]. Clearly, a SSP cannot produce such a secondary RC in its CMD. We found most of these secondary RC stars located below the position indicated by the 1.48 Gyr ($\log(t/\mathrm{yr}) = 9.17$) isochrone, they totally occupy ∼25% of the full RC population. We thus slightly change our simulated sample by adding two stellar populations with ages of 1.38 and 1.48 Gyr to the bulk population, with number fractions of 12.5% each. Then we check whether the addition of these younger populations to our model can improve the significance of the comparison. We performed the same approaches to the synthetic CMDs as before, and compared their derived SFHs with observations, the K–S test again shows that the distribution of the observed SGB and RC stars are consistent with the SFHs of the synthetic samples, but with higher P values of 0.93 and 0.67, respectively. The SFH of the eMSTO remain inconsistent with the synthetic sample, with $(H,\ P) = (1, 2.6 \times 10^{-9})$. The comparisons are shown in Fig. 6.8. These results clearly indicate that the SGB and RC morphologies of NGC411 do not agree with the eMSTO if the width of the eMSTO reflect an eSFH.

6.3.3 NGC419

The CMD of NGC419 is shown in Fig. 6.9, which is already decontaminated. The attached isochrones that describe the boundaries of its eMSTO region as well as the bulk of SGB are obtained from the Padova stellar evolution models [24]. The fitting

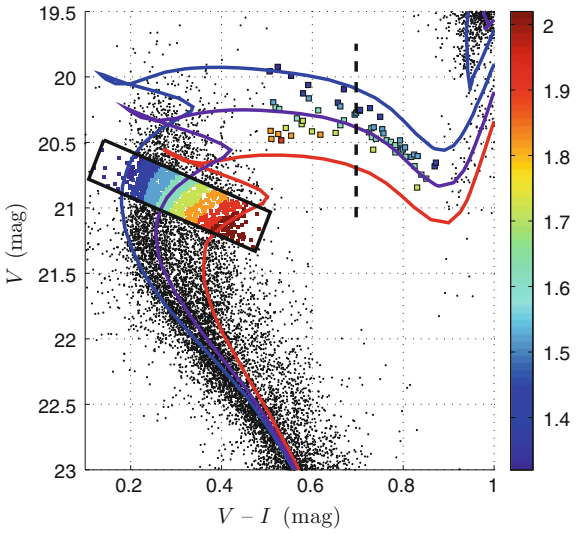

Fig. 6.9 The CMD of NGC419, showing isochrones of 1.32 Gyr (*blue solid line*, corresponding to the *blue* boundary of the eMSTO region), 1.52 Gyr (*purple solid line*, which describe the peak in the cluster's SFH based on the morphology of the *red* part SGB), and 2.02 Gyr (*red solid line*, corresponding to the *red* boundary of the eMSTO region). The color bar indicates the age of SGB stars and the eMSTO stars (stars in the *black* box), based on the assumption that these features can be explained solely by stellar age ranges (in Gyr). The vertical *dashed black line* divided the SGB stars into *blue* and *red* samples

parameters are $Z = 0.004$ [68, 248], $(m - M)_0 = 18.90$, $E(B - V) = 0.06$ [198], different color represent isochrones with different ages, they are $\log(t/\mathrm{yr}) = 9.12$ (1.32 Gyr, the blue solid line), $\log(t/\mathrm{yr}) = 9.18$ (1.52 Gyr, the magenta solid line) and $\log(t/\mathrm{yr}) = 9.31$ (2.02 Gyr, the red solid line). The youngest and oldest isochrones indicate an age spread of ~700 Myr for NGC419. Although at first glance, it seems NGC419 also harbor a broadened SGB, however, if we take a carful exploration focus on the width of the SGB for the entire color range, one will find it exhibits an SGB that is broad only on the blue side, for the range of $(V - I) \geq 0.7$ mag, the SGB becomes significantly narrower. This feature is even apparent before we decontaminate the background pollution, thus cannot be caused by data reduction. In addition, the significance level of our field-star decontamination is high enough along the SGB, and both the photometric results from the packages of IRAF/DAOPHOT and DOLPHOT confirm the reality of the 'converging' SGB morphology. AS test also reveals that blending cannot cause the observed narrowing. Because of this, the observed converging of the NGC419 SGB is real and not caused by artifacts related our data reduction.

In order to characterize the narrowing of the SGB, we firstly divided SGB into two parts. The red part SGB stars are selected by constrain their color in $0.50 \leq (V-I) \leq 0.7$ mag, and the blue part SGB stars have their color of $0.7 \leq (V - I) \leq 0.89$ mag.

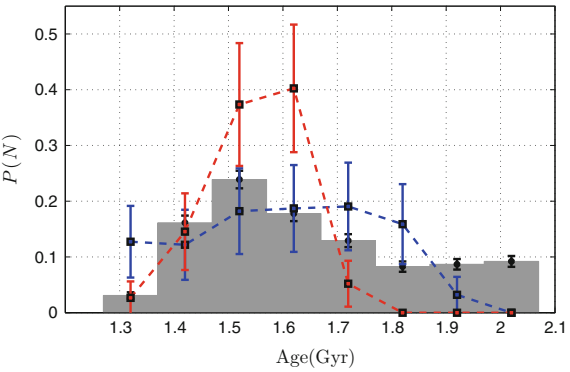

Fig. 6.10 SFHs derived from *red*, *blue* SGB stars, as well as eMSTO stars. *Blue*, *red dashed lines* represent the SFHs of the *blue*, *red* SGB samples, respectively. *Grey* histogram is the SFH of the eMSTO stars

This division will make these two sub-samples contain equal number of SGB stars. The blue SGB stars span a broad range in luminosity, in contrast to the red SGB stars, where the letter almost all converge to a significantly narrower distribution. For each SGB star we arrange the same method that used for NGC411 SGB stars to determine their model-fitted age, then we counted the fractions of SGB stars with different ages to derive the SGB's SFHs.

The SGB lifetime is a monotonically increasing function of the stellar age, ranging from 9 Myr for the 1.32 Gyr population to 22 Myr for the 2.02 population [24], this difference is significantly shorter than the adopted age resolution of 100 Myr. The small variation in SGB lifetimes therefore does not affect the derived SFHs, also the probability of an SGB star to be associated with a given isochrone is nearly constant for all ages.

The typical photometric uncertainties in SGB photometry will cause a age dispersion of $\leq$50 Myr, indicating that the isochrone fits are well-constrained. Figure 6.10 shows the SFHs derived from the blue and red SGB subsamples, the former is apparently wider than the latter, which is characterized by a peak at 1.52–1.62 Gyr (corresponding to the purple isochrone in Fig. 6.9). The average period times of stars spend in the red and blue SGB range are approximately equal, therefore our derived SFHs are reliable, which represent the real SFHs. As expectation, the SFH of eMSTO (grey histogram in Fig. 6.10) is much broadened, indicating an age spread from 1.32 to 2.02 Gyr. This maybe consistent with the SFH of blue SGB stars, where the letter also seems have an age spread of $\sim$600 Myr, but apparently not with the SFH of red SGB stars. Based on 1000 synthetic clusters characterized by an age spread of 700 Myr, we found the 'convergence' of the SGB in NGC419 is unlikely owning to stochastic sampling: the probability of detecting fewer than 10% of the red SGB stars associated with the oldest isochrones is $P \leq 0.05$. This is thus exclude the presence of a genuine age spread in the cluster. There must be one or more mechanisms that have affected the morphology of the NGC419's MSTO region.

6.4 Physical Discussion

Apparently, all these results deny the presences of dramatic age spread in these clusters. If a SC can constantly build its mass in a period of several hundred million years, then we would expect to see many YMCs with ages of several tens of hundreds million years are still building up their stellar masses, however, as already introduced, observed YMCs do not show evidence of ongoing star formation [100].

Although both NGC1651, NGC411 and NGC419 show apparent eMSTO regions, their current mass are significantly different. NGC1651 and NGC411 have a total mass of only $\log M_{\rm cl}/{\rm M}_{\odot} \sim 4.64$ and 4.51, respectively [264], while NGC419 has a total mass that reaches $M_{\rm cl}/{\rm M}_{\odot} \sim 5.38$ [99], assuming their half-mass radii are roughly equal to their half-light radii [99], based on the formula of [48]

$$v_{\rm esc}(t) = f_{\rm c}\sqrt{\frac{M_{\rm cl}(t)}{r_{\rm h}(t)}}\ \ {\rm km\ s^{-1}}, \tag{6.1}$$

where $M_{\rm cl}(t)$ is the cluster current mass (in units of $\rm M_{\odot}$), $r_{\rm h}(t)$ is the cluster's current half-light radius in pc, $f_{\rm c}$ is a coefficient which depends on the concentration index c of King models [265]. This finally gives the escape velocities of NGC1651, NGC411 and NGC419 of $v_{\rm esc} \sim 5.80$, 7.24 and 17.55 Km $\rm s^{-1}$, respectively. Count the initial velocity of runaway gas in a SC is in order of 10 km $\rm s^{-1}$, and the intermediate-age AGB stellar winds can have velocities of 10–40 km $\rm s^{-1}$, only NGC419 would have the capacity to capture its runaway gas to make new stars. However, since all these SCs have a suspected SFH of several hundred million years, the multi-supernovae explosions must have strongly accelerated the gas remnants at very early stage, that means the runaway velocities of these gas remnants should be at least in order of 100 km $\rm s^{-1}$. Clearly, it is indeed reluctantly for they to retain their runaway gas for such a long period.

Instead, our results seem favor stellar fast rotation scenario: for NGC1651 and NGC411, the observed eMSTO regions as well as their tight SGBs may indicate that their TO regions are expanded by the effect of stellar rotation. When those TO stars quench their central hydrogen burning, their internal expansion will lead their self rotation quickly slow down, if rotation has not affect their core size, then these slowing down will lead their luminosity converging into the prediction of the SSP. The feature of converging SGB indeed appears in NGC419, which could be produced if the cluster is mostly composed of rapidly rotating stars and slow down over time when they evolved off, because of the conservation of angular momentum. However, the assumption of that the rotation will not affect the stellar core size is really surprising, if a coeval stellar population is composed by stars with zero rotational rate ($\Omega = 0$) to critical rotational rate ($\Omega = \Omega_{\rm c}$), the rotational mixing effect will lead a fast rotating star to appear brighter in about 0.5 mag than a none rotating star, if their total masses are equal, because the fast rotating star will have a heavier core, that is equal to it is more massive than its none rotating counterpart. For example, as shown in Fig. 6.9, NGC419 has its SGB that is wide in the blue

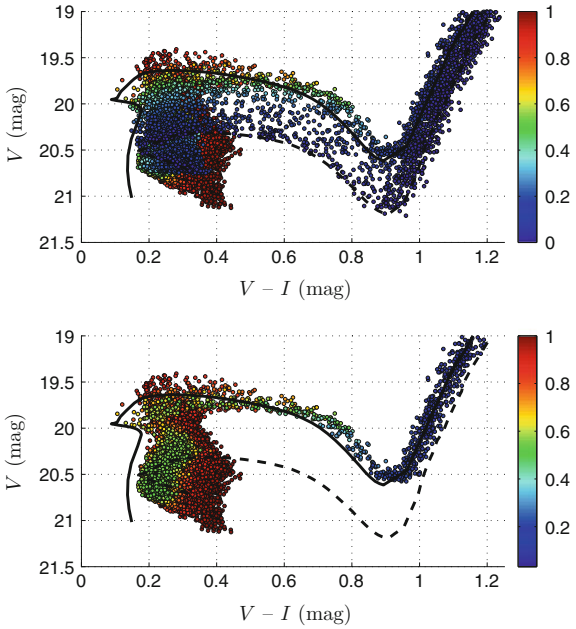

Fig. 6.11 *Top* panel, the $(V, V-I)$ CMD of a synthetic cluster based on Geneva stellar rotation models, with $Z = 0.006$ and $\log(tyr^{-1}) = 9.1$, adopting a flat initial rotation distribution, $\Omega_{\rm int}/\Omega_{\rm crit} \in [0,1]$. Color bar indicates each star's current (not initial) rotational rate, $\Omega/\Omega_{\rm crit}$; *bottom* panel: as the *top* panel, but for all stars have their initial rotational rates larger than 0.5, $\Omega_{\rm int}/\Omega_{\rm crit} \geq 0.5$, in this case, a converging SGB appears. The *black solid* and *dashed lines* are isochrones for the same metallicity, but for none-rotating stellar populations with different isochronal ages, $\log(t\ {\rm yr}^{-1}) = 8.9$ and 9.1, respectively, which provide a comparison between stellar fast rotation scenario and age spread scenario

range and tight in the red range, which cannot be explained by an age spread of 700 Myr (derived from its eMSTO region). However, if assume NGC419 is a SSP with its member stars have different self-rotational rates from $\Omega = 0$ to $\Omega = 1$, it would also produce a apparent inconsistency between the stellar evolutionary model (under the consideration of stellar rotation) and observations. In Fig. 6.11, we show the CMDs of synthetic clusters, which are composed by SSPs with different rotational rates in Johnson—Cousins V and I bands. Based on this figure, we found only very rapidly rotating stars will converge into a narrower sequence, while the slow rotators would still occupy a much broader luminosity range.

Because NGC1651, NGC411 and NGC419 all show a tight or converging SGB, this may indicate that the eMSTO stars in these clusters are rotating much faster than expected, adopting their rotational rates homogeneously distributed from 0 to 1 is not proper. As for slowly rotating stars, the rotational mixing will produce dramatic difference in their luminosity of SGB phase, which will make these normal rotating stars occupy the bottom part of the SGB and broaden it to a large extent. If all stars

are extremely fast rotating stars, then this difference in their SGB stars' luminosity become smaller, but the gravity darkening still play a important role on their MS stage, thus produces a broadened TO region. However, it seems unrealistic that a cluster would only contain rapid rotators, direct measurements of stellar rotational rates of stars in a dense SC is required.

The inconsistency may also reflect our lack of knowledges, because the effects of rapid stellar rotation will significantly complicate our understanding of stellar evolution. The discovery of nitrogen and helium enhancements in massive MS stars has been generally recognized as a result of rotational mixing [266, 267], which will further affect the morphology of the observed CMD, this is also applied for RC stars. The discovery of a weak secondary RC in NGC411 is also consistent with previous work on younger clusters [268], although they are narrower than that in the case of real age spread as suggested by the eMSTO regions, but still more extended than for an SSP. To understand the eMSTO conundrum, more explorations of the rapid stellar rotation, binaries, as well as the chemical compositions of stellar populations in intermediate-age star clusters are required. At this stage, we still lack direct comparison between comprehensive models that consider all those effects and observations.

6.5 Conclusion

In this Chapter, I introduced our latest researches on three intermediate-age SCs in LMC and SMC, all these three SCs show apparent eMSTO regions, which strongly indicate that they may have initially formed its bulk stars within a star forming period of several million years. This is much longer than that allowed by their initial gas expulsions. However, the stellar populations in intermediate-age SCs are different compare with that in GCs, the latter always show multiple features in their TO regions, SGBs, RGBs or even HBs. When we explored the SGBs or RCs in these SCs, features that consistent with a dramatic age spread disappear, in particular for their SGBs, which are usually narrower than that for multi-aged stellar populations, but close or consistent with SSPs instead. That means the observed complex TO regions may caused by mechanisms that related to stellar evolution rather than a global extended star formation period, like stellar fast rotation. If confirm, this may push us to reevaluate our understanding of stellar evolution, as these mechanisms that we did not consider into our models may actually important for stellar evolution, and finally affect our estimations of many physical parameters of stellar systems.

Our studies of SGBs (also the RC) in these SCs exclude the presence of a significant age spread. Except for NGC419, other two SCs are too light to have the capacity to retain the initial runaway gas, but they all show apparent broadened TO regions, that means any scenario that suggest continued gas accretion as the solution to the eMSTO regions is incorrect. In particular a recent study of two intermediate-age LMC clusters with masses of only $\sim$5000 $M_{\odot}$ shows that they all harbor eMSTOs [269]. The converging morphology of SGB in NGC419 strongly suggest that the

distribution of SGB stars have been affected by their evolutionary stage, which is most likely the stellar rotation. If this speculation is correct, then the broadening of the blue range SGB is thus caused by the differential rotation of sample stars, it would naturally lead us to speculate that its eMSTO region is also owning to the differential rotation.

The study of stellar populations in YMCs, intermediate-age SCs and GCs is a very active field among all topics that related to SCs. Our current understandings on this issue are far from perfect, and it is of paramount importance because it may affect our basic understanding on star formation, stellar evolution as well as the relationship between GCs and galaxies. In Part III of this book, we will go into a chapter of comprehensive discussions and summaries based on all the results obtained from observations that introduced in this work, since there is no final answer to the origin of MSPs in SCs, one should try to sort out all these observational results and gain their own perspective on this topic.

Part III
Not-So-Simple Stellar Populations in Massive Star Clusters, Where Do We Stand?

Chapter 7
Lessons Learned from This Thesis

It is thus of fundamental importance to explore the origin of MSPs in SCs. If the infancy GCs were such massive, then most observed YMCs and intermediate-age SCs would fail to represent a young GC. SCs are the building blocks of their host galaxies, investigating the stellar populations in SCs (which relates to how they form and evolve), would become inevitable if one wants to understand the evolution of galaxies as a whole. The discovery of possible MSPs in intermediate-age SCs also push us to reconsider our understanding on stellar evolution. On the other hand, if the GCs did not formed in situ, indicating that they are different to our currently observed young SCs, then it may suggest that they are related to galactic mergers. The ubiquitous GCs in the Galactic halo would strongly indicate a large number of satellite galaxies around the MW, which would help us better understand the "missing satellite" problem. This also relates the study of stellar populations in SCs to cosmology.

Because of this, it is deserve to make a summary about what we have learned from previous chapters and see where do we stand for the topic of stellar populations of SCs.

7.1 Do the Young Massive Clusters Harbor Multiple Stellar Populations?

Based on Chap. 3, we learn that the YMCs NGC1805 and NGC1818 can be ideally described by SSPs. But this only means we have not found any photometric evidence of MSPs for these two clusters in V and I bands. Indeed, recent observations which involve the U band data have revealed at least for three YMCs, NGC1755 [113], NGC1850 [63] and NGC1856 [62], the morphology of their MSs are inconsistent with SSPs. But it seems the complex of their MSs are caused by stellar fast rotation rather than a prolonged SFH [63, 110, 113]. For NGC1805 and NGC1818, they show

C. Li, *Not-So-Simple Stellar Populations in Star Clusters*, Springer Theses,
DOI 10.1007/978-981-10-5681-9_7

apparently broadened MSs, but it seems caused by unresolved binaries or blending instead of spread in their chemical abundances.

Most soft binaries (binaries with low binding energy) would be disrupted during their very early evolutionary stage. The time-scale of the disruption depends on the local environment and global parameters: NGC1818 is characterized by a relatively shorter time-scale because it is more massive and contains more member stars, and the velocity dispersion for its bulk stars is higher than NGC 1805. The remaining hard binaries would become gradually harder, that is, their components stars would evolve to become closer and closer, and finally merge [139, 170]. The most massive binaries, in the mean time, are the "hardest" binaries, which would quickly evolve to be close binaries. Based on [115], such massive binaries ($\sim$20 $M_{\odot}$) could possibly be the sources of abundance anomalies in GCs.

However, star with a mass of 20 $M_{\odot}$ would only have a lifetime of roughly 10 Myr. This is significantly shorter than the age of NGC1805 and NGC1818. That means if the massive binaries would contribute to the SCs' abundance enhancement, this should already complete when we observed them. From Chap. 1 we know both the enhanced helium abundance and metallicity in stellar populations would show features in their CMD. However, the effect of helium enhancement is opposite to that of metallicity enhancement, since the former would causes a MS blueshift and the latter would make the MS redshift (see Figs. 1.9 and 1.10). It is reasonable to expect that an enhancement of the helium abundance would be associated with that of metallicity. Since their effects on the MS compensate each other, this would still lead to a tight MS.

As introduced in Chap. 1, an abundance spread would introduce an apparent split or broadening of the SGB and RGB in a cluster's CMD, which has been confirmed in most GCs and in 47 Tucanae in this book (Chap. 5). However, NGC1805 and NGC1818 are so young that they show no clear SGB or RGB in their CMDs. Because only very massive stars at this age would have evolved off the MS, but the more massive the stars, the faster they evolve, hence their SGB and RGB phases would be so short that it would be very hard to catch an entire branch of such stars. This difficulty pushes us to investigate intermediate-age SCs.

At this stage, we can only conclude that we found no evidence of the absence of MSPs in the YMCs NGC1805 and NGC1818: their MS is tight, the broadened sub-sequence at the red-side of the MS can be explained as due to unresolved binaries and blending. However, based on recent discoveries of multiple or broadened MSs in YMCs NGC1755, NGC1850 and NGC1856 [62, 63, 113], NGC1805 and NGC1818 may also appear similar features if ultraviolet data is involved. If this confirmed in the future, it may indicate the importance of stellar fast rotations for their photometric properties. It is reasonable to expect that at the time of cluster formation, there would be very massive fast-rotating stars, but whether they already transferred their effect to the MS stars' abundance is still unclear, because we lack apparent SGB and RGB features. This is the key to determine abundance spread in photometry.

Binaries would also affect the stellar evolution, a direct binary product is provided by the BSS. In principle, the refreshed BSSs are no longer belong to the first generation stars, which offers us a good chance to study stars that are younger than

the cluster's typical age. In Chap. 3, we know that most binaries would be disrupted within a very short period. The remaining counterparts would continue to evolve, some of them may be disrupted in the future, but some of them would finally merge or trigger mass transfer, leading to the formation of BSSs. Geller and Mathieu (2012) found for NGC 188, the hard-binary frequency is $23 \pm 2\%$ [270]. In the mean time, it was reported that 76% of the BSSs in NGC 188 are actually in binary systems [130]. Chapter 4 exhibits the presence of BSSs in the extragalactic GC Hodge 11, except for the central extremely dense region, where the BSSs with collisional origin dominate the whole sample. We found that BSSs can also form in less dense regions like a cluster's outskirt, where binaries play an important role. In fact, only for extremely old GCs, BSSs with a binary mass transfer/merger origin would have a comparable number to collisional BSS. In most evolutionary stages of clusters, the BSSs with the binary origin would be more important than those resulting from the collisional channel [182].

7.2 No Evidence of Multiple Stellar Populations in Intermediate-Age Star Clusters

In Chap. 6, the discovery of eMSTO in intermediate-age SCs provides a exciting hint. It may indicate that SCs were not born as SSPs. However, as we pointed out in that chapter, such an individual puzzling feature is far from excluding the SSPs origin for SCs. To confirm the presence of spreads of age and abundance, one should find multiple features in the SGB and RGB. We still do not reach a final conclusion before we can exclude the effect of stellar fast rotation.

In photometry, MSPs would most apparently show their features on the SGB and RGB. However, the morphologies of the SGBs in NGC1651, NGC411 and NGC419 are conflict with this speculation, in stead they favor the stellar rotation scenario. Since a scenario has predicted that the massive fast rotating stars would contribute the abundance enhancement in SCs [32], if this scenario works, we would expect a split or broadened SGB in their CMD. Our results clearly refutes this prediction.

But we already concluded that the intermediate-age SCs may harbor no age spread, so if their member stars are not fast rotators, how can we explain the eMSTO? One possible explanation is that the rotational rates of massive stars ($\sim$20 $M_\odot$ in [32]) are all extremely high. As shown in Fig. 6.11, slowly rotating stars would mainly contribute the broadening of the SGB, if we confine all stars have their rotational rates greater than 0.5, then gravity darkening would play a important role on these stars' MS phase, producing a broadened TO region while keep the SGB tight. However, this speculation is surprising, because a cluster would only contain rapid rotators is somehow unrealistic. Direct measurements of stellar rotational rates in a dense SC is desiderate.

The LMC intermediate-age SCs are similar to YMCs in many physical parameters: both their masses span from 5000 $M_\odot$ to 50000 $M_\odot$ (see Fig. 5 [top 1st to 3rd panels]

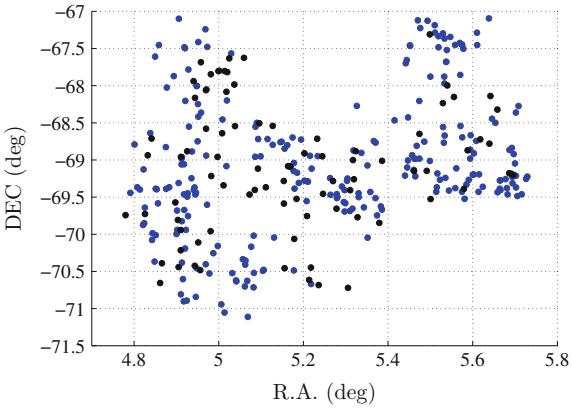

Fig. 7.1 Spatial distribution of LMC YMCs (*blue* filled *circles*, $\log(t/\mathrm{yr}) \leq 30$ Myr.) and intermediate-age SCs (*black* filled *circles*, $\log(t/\mathrm{yr}) \in [500, 3000]$ Myr). Data comes from [272]

in [271]), and they all contain 10^3 to 10^5 member stars. They are also associated in spatial distribution (see Fig. 7.1). It is therefire reasonable to expect that they are the same kind of SCs at different evolutionary stages. The tight and converging SGB observed in intermediate-age SCs may reflect that both they and YMCs are born as SSPs.

Hence we can reach a relatively conservative conclusion, at least YMCs and intermediate-age SCs in the LMC are SSPs. If GCs' MSPs originate from the ejecta of massive, fast rotating stars or binaries, they would enhance the abundance within a very short period. In that case, we would observe a broadened or split SGB and RGB for YMCs or intermediate-age SCs. The tight SGB in intermediate-age SCs is at odds with this scenario. Additionally, both these scenarios suggest an initially at least 10 times more massive origin for GCs. We would then immediately have found that the YMCs are not sufficient massive to hold the stellar ejecta to form the next generation stars. But currently no YMC is this massive and they have all gotten rid of gas [100].

7.3 Do Globular Clusters have Another Origin?

It seems that we already excluded all the possibility that GCs are originated from YMCs. Does that mean GCs are different to YMCs? This is possibly true for some of the observed GCs, like the GC ω Centauri, whose mass reaches $\sim 4 \times 10^6$ $M_\odot$ [273]. If such a tremendously massive GC were initially comes from an individual YMC, and its abundance enhancement is due to the initial massive stars/binaries, then the GC's initial mass would reach 4×10^7 $M_\odot$. Such a mass scale for an individual SC seems incredible, given that we never observed such a "super" YMC.

But now we have a better constraint: Larsen et al. (2012) estimated that the initial mass of GCs in the Fornax dwarf spheroidal galaxy would only need to be 4–5 times more massive than their current mass on average [274]. That means that at least a

number of less massive GCs would have a initial mass like the YMCs that we observe today (like NGC6362, whose initial mass would be just over 10^5 $M_\odot$ [275]).

However, the tight SGB of intermediate-age SCs tells us that at least for SCs that are younger than 2 Gyr, they would not contain large numbers of secondary population stars, despite that they may already have formed a small number of BSSs. So other scenarios that would generate the secondary population stars after the timescale of about 2 Gyr, such scenarios should meet:

1. They should reproduce the MSPs as observed in GCs today.
2. The reproduction process should not be too quick, the typical time-scale for the formation of MSPs in this scenario should longer than 2 Gyr.

Another promising scenario is again the binary interactions, but instead of the very massive OB stars ($\sim$20 $M_\odot$), the main contributors are binaries with F-type primary stars (1.0–1.4 $M_\odot$). In this scenario, "**the stars with anomalous abundances observed in GCs are merged stars and the accretor stars produced by binary interactions, and these binary products are rapidly rotating and more massive than the normal stars. These binary products have different effective temperatures, luminosities, and surface abundances from single stars in the same evolutionary stage due to their evolution. Thus, the stellar population with binaries can reproduce the observations of multiple stellar populations because this binary population includes two sub-populations: (1) normal single stars with normal abundance (the initial abundance of GCs) and (2) merged stars and acceretor stars (produced by binary interactions) that have abnormal surface abundances through their own evolution.**" [127]. Based on this model, one can reproduce the observed MSPs in GCs on a relatively long timescale: there are three channels to reproduce the secondary stellar populations, with two of them needing binaries to evolve into their Roche lobe overflow, which already reaches the red-giant stage of primary star. Since the F-type stars' typical MS lifetime is 2–10 Gyr, they would not produce any multiple features in intermediate-age SCs and YMCs. Another channel involves the initially very close binaries. The timescale for close binary mergers is uncertain, typically from 0.25 Gyr [276] to 8 Gyr [277]. If close binary mergers are not as fast as expected, then the SCs that are younger than 2 Gyr may still resemble SSPs. On the other hand, if the timescale for binary mergers is short enough, then we should find significant numbers of BSSs in YMCs or intermediate-age SCs. However, because it is difficult to determine the MSTO in YMCs, it is hard to distinguish BSSs from MS stars. For intermediate-age SCs, we do find such features: in Fig. 7.2, we present the CMD of NGC2213, where we found at least 53 BSSs candidates (highlighted by black filled circles) are in this region, indicating that binary mergers may already work at the age of NGC2213 (1.4 Gyr).

When we say BSSs are another kind of secondary stellar populations, we mean that they are not formed in the first generations, but such secondary stellar populations only occupy a very small fraction in the whole SCs. However, the existence of BSSs may indicate that a large number of secondary stellar population stars are around to form: the binary interaction enhances the abundance, leading us to observe

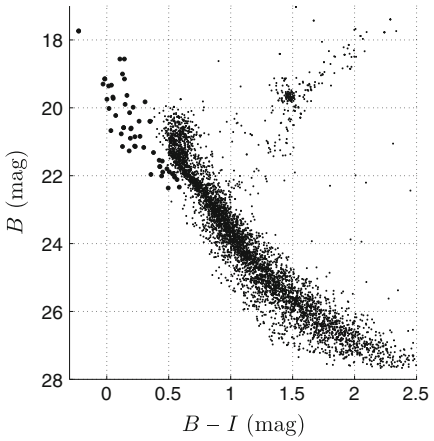

Fig. 7.2 Possible BSSs in intermediate-age star cluster NGC2213(1.4 Gyr), the 53 BSS candidates are highlighted

multiple features in the SGB, RGB and HB in a SC's CMD. If the secondary stellar populations come from the most massive objects, then the initial mass of GCs would be tremendously massive (10–20 times massive than their current mass). This is because, in order to form a large number of secondary stars, we need the corresponding very massive ejecta from the most massive stars. If the IMF of a globular is Kroupa-like [163], the initial number of low mass stars in a GC would be very large, which contributes most of its initial mass. In the mean time, if the first generation F-type stars are the main progenitor of GCs' MSPs, then such a massive initial for GCs may be not required.

As introduced in Chap. 2, although the current observed young SCs seem lack the capacity to capture their initially runaway gas, it may accrete materials when they went through a background medium. A possible hint of such a external accretion has been observed recently, in 2016, we found two well-populated SSPs in 1.4 Gyr-old cluster NGC1783 [75] (Fig. 7.3), at first glance, it seems there are two BSS populations which represent two star burst events. If the observed tight young sequences resemble a set of BSSs, it would indicate that these BSSs are produced by stellar collision, however, the observed spatial distribution of these young sequence stars is even more extended than those same luminosity RGB stars, which thus refutes these stars' blue straggler nature.[1] Similar features were also found in LMC cluster NGC1806 and SMC cluster NGC411 (see [75]).

The more extended (than RGB stars) nature of these young stars may indicate an external origin: when clusters orbit with their host galaxy, they may occasionally collide with some GMCs and accrete gas from them, producing new stars that are less segregated than the massive primordial population stars. However, because the observed young populations in those SCs only occupy small mass fractions, addi-

[1] They are not field stars, neither, because field stars with different ages and metallicities could not populate SSPs, also their spatial distribution is more concentrated than homogeneous field, see [278].

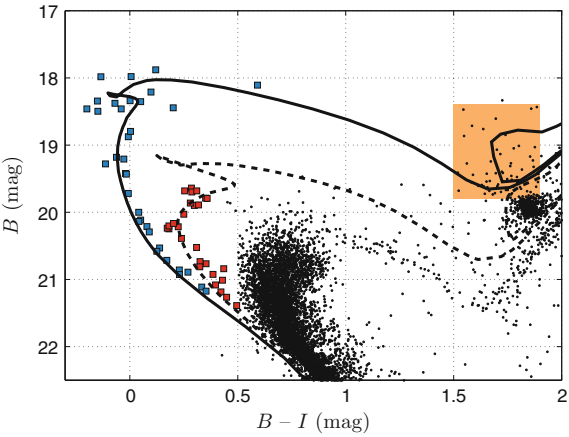

Fig. 7.3 CMD of the LMC cluster NGC1783 (1.4 Gyr old), which hosts two younger stellar populations, they are tightly associated with two isochrones (shown as the *black dashed* and *solid lines*), as indicated by *blue* and *red squares*. For the younger population stars, it also associates with a secondary RC (as indicated by the *orange* background)

tional numerical simulations are required to further study the implications of these observations.

7.4 Epilogue

It has been confirmed that almost all GCs have MSPs with different significances, evidence have accumulated for YMCs and intermediate-age SCs as well. However, how to produce MSPs in a SCs is still an open question, which relates our understanding of star formation and evolution. To shed light on this topic, an important point is to find out the key parameter that would determine the stellar populations in SC. Two possible parameters may be the cluster's mass or age. If the former is the determinant of MSPs in SCs, then it may imply that the GCs may have different origin to current observed young SCs, or at least their initial mass are much massive than that for current YMCs, which forces people to solve the "mass-budget problem" [119]. On the other hand, if there is a distinct age boundary to divide SCs into two different types (with or without MSPs), then it would strongly indicate when SCs evolve to a given stage, some unknown physical mechanisms would make their stellar populations diverse, as introduced, such mechanisms may include stellar rotation and binary merger.

In this book, I investigate the stellar population properties of seven SCs with ages spanning from extremely young ($\sim$25 Myr) via intermediate ages ($\sim$1–2 Gyr) to the cosmic age ($\geq$10 Gyr). All sample clusters exhibit features in the diagnostic CMD which make them significantly different from SSPs. We found for the extremely YMCs, NGC1805 and NGC1818, that even though they can still be very well described by the SSP model, evidence of frequent interactions involving binary stars has already become apparent. In the CMDs of intermediate-age sample clusters, NGC1651, NGC411, and NGC419, complex eMSTO regions appear, indicating that

their initial star-forming processes may have lasted in several million years. This would dramatically change our traditional understanding of SC formation scenarios. However, upon careful analysis of the SGB morphology for these 1–2 Gyr-old clusters, to our surprise we found that the SSP origin might still apply. We interpret the observed eMSTO as evidence of the presence of a population of rapidly rotating stars in the cluster. In extremely old GCs, Hodge 11 and 47 Tucanae, we confirm the existence of rejuvenated and secondary stellar populations. Their spatial distributions indicate that their more recent formation mechanism would have been more centrally concentrated rather than homogeneously distributed. We also found a dramatically rejuvenated stellar population in the form of BSSs in Hodge 11, which can be split into subpopulations that may have formed through different formation channels, depending on the local stellar density. Our analysis has revealed the stellar population distribution in SCs of different ages, as well as their formation processes.

It is important to study the stellar composition in young SCs, as they are usually dynamically young, compare to GCs, the young SCs' current mass are more close to their initial mass. Currently only three young SCs, NGC1755 [113], NGC1850 [63] and NGC1856 [62] have been confirmed to have multiple sequences in their CMDs, but their masses are very different, where NGC1755 only has a total mass of $10^{4.0}$ $M_\odot$ [279], while NGC1856 is as massive as $10^{5.0}$ $M_\odot$ [157]. This may indicate that mass is not the parameter that determines the MSPs in SCs. Although a large sample of young SCs are required in the future,[2] obviously we are on the right track now.

If age were finally determined as the key parameter that lead to the observed MSPs in SCs, then it would push us to reevaluate the importance of stellar dynamics for their evolution. If the scenario that using F-type binary stars to generate the MSPs [127] is promising, then possibly we have found "the last tangram": when a SC forms, it is initially 4–5 massive than its current mass, containing a large fraction of binaries. These binaries would be quickly disrupt and segregate into the cluster core, accelerating the dynamical evolution of the SC. In the cluster core, the surviving binaries would almost all be hard binaries. They would evolve to be closer interacting binaries, and eventually coalesce to BSSs, which has already been observed in some intermediate-age SCs and most GCs. The resulting fast rotating BSSs may mimic their surface abundances like they are the second stellar population stars. The timescale for binaries to evolve to the mass transfer stage may be 2–10 Gyr (the typical life time of F-type stars), hence for SCs younger than 2 Gyr, no significant feature of MSPs appears. That is why the intermediate-age SCs show no evidence of abundance spreads, and their eMSTOs seem to have been caused by other dynamical scenarios (e.g., stellar fast rotation) instead of MSPs.

This scenario actually suggests that the potential dynamics that would affect the stellar evolution is the self-rotation, this is also consistent with scenarios that aim to explain the eMSTO problem in intermediate-age SCs. How can we shed light on this topic in the future? A promising project is to use spectroscopy to further investigate the eMSTO stars' rotating rate. The principle is: stellar self rotation would broaden

[2] with U band photometric data involved.

some of their absorption lines in their spectrum, which would help us estimating their self-rotating velocity.

Observing the stellar populations in a extremely young ($\leq$10 Myr, close to the gas expulsion timescale) and massive ($\geq 10^6$ $M_\odot$) SC is also a creditable project. Currently only SCs in the MW and Magellanic Clouds have been deeply resolved to individual stars, which enables us to study their stellar populations in photometric way. However, some more massive SCs may exist in other distant starburst galaxies (galaxies undergoing an exceptionally high rate of star formation), e.g., [?] found five possible supermassive cluster candidates in galaxy M82, the mass of one of these "clusters" (M82-A1) are estimated reach to $1.3^{+0.5}_{-0.4} \times 10^6$ $M_\odot$, while its age is determined as only 6.4 ± 0.5 Myr. If it is really an individual YMCs, then it may be a good candidate that represent the predecessor of GCs. It is much younger than most of the YMCs that observed in the LMC ($\sim$30 Myr) and it is also extremely massive. Can we investigate the stellar populations in such an extremely young and massive SC? Our current facilities are reluctant to resolve its member stars, but probably our next generation telescopes can. If we can directly observe the stellar populations in such a extremely young and massive SC, it would significantly help us gain a better understanding of the origin of stellar populations in SCs.

References

1. D'Onofrio, M., Burigana, C.: Questions of Modern Cosmology: Galileo's Legacy. Springer, Heidelberg (2009)
2. Champman, A.: William Herschel and the measurement of space quarterly. J. R. Astronomical Soc. **30**, 399–418 (1989)
3. Lada, C.J., Lada, E.A.: Embedded clusters in molecular clouds. Ann. Rev. Astron. Astrophys. **41**, 57–115 (2003)
4. de Grijs, R.: A revolution in star cluster research: setting the scene. Philosophical Trans. R. Soc. A **368**(368), 693–711 (2010)
5. Larson, S.S.: Young and intermediate-age massive star clusters. Philosophical Trans. R. Soc. A **368**(368), 867–887 (2010)
6. Richer, H.B., Fahlman, G.G., Rosvick, J., Ibata, R.: The white dwarf cooling age of M67. Astrophys. J. Lett. **504**, L91–L94 (1998)
7. Adams, F.C., Myers, P.C.: Modes of multiple star formation. Astrophys. J. **553**, 744–753 (2001)
8. Frommet, H.: Milky way globular clusters. http://spider.seds.org/spider/MWGC/mwgc.html
9. Spitzer Jr., L.: Dynamical Evolution of Globular Clusters. Princeton University Press, Princeton (1987)
10. Clusters, Y.M.S.: Portegies Zwart, S.F., McMillan, S.L.W., Gieles, M. Ann. Rev. Astron. Astrophys. **48**, 431–493 (2010)
11. Caffau, E., Ludwig, H.G., Steffen, M., Freytag, B., Bonifacio, P.: Solar chemical abundances determined with a CO5BOLD 3D model atmosphere. Sol. Phys. **268**, 255–269 (2011)
12. Hertzprung, E.: Über die Sterne der Unterabteilung c und ac nach der Spektral klassifikation von Antonia C Maury. Astronomische Nachrichten **179**, 373–380 (1909)
13. Russell, H.N.: Relations between the spectra and other characteristics of the stars. Pop. Astronomy **22**, 275–294 (1914)
14. Harris, D. L.: The Stellar Temperature Scale and Bolometric Corrections. in Basic Astronomical Data, Chapter 15. University of Chicago press (1963)
15. Prialnik, D.: An Introduction to the Theory of Stellar Structure and Evolution. Chapter 9.4. Cambridge University Press (2000)
16. Kippenhahn, R., Weigert, A.: Stellar Structure and Evolution. Springer, New York (1991)
17. Valcarce, A.A.R., Catelan, M., Sweigart, A.V.: Effects of helium enrichment in globular clusters. I. Theoretical plane with PGPUC stellar evolution code. Astronomy Astrophys. **547**, A5 (2012)
18. Duric, N.: Advanced Astrophysics, vol. 29. Cambridge University Press, Cambridge (2004)

C. Li, *Not-So-Simple Stellar Populations in Star Clusters*, Springer Theses,
DOI 10.1007/978-981-10-5681-9

19. Salaris, M., Cassisi, S.: Evolution of Stars and Stellar Populations, p. 138. Wiley, Chichester (2005)
20. Cabrera-Ziri, I., Bastian, N., Davies, B., Magris, G., Bruzual, G., Schweizer, F.: Constraining globular cluster formation through studies of young massive clusters - II. A single stellar population young massive cluster in NGC34. Monthly Not. R. Astronomical Soc. **441**, 2754–2759 (2014)
21. Pelupessy, F.I., van Elteren, A., de Vries, N., McMillan, S.L.W., Drost, N., Portegies Zwart, S.F.: The astrophysical multipurpose software environment. Astronomy Astrophys. **557**, A84 (2013)
22. Bastian, N., Strader, J.: Constraining globular cluster formation through studies of young massive clusters. III. A lack of gas and dust in massive stellar clusters in the LMC and SMC. Monthly Not. R. Astronomical Soc. **443**, 3594–3600 (2014)
23. Murray, N.: Star formation efficiencies and lifetimes of giant molecular clouds in the milky way. Astrophys. J. **729**, 133–147 (2011)
24. Bressan, A., Marigo, P., Girardi, L., Salasnich, B., Dal Cero, C., Rubele, S., Nanni, A.: PARSEC: stellar tracks and isochrones with the PAdova and TRieste stellar evolution code. Monthly Not. R. Astronomical Soc. **427**, 127–145 (2012)
25. Bekki, K., Freeman, K.C.: Formation of ω centauri from an ancient nucleated dwarf galaxy in the young galactic disc. Monthly Not. R. Astronomical Soc. **346**, L11–L15 (2003)
26. Mayya, Y.D., Rosa-González, D., Santiago-Cortés, M., Rodríguez-Merino, L.H., Vega, O., Torres-Papaqui, J.P., Bressan, A., Carrasco, L.: On the nature of the brightest globular cluster in M81. Monthly Not. R. Astronomical Soc. **436**, 2763–2773 (2013)
27. Brüns, R.C., Kroupa, P., Fellhauer, M.: Faint fuzzy star clusters in NGC1023 as remnants of merged star cluster complexes. Astrophsycal J. **702**, 1268–1274 (2009)
28. Brüns, R.C., Kroupa, P.: A new formation scenario for the milky way cluster NGC2419. Astrophsycal J. **729**, 69–81 (2011)
29. Fujii, M.S., Saitoh, T.R., Portegies Zwart, S.F.: The formation of young dense star clusters through mergers. Astrophys. J. **753**, 85–97 (2012)
30. Bekki, K.: Secondary star formation within massive star clusters: origin of multiple stellar populations in globular clusters. Monthly Not. R. Astronomical Soc. **412**, 2241–2259 (2011)
31. Renzini, A.: Origin of multiple stellar populations in globular clusters and their helium enrichment. Monthly Not. R. Astronomical Soc. **391**, 354–362 (2008)
32. Decressin, T., Meynet, G., Charbonnel, C., Prantzos, N., Ekström, S.: Fast rotating massive stars and the origin of the abundance patterns in galactic globular clusters. Astron. Astrophys. **464**, 1029–1044 (2007)
33. Maeder, A., Meynet, G.: On the origin of the high helium sequence in ω centauri. Astron. Astrophys. **448**, L37–L41 (2006)
34. Carney, B.W., Latham, D.W., Laird, J.B., Grant, C.E., Morse, J.A.: A survey of proper-motion stars. XIV. Spectroscopic Binaries among metal-poor field blue stragglers. Astron. J. **122**, 3419–3435 (2001)
35. McCrea, W.H.: Extended main-sequence of some stellar clusters. Monthly Not. R. Astronomical Soc. **128**, 147–155 (1964)
36. Hills, J.G., Day, C.A.: Stellar collisions in globular clusters. Astrophys. J. **17**, 87–93 (1976)
37. Lombardi Jr., J.C., Warren, J.S., Rasio, F.A., Sills, A., Warren, A.R.: Stellar collisions and the interior structure of blue stragglers. Astrophys. J. **568**, 939–953 (2002)
38. Cassisi, S., Maurizio, S.: Old Stellar Populations: How to Study the Fossil Record of Galaxy Formation. p. 134. Wiley-VCH Verlag GmbH & Co. KGaA (2013)
39. Ciardullo, R.: Lecture: Stellar Structure and Evolution. Springer (2007). http://www2.astro.psu.edu/users/rbc/a534/lec18.pdf. Cited 15 Jan 2015
40. Zoccali, M., Cassisi, S., Piotto, G., Bono, G., Salaris, M.: Comparison between Predicted and Empirical $\Delta V_{\mathrm{HB}}^{\mathrm{bump}}$ Bump in Galactic Globular Clusters. Astrophysical Journal Letters. **518**, L49–L52 (1999)
41. Bertelli, G., Girardi, L., Marigo, P., Nasi, E.: Scaled solar tracks and isochrones in a large region of the Z-Y Plane. I. From the ZAMS to the TP-AGB end for 0.15-2.5 $M_{\odot}$ stars. Astron. Astrophys. **484**, 815–830 (2008)

42. Allison, Richard J., Goodwin, Simon P., Parker, Richard J., de Grijs, Richard, Portegies Zwart, Simon F., Kouwenhoven, M.B.N.: Dynamical mass segregation on a very short timescale. Astrophys. J. Lett. **700**, L99–L103 (2003)
43. Moeckel, N., Burkert, A.: The formation of filamentary bundles in turbulent molecular clouds. Monthly Not. R. Astronomical Soc. **807**, 67–73 (2015)
44. de Silva, G.M., Gibson, B.K., Lattanzio, J., Asplund, M.: O and Na abundance patterns in open clusters of the galactic disk. Astron. Astrophys. **500**, L25–L28 (2009)
45. Krumholz, M.R., Matzner, C.D.: The dynamics of radiation-pressure-dominated H II regions. Astrophys. J. **703**, 1352–1362 (2009)
46. Banerjee, S., Kroupa, P.: Formation of very young massive clusters and implications for globular clusters. In: Stahler, S (ed.) The Origin of Stellar Clusters. Springer (2015). arXiv:1512.03074
47. Shustov, B.M., Wiebe, D.S.: First supernovae in galactic globular clusters. Mon. Not. R. Astron. Soc. **319**, 1047–1055 (2000)
48. Georgiev, I.Y., Hilker, M., Puzia, T.H., Goudfrooij, P., Baumgardt, H.: Globular cluster systems in nearby dwarf galaxies - II. Nuclear star clusters and their relation to massive galactic globular clusters. Mon. Not. R. Astron. Soc. **396**, 1075–1085 (2009)
49. Djorgovski, S., Meylan, G.: The galactic globular gluster system. Astron. J. **108**, 1292–1311 (1994)
50. McLaughlin, D.E., Fall, S.M.: Shaping the globular cluster mass function by stellar-dynamical evaporation. Astrophys. J. **679**, 1272–1287 (2008)
51. Shen, Z.-X., Jones, B., Lin, D.N.C., Liu, X.-W., Li, S.L.: Spectroscopic abundance analysis of dwarfs in the young open cluster IC 4665. Astrophys. J. **635**, 608–624 (2005)
52. D'Orazi, V., Bragaglia, A., Tosi, M., Di Fabrizio, L., Held, E.V.: The old anticentre open cluster berkeley 32: membership and fundamental parameters. Mon. Not. R. Astron. Soc. **368**, 471 (2006)
53. Ting, Y.-S., De Silva, G.M., Freeman, K.C., Parker, S.J.: High-resolution elemental abundance analysis of the open cluster IC 4756. Mon. Not. R. Astron. Soc. **427**, 882–892 (2012)
54. Norris, J., Smith, G.H.: The chemical homogeneity of NGC 188. Astron. J. **90**, 2526–2531 (1985)
55. De Silva, G.M., D'Orazi, V., Melo, C., Torres, C.A.O., Gieles, M., Quast, G.R., Sterzik, M.: Search for associations containing young stars: chemical tagging IC 2391 and the argus association. Mon. Not. R. Astron. Soc. **431**, 1005–1018 (2013)
56. Nieva, M.-F., Simón-Díaz, S.: The chemical composition of the orion star forming region. III. C, N, Ne, Mg, and Fe abundances in b-type stars revisited. Astron. Astrophys. **532**, A2 (2011)
57. Soderblom, D.R.: The ages of stars. Ann. Rev. Astron. Astrophys. **48**, 581–629 (2010)
58. Duncan, D.K., Jones, B.F.: Lithium abundance and age spread in the pleiades. Astrophys. J. **271**, 663–671 (1983)
59. Palla, F., Randich, S., Pavlenko, Y.V., Flaccomio, E., Pallavicini, R.: Old stars in young clusters: lithium-depleted low-mass stars of the orion nebula cluster. Astrophys. J. Lett. **659**, L41–L44 (2007)
60. Eggen, O.J.: The age range of hyades stars. Astron. J. **116**, 284–292 (1998)
61. Palla, F., Stahler, S.W.: Accelerating star formation in clusters and associations. Astrophys. J. **540**, 255–270 (2000)
62. Milone, A.P., Bedin, L.R., Piotto, G., Marino, A.F., Cassisi, S., Bellini, A., Jerjen, H., Pietrinferni, A., Aparicio, A., Rich, R.M.: Multiple stellar populations in magellanic cloud clusters - III. The first evidence of an extended main sequence turn-off in a young cluster: NGC 1856. Mon. Not. R. Astron. Soc. **450**, 3750–3764 (2015)
63. Bastian, N., Niederhofer, F., Kozhurina-Platais, V., Salaris, M., Larsen, S., Cabrera-Ziri, I., Cordero, M., Ekström, S., Geisler, D., Georgy, C., Hilker, M., Kacharov, N., Li, C., Mackey, D., Mucciarelli, A., Platais, I.: A young cluster with an extended main sequence turnoff: confirmation of a prediction of the stellar rotation scenario. Mon. Not. R. Astron. Soc. **460**, L20–L24 (2016)

64. Mackey, A.D., Broby Nielsen, P.: A double main-sequence turn-off in the rich star cluster NGC 1846 in the large magellanic cloud. Mon. Not. R. Astron. Soc. **379**, 151–158 (2007)
65. Mackey, A.D., Broby Nielsen, P., Ferguson, A.M.N., Richardson, J.C.: Multiple stellar populations in three rich large magellanic cloud star clusters. Astrophys. J. Lett. **681**, L17–L20 (2008)
66. Milone, A.P., Bedin, L.R., Piotto, G., Anderson, J.: Multiple stellar populations in magellanic cloud clusters. I. An ordinary feature for intermediate age globulars in the LMC? Astron. Astrophys. **497**, 755–771 (2009)
67. Girardi, L., Goudfrooij, P., Kalirai, J.S., Kerber, L., Kozhurina-Platais, V., Rubele, S., Bressan, A., Chandar, R., Marigo, P., Platais, I., Puzia, T.H.: An extended main-sequence turn-off in the small magellanic cloud star cluster NGC 411. Mon. Not. R. Astron. Soc. **431**, 3501–3509 (2013)
68. Girardi, L., Rubele, S., Kerber, L.: Discovery of two distinct red clumps in NGC 419: a rare snapshot of a cluster at the onset of degeneracy. Mon. Not. R. Astron. Soc. **394**, L74–L78 (2009)
69. Li, C.-Y., de Grijs, R., Deng, L.-C.: Not-so-simple stellar populations in the intermediate-age large magellanic cloud star clusters NGC 1831 and NGC 1868. Astrophys. J. **784**, 157–170 (2014)
70. Cabrera-Ziri, I., Bastian, N., Hilker, M., Davies, B., Schweizer, F., Kruijssen, J.M.D., Mejía-Narváez, A., Niederhofer, F., Brandt, T.D., Rejkuba, M., Bruzual, G., Magris, G.: Is the escape velocity in star clusters linked to extended star formation histories? using NGC 7252: W3 as a test case. Mon. Not. R. Astron. Soc. **457**, 809–821 (2016)
71. Mucciarelli, A., Dalessandro, E., Ferraro, F.R., Origlia, L., Lanzoni, B.: No evidence of chemical anomalies in the bimodal turnoff cluster NGC 1806 in the large magellanic cloud. Astrophys. J. Lett. **793**, L6–L11 (2014)
72. Li, C.-Y., de Grijs, R., Deng, L.-C.: The exclusion of a significant range of ages in a massive star cluster. Nature **516**, 367–369 (2014)
73. Bastian, N., Niederhofer, F.: The morphology of the sub-giant branch and red clump reveal no sign of age spreads in intermediate-age clusters. Mon. Not. R. Astron. Soc. **448**, 1863–1873 (2015)
74. Goudfrooij, P., Girardi, L., Rosenfield, P., Bressan, A., Marigo, P., Correnti, M., Puzia, T.H.: On the interpretation of sub-giant branch morphologies of intermediate-age star clusters with extended main sequence turnoffs. Mon. Not. R. Astron. Soc. **450**, 1693–1704 (2015)
75. Li, C.-Y., de Grijs, R., Bastian, N., Deng, L.-C., Niederhofer, F., Zhang, C.-L.: The tight subgiant branch of the intermediate-age star cluster NGC 411 implies a single-aged stellar population. Mon. Not. R. Astron. Soc. **461**, 3212–3221 (2016)
76. Hesser, J.E., Bell, R.A.: CN variations among main-sequence 47 tucanae stars. Astrophys. J. Lett. **238**, L149–L153 (1980)
77. Smith, G.H.: The cyanogen inhomogeneity of NGC 362. Astron. J. **88**, 410–417 (1983)
78. Smith, G.H.: CN and CH Variations among Red Giants in the Globular Cluster NGC. **6171**(95), 755–761 (1988)
79. Penny, A.J., Smith, G.H., Churchill, C.W.: CN and CH inhomogeneities among lower giant branch stars in M71. Mon. Not. R. Astron. Soc. **257**, 89–96 (1992)
80. Smith, G.H.: CN abundance inhomogeneities in the globular cluster M3: results based on merged data sets from the literature. Publ. Astron. Soc. Pac. **114**, 1097–1107 (2002)
81. Smith, G.H., Briley, M.M.: CN abundance inhomogeneities in the globular cluster messier 13 (NGC 6205): results based on merged data sets from the literature. Publ. Astron. Soc. Pac. **118**, 740–753 (2006)
82. Piotto, G., Milone, A.P., Bedin, L.R., et al.: The hubble space telescope UV legacy survey of galactic globular clusters. I. Overview of the project and detection of multiple stellar populations. Astrophys. J. **149**, 91–119 (2015)
83. Carretta, E., Bragaglia, A., Cacciari, C.: Star-to-star Na and O abundance variations along the red giant branch in NGC 2808. Astrophys. J. Lett. **610**, L25–L28 (2004)

84. Carretta, E., Gratton, R.G., Bragaglia, A., Bonifacio, P., Pasquini, L.: Abundance analysis of turn-off and early subgiant stars in the globular cluster 47 Tuc (NGC 104). Astron. Astrophys. **416**, 925–940 (2004)
85. Gratton, R., Sneden, C., Carretta, E.: Abundance variations within globular clusters. Ann. Rev. Astron. Astrophys. **42**, 385–440 (2004)
86. Johnson, J.A., Ivans, I.I., Stetson, P.B.: Chemical Compositions of Red Giant Stars in Old Large Magellanic Cloud Globular Clusters. **640**, 801–822 (2006)
87. Gratton, R.G., Bonifacio, P., Bragaglia, A., et al.: The O-Na and Mg-Al anticorrelations in turn-off and early subgiants in globular clusters. Astron. Astrophys. **369**, 87–98 (2001)
88. Yong, D., Grundahl, F., Lambert, D.L., Nissen, P.E., Shetrone, M.D.: Mg isotopic ratios in giant stars of the globular cluster NGC 6752. Astron. Astrophys. **402**, 985–1001 (2003)
89. Marino, A.F., Milone, A.P., Piotto, G., Villanova, S., Bedin, L.R., Bellini, A., Renzini, A.: A double stellar generation in the globular cluster NGC 6656 (M 22). Two stellar groups with different iron and s-process element abundances. Astron. Astrophys. **505**, 1099–1113 (2009)
90. Yong, D., Roederer, I.U., Grundahl, F.: Iron and neutron-capture element abundance variations in the globular cluster M2 (NGC 7089). Mon. Not. R. Astron. Soc. **441**, 3396 (2014)
91. Carretta, E., Gratton, R.G., Lucatello, S., Bragaglia, A., Catanzaro, G., Leone, F., Momany, Y., D'Orazi, V., Cassisi, S., D'Antona, F., Ortolani, S.: Abundances for a large sample of red giants in NGC 1851: hints for a merger of two clusters? Astrophys. J. Lett. **722**, L1–L6 (2010)
92. Cassisi, S., Salaris, M., Pietrinferni, A., Piotto, G., Milone, A.P., Bedin, L.R., Anderson, J.: The double subgiant branch of NGC 1851: The role of the CNO abundance. Astrophys. J. Lett. **672**, L115–L118 (2008)
93. Piotto, G., Bedin, L.R., Anderson, J., King, I.R., Cassisi, S., Milone, A.P., Villanova, S., Pietrinferni, A., Renzini, A.: A triple main sequence in the globular cluster NGC 2808. Astrophys. J. Lett. **661**, L53–L56 (2007)
94. Milone, A.P., Marino, A.F., Piotto, G.: The hubble space telescope UV legacy survey of galactic globular clusters - II. The Seven stellar populations of NGC 7089 (M2). Mon. Not. R. Astron. Soc. **447**, 927–938 (2015)
95. Milone, A.P., Piotto, G., Bedin, L.R., et al.: Multiple stellar populations in 47 tucanae. Astrophys. J. **744**, 58–80 (2012)
96. Li, C.-Y., de Grijs, R., Deng, L.-C.: The VMC survey. XI. Radial stellar population gradients in the galactic globular cluster 47 tucanae. **790**, 35–49 (2014)
97. Carretta, E., Bragaglia, A., Gratton, R.G., Lucatello, S., D'Orazi, V., Bellazzini, M., Catanzaro, G., Leone, F., Momany, Y., Sollima, A.: NGC 362: another globular cluster with a split red giant branch. Astron. Astrophys. **557**, 138–153 (2013)
98. Lardo, C., Bellazzini, M., Pancino, E., Carretta, E., Bragaglia, A., Dalessandro, E.: Mining SDSS in search of multiple populations in globular clusters. Astron. Astrophys. **525**, 114–125 (2011)
99. Goudfrooij, P., Girardi, L., Kozhurina-Platais, V., et al.: Extended main sequence turnoffs in intermediate-age star clusters: a correlation between turnoff width and early escape velocity. Astrophys. J. **797**, 35–56 (2014)
100. Bastian, N., Cabrera-Ziri, I., Davies, B., Larsen, S.S.: Constraining globular cluster formation through studies of young massive clusters - I. A lack of ongoing star formation within young clusters. Mon. Not. R. Astron. Soc. **436**, 2852–2863 (2013)
101. Bekki, K., Mackey, A.D.: On the origin of double main-sequence turn-offs in star clusters of the magellanic clouds. Mon. Not. R. Astron. Soc. **394**, 124–132 (2009)
102. Schatzman, E.: A theory of the role of magnetic activity during star formation. Annales d'Astrophysique **25**, 18–44 (1962)
103. Mestel, L., Spruit, H.C.: On magnetic braking of late-type stars. Mon. Not. R. Astron. Soc. **226**, 57–66 (1987)
104. McNally, D.: The distribution of angular momentum among main sequence stars. Observatory. **85**, 166–169 (1965)
105. Royer, F., Zorec, J., Gómez, A.E.: Rotational Velocities of A-type stars III. Velocity distributions. Astron. Astrophys. **463**, 671–682 (2007)

106. Bastian, N., de Mink, S.E.: The effect of stellar rotation on colour-magnitude diagrams: on the apparent presence of multiple populations in intermediate age stellar clusters. Mon. Not. R. Astron. Soc. **398**, L11–L15 (2009)
107. Girardi, L., Eggenberger, P., Miglio, A.: Can rotation explain the multiple main-sequence turn-offs of magellanic cloud star clusters? Mon. Not. R. Astron. Soc. **412**, L103–L107 (2011)
108. Yang, W.-M., Bi, S.-L., Meng, X.-C., Liu, Z.-E.: The effects of rotation on the main-sequence turnoff of intermediate-age massive star clusters. Astrophys. J. **776**, 112–126 (2013)
109. Niederhofer, F., Hilker, M., Bastian, N., Silva-Villa, E.: No evidence for significant age spreads in young massive LMC clusters. Astron. Astrophys. **575**, 62–80 (2015)
110. Correnti, M., Goudfrooij, P., Puzia, T.H., de Mink, S.E.: New constraints on the star formation history of the star cluster NGC 1856. Mon. Not. R. Astron. Soc. **450**, 3054–3068 (2015)
111. Georgy, C., Ekström, S., Granada, A., Meynet, G., Mowlavi, N., Eggenberger, P., Maeder, A.: Populations of rotating stars. I. Models from 1.7 to 15 $M_{\odot}$ at $Z = 0.014$, 0.006, and 0.002 with $\Omega/\Omega_{\rm crit}$ between 0 and 1. Astron. Astrophys. **553**, 24–41 (2013)
112. Wu, X.-H., Li, C.-Y., de Grijs, R., Deng, L.-C.: First observational signiture of rotational deceleration in an intermediate-age star cluster. Astrophys. J. Lett. **826**, L14–L22 (2016)
113. Milone, A.P., Marino, A.F., D'Antona, F., Bedin, L.R., Da Costa, G.S., Jerjen, H., Mackey, A.D.: Multiple stellar populations in magellanic cloud clusters - IV. The double main sequence of the young cluster NGC 1755. Mon. Not. R. Astron. Soc. **458**, 4368–4382 (2016)
114. Kraft, R.P.: Abundance Differences among Globular-cluster Giants: Primordial versus Evolutionary Scenarios. Astronomical Society of the Pacific, Publications. **106**, 553–565 (1994)
115. de Mink, S.E., Pols, O.R., Langer, N., Izzard, R.G.: Massive binaries as the source of abundance anomalies in globular clusters. Astron. Astrophys. **507**, L1–L4 (2009)
116. Ventura, P., D'Antona, F.: Massive AGB models of low metallicity: the implications for the self-enrichment scenario in metal-poor globular clusters. Astron. Astrophys. **499**, 835–846 (2009)
117. Valcarce, A.A.R., Catelan, M.: Formation of multiple populations in globular clusters: another possible scenario. Astron. Astrophys. **533**, 120–135 (2011)
118. D'Antona, F., Vesperini, E., D'Ercole, A., Ventura, P., Milone, A. P., Marino, A. F., Tailo, M.: A single model for the variety of multiple-population Formation(s) in globular clusters: a temporal sequence. **458**, 2122–2139 (2016)
119. Bastian, N., Cabrera-Ziri, I., Salaris, M.: A general abundance problem for all self-enrichment scenarios for the origin of multiple populations in globular clusters. Mon. Not. R. Astron. Soc. **449**, 3333–3346 (2015)
120. Bastian, N., Hollyhead, K., Cabrera-Ziri, I.: Constraining globular cluster formation through studies of young massive clusters - IV. Testing the fast rotating massive star scenario. Mon. Not. R. Astron. Soc. **445**, 378–384 (2014)
121. Hollyhead, K., Bastian, N., Adamo, A., Silva-Villa, E., Dale, J., Ryon, J.E., Gazak, Z.: Studying the YMC population of M83: how long clusters remain embedded, their interaction with the ISM and implications for GC formation theories. Mon. Not. R. Astron. Soc. **449**, 1106–1117 (2015)
122. Naiman, J.P., Ramirez-Ruiz, E., Lin, D.N.C.: External mass accumulation onto core potentials: implications for star clusters, galaxies, and galaxy clusters. Astrophys. J. **735**, 25–38 (2011)
123. Amaro-Seoane, P., Konstantinidis, S., Brem, P., Catelan, M.: Mergers of multimetallic globular clusters: the role of dynamics. Mon. Not. R. Astron. Soc. **435**, 809–821 (2013)
124. Bastian, N., Trancho, G., Konstantopoulos, I.S., Miller, B.W.: Gemini spectroscopic survey of young star clusters in merging/interacting galaxies III. The antennae. Astrophys. J. **701**, 607–619 (2009)
125. Lee, J.-W.: Variations in the Na-O anticorrelation in globular clusters: evidence for a deep mixing episode in red giant branch stars. Mon. Not. R. Astron. Soc. **405**, L36–L40 (2010)
126. Nucci, M.C., Busso, M.: Magnetohydrodynamics and deep mixing in evolved stars. I. Two- and three-dimensional analytical models for the asymptotic giant branch. Astrophys. J. **787**, 141–156 (2014)

127. Jiang, D.-K., Han, Z.W., Li, L.F.: Binary interactions as a possible scenario for the formation of multiple stellar populations in globular clusters. Astrophys. J. **789**, 88–93 (2014)
128. Hu, Y., Deng, L.-C., de Grijs, R., Liu, Q., Goodwin, S.P.: The binary fraction of the young cluster NGC 1818 in the large magellanic cloud. Astrophys. J. **724**, 649–656 (2010)
129. de Grijs, R., Li, C.-Y., Zheng, Y., Deng, L.-C., Hu, Y., Kouwenhoven, M.B.N., Wicker, J.E.: Gravitational conundrum? Dynamical mass segregation versus disruption of binary stars in dense stellar systems. Astrophys. J. **765**, 4–12 (2013)
130. Mathieu, R.D., Geller, A.M.: A binary star fraction of 76 per cent and unusual orbit parameters for the blue stragglers of NGC 188. Nature **462**, 1032–1035 (2009)
131. Duquennoy, A., Mayor, M.: Multiplicity among solar-type stars in the solar neighbourhood. II - Distribution of the orbital elements in an unbiased sample. Astron. Astrophys. **248**, 485–524 (1991)
132. Griffin, R.F., Suchkov, A.A.: The nature of overluminous F stars observed in a radial-velocity survey. Astrophys. J. Suppl. **147**, 103–144 (2003)
133. Halbwachs, J.L., Mayor, M., Udry, S., Arenou, F.: Multiplicity among solar-type stars. III. Statistical properties of the F7-K binaries with periods up to 10 years. Astron. Astrophys. **397**, 159–175 (2003)
134. Kouwenhoven, M.B.N., Brown, A.G.A., Zinnecker, H., Kaper, L., Portegies Zwart, S.F.: The primordial binary population. I. A near-infrared adaptive optics search for close visual companions to A star members of scorpius OB2. Astron. Astrophys. **430**, 137–154 (2005)
135. Rastegaev, D.A.: Multiplicity and period distribution of population II field stars in solar vicinity. Astron. J. **140**, 2013–2024 (2010)
136. de Grijs, R., Johnson, R.A., Gilmore, G.F., Frayn, C.M.: Mass segregation in young compact star clusters in the large magellanic cloud - I. Data and luminosity functions. Mon. Not. R. Astron. Soc. **331**, 228–244 (2002)
137. de Grijs, R., Gilmore, G.F., Johnson, R.A., Mackey, A.D.: Mass segregation in young compact star clusters in the large magellanic cloud - II. Mass functions. Mon. Not. R. Astron. Soc. **331**, 245–258 (2002)
138. de Grijs, R., Gilmore, G.F., Mackey, A.D., Wilkinson, M.I., Beaulieu, S.F., Johnson, R.A., Santiago, B.X.: Mass segregation in young compact clusters in the large magellanic cloud - III. Implications for the initial mass function. Mon. Not. R. Astron. Soc. **337**, 597–608 (2002)
139. Heggie, D.C.: Binary evolution in stellar dynamics. Mon. Not. R. Astron. Soc. **173**, 729–787 (1975)
140. Ivanova, N., Belczynski, K., Fregeau, J.M., Rasio, F.A.: The evolution of binary fractions in globular clusters. Mon. Not. R. Astron. Soc. **358**, 572–584 (2005)
141. Trenti, M., Heggie, D.C., Hut, P.: Star clusters with primordial binaries - ii. dynamical evolution of models in a tidal field. Mon. Not. R. Astron. Soc. **374**, 344–356 (2007)
142. Parker, R.J., Goodwin, S.P., Kroupa, P., Kouwenhoven, M.B.N.: Do binaries in clusters form in the same way as in the field? Mon. Not. R. Astron. Soc. **397**, 1577–1586 (2009)
143. Kaczmarek, T., Olczak, C., Pfalzner, S.: Evolution of the binary population in young dense star clusters. Astron. Astrophys. **528**, 144–152 (2011)
144. Trenti, M., Ardi, E., Mineshige, S., Hut, P.: Star clusters with primordial binaries - III. Dynamical interaction between binaries and an intermediate-mass black hole. Mon. Not. R. Astron. Soc. **374**, 857–866 (2007)
145. Rubenstein, E.P., Bailyn, C.D.: Hubble space telescope observations of the post-core-collapse globular cluster NGC 6752. II. A large main-sequence binary population. Astrophys. J. **474**, 701–709 (1997)
146. Zhao, B., Bailyn, C.D.: Hubble space telescope WFPC2 photometry of the globular clusters M3 and M13: binaries and intrinsic broadening on the main sequence. Astron. J. **129**, 1934–1953 (2005)
147. Sollima, A., Beccari, G., Ferraro, F.R., Fusi Pecci, F., Sarajedini, A.: The fraction of binary systems in the core of 13 low-density galactic globular clusters. Mon. Not. R. Astron. Soc. **380**, 781–791 (2007)

148. Sollima, A., Carballo-Bello, J.A., Beccari, G., Ferraro, F.R., Pecci, F.F., Lanzoni, B.: The fraction of binary systems in the core of five galactic open clusters. Mon. Not. R. Astron. Soc. **401**, 577–585 (2010)
149. Milone, A.P., Piotto, G., Bedin, L.R., et al.: The ACS survey of galactic globular clusters. XII. Photometric binaries along the main sequence. Astron. Astrophys. **540**, 16–57 (2012)
150. Elson, R.A.W., Sigurdsson, S., Davies, M., Hurley, J., Gilmore, G.: The binary star population of the young Cluster NGC 1818 in the large magellanic cloud. Mon. Not. R. Astron. Soc. **300**, 857–862 (1998)
151. Dolphin, A.E.: WFPC2 stellar photometry with HSTPHOT. Publ. Astron. Soc. Pac. **112**, 1383–1396 (2000)
152. Liu, Q., de Grijs, R., Deng, L.-C., Hu, Y., Baraffe, I., Beaulieu, S.F.: The initial mass function of the rich young cluster NGC 1818 in the large magellanic cloud. Mon. Not. R. Astron. Soc. **396**, 1665–1674 (2009)
153. Will, J.-M., Bomans, D.J., Tucholke, H.-J., de Boer, K.S., Grebel, E.K., Richtler, T., Seggewiss, W., Vallenari, A.: CCD photometry and astrometry in the selected regions C and E in the large magellanic cloud. Astron. Astrophys. Suppl. **112**, 367–369 (1995)
154. Johnson, R.A., Beaulieu, S.F., Gilmore, G.F., Hurley, J., Santiago, B.X., Tanvir, N.R., Elson, R.A.W.: Young star clusters in the large magellanic cloud: NGC 1805 and 1818. Mon. Not. R. Astron. Soc. **324**, 367–380 (2001)
155. Santos, J.F.C., Dottori, H., Grosbøl, P.: Properties of young star cluster systems: the age signature from near-infrared integrated colours. Astron. Astrophys. **553**, 74–83 (2013)
156. Bate, M.R.: Stellar, brown dwarf and multiple star properties from hydrodynamical simulations of star cluster formation. Mon. Not. R. Astron. Soc. **392**, 590–616 (2009)
157. Mackey, A.D., Gilmore, G.F.: Surface brightness profiles and structural parameters for 53 rich stellar clusters in the large magellanic cloud. Monthly Not. R. Astron. Soc. **338**, 85–119 (2003)
158. Salpeter, E.E.: The luminosity function and stellar evolution. Astrophys. J. **121**, 161–167 (1955)
159. Kouwenhoven, M.B.N., Brown, A.G.A., Portegies Zwart, S.F., Kaper, L.: The primordial binary population. II. Recovering the binary population for intermediate mass stars in scorpius OB2. Astron. Astrophys. **474**, 77–194 (2007)
160. Reggiani, M.M., Meyer, M.R.: Binary formation mechanisms: constraints from the companion mass ratio distribution. Astrophys. J. **738**, 60–67 (2011)
161. Wall, J.V.: Practical statistics for astronomers - II. Correlation, data-modelling and sample comparison. Q. J. R. Astron. Soc. **37**, 519–563 (1996)
162. Allison, R.J., Goodwin, S.P., Parker, R.J., Portegies Zwart, S.F., de Grijs, R.: The early dynamical evolution of cool, clumpy star clusters. Mon. Not. R. Astron. Soc. **407**, 1098–1107 (2010)
163. Kroupa, P.: On the variation of the initial mass function. Mon. Not. R. Astron. Soc. **322**, 231–246 (2001)
164. Elson, R.A.W., Fall, S.M., Freeman, K.C.: The Structure of Young Star Clusters in the Large Magellanic Cloud. **323**, 54–78 (1987)
165. Gürkan, M.A., Freitag, M., Rasio, F.A.: Formation of massive black holes in dense star clusters. I. Mass segregation and core collapse. Astrophys. J. **604**, 632–652 (2004)
166. Inagaki, S., Saslaw, W.C.: Equipartition in multicomponent gravitational systems. Astrophys. J. **292**, 339–347 (1985)
167. Nemec, J.M., Harris, H.C.: Blue straggler stars in the globular cluster NGC 5466. Astrophys. J. **316**, 172–188 (1987)
168. de Marchi, G., Paresce, F.: Very blue stars and mass segregation in the core of M15. Astrophys. J. **467**, 658–665 (1996)
169. Bonnell, I.A., Davies, M.B.: Mass segregation in young stellar clusters. Mon. Not. R. Astron. Soc. **295**, 691 (1998)
170. Binney, J., Tremaine, S.: Galactic Dynamics. Princeton University Press, Princeton (1987)
171. Sollima, A.: The evolution of the binary population in globular clusters: a full analytical computation. Mon. Not. R. Astron. Soc. **388**, 307–322 (2008)

172. Sana, H., de Mink, S.E., de Koter, A., Langer, N., Evans, C.J., Gieles, M., Gosset, E., Izzard, R.G., Le Bouquin, J.-B., Schneider, F.R.N.: Binary interaction dominates the evolution of massive stars. Science **337**, 444–446 (2012)
173. Bastian, N., Lamers, H.J.G.L.M., de Mink, S.E., Longmore, S.N., Goodwin, S.P., Gieles, M.: Early disc accretion as the origin of abundance anomalies in globular clusters. Mon. Not. R. Astron. Soc. **436**, 2398–2411 (2013)
174. Sandage, A.R.: The color-magnitude diagram for the globular cluster M3. Astron. J. **58**, 61–75 (1953)
175. Stryker, L.L.: Blue stragglers. Publ. Astron. Soc. Pac. **105**, 1081–1100 (1993)
176. Zinn, R., Searle, L.: The masses of the anomalous cepheids in the draco system. Astrophys. J. **209**, 734–747 (1976)
177. Tian, B., Deng, L.-C., Han, Z., Zhang, X.B.: The blue stragglers formed via mass transfer in old open clusters. Astron. Astrophys. **455**, 247–254 (2006)
178. Lu, P., Deng, L.-C., Zhang, X.B.: Blue straggler formation via close binary mass transfer. Mon. Not. R. Astron. Soc. **409**, 1013–1021 (2010)
179. Lu, P., Deng, L.-C., Zhang, X.B.: Modeling blue straggler stars in young clusters. Res. Astron. Astrophys. **11**, 1336–1350 (2011)
180. Knigge, C., Leigh, N., Sills, A.: A binary origin for 'blue stragglers' in globular clusters. Nature **457**, 288–290 (2009)
181. Piotto, G., De Angeli, F., King, I.R., Djorgovski, S.G., Bono, G., Cassisi, S., Meylan, G., Recio-Blanco, A., Rich, R.M., Davies, M.B.: Relative frequencies of blue stragglers in galactic globular clusters: constraints for the formation mechanisms. Astrophys. J. Lett. **604**, L109–L112 (2004)
182. Hypki, A., Giersz, M.: MOCCA code for star cluster simulations - I. Blue stragglers, first results. Mon. Not. R. Astron. Soc. **429**, 1221–1243 (2013)
183. Ferraro, F.R., Lanzoni, B., Dalessandro, E., Beccari, G., Pasquato, M., Miocchi, P., Rood, R.T., Sigurdsson, S., Sills, A., Vesperini, E., Mapelli, M., Contreras, R., Sanna, N., Mucciarelli, A.: Dynamical age differences among coeval star clusters as revealed by blue stragglers. Nature **492**, 393–395 (2012)
184. Mapelli, M., Sigurdsson, S., Ferraro, F.R., Colpi, M., Possenti, A., Lanzoni, B.: The radial distribution of blue straggler stars and the nature of their progenitors. Mon. Not. R. Astron. Soc. **373**, 361–368 (2006)
185. Ferraro, F.R., Paltrinieri, B., Fusi Pecci, F., Cacciari, C., Dorman, B., Rood, R.T., Buonanno, R., Corsi, C.E., Burgarella, D., Laget, M.: HST observations of blue straggler stars in the core of the globular cluster M 3. Astron. Astrophys. **324**, 915–928 (1997)
186. Ferraro, F.R., Beccari, G., Dalessandro, E., Lanzoni, B., Sills, A., Rood, R.T., Pecci, F.F., Karakas, A.I., Miocchi, P., Bovinelli, S.: Two distinct sequences of blue straggler stars in the globular cluster M 30. Nature **462**, 1028–1031 (2009)
187. Bailyn, C.D., Pinsonneault, M.H.: On the luminosity function, lifetimes, and origin of blue stragglers in globular clusters. Astrophys. J. **439**, 705–714 (1995)
188. Sills, A., Adams, T., Davies, M.B., Bate, M.R.: High-resolution simulations of stellar collisions between equal-mass main-sequence stars in globular clusters. Mon. Not. R. Astron. Soc. **332**, 49–54 (2002)
189. Shara, M.M., Fall, S.M., Rich, R.M., Zurek, D.: Hubble space telescope observations of NGC 121: First detection of blue stragglers in an extragalactic globular cluster. Astrophys. J. **508**, 570–575 (1998)
190. Johnson, J.A., Bolte, M., Stetson, P.B., Hesser, J.E., Somerville, R.S.: Hubble space telescope observations of the oldest star clusters in the large magellanic cloud. Astrophys. J. **527**, 199–218 (1999)
191. Mackey, A.D., Payne, M.J., Gilmore, G.F.: Photometry of magellanic cloud clusters with the advanced camera for surveys - II. The unique LMC cluster ESO 121-SC03. Mon. Not. R. Astron. Soc. **369**, 921–932 (2006)
192. Castro, R., Santiago, B.X., Gilmore, G.F., Beaulieu, S., Johnson, R.A.: Deep colour-magnitude diagrams of LMC field stars imaged with HST. Mon. Not. R. Astron. Soc. **326**, 333–341 (2001)

193. Cowley, A.P., Hartwick, F.D.A.: Some implications for the early chemical and dynamical evolution of the large magellanic cloud from observations of the oldest globular clusters. Astrophys. J. **259**, 89–95 (1982)
194. Olszewski, E.W., Schommer, R.A., Suntzeff, N.B., Harris, H.C.: Spectroscopy of giants in LMC clusters. I - Velocities, abundances, and the age-metallicity relation. Astron. J. **101**, 515–537 (1991)
195. Grocholski, A.J., Cole, A.A., Sarajedini, A., Geisler, D., Smith, V.V.: Ca II triplet spectroscopy of large magellanic cloud red giants. I. Abundances and velocities for a sample of populous clusters. Astron. J. **132**, 1630–1644 (2006)
196. Ferraro, F.R., Fusi Pecci, F., Bellazzini, M.: Blue stragglers in galactic globular clusters: playing with specific quantities. Astron. Astrophys. **294**, 80–88 (1995)
197. Sigurdsson, S., Davies, M.B., Bolte, M.: Modeling the radial distribution of blue stragglers in M3. Astrophys. J. Lett. **431**, L115–L118 (1994)
198. Rubele, S., Kerber, L., Girardi, L.: The star-formation history of the small magellanic cloud star cluster NGC 419. Mon. Not. R. Astron. Soc. **403**, 1156–1164 (2010)
199. Goudfrooij, P., Puzia, T.H., Kozhurina-Platais, V., Chandar, R.: Population parameters of intermediate-age star clusters in the large magellanic cloud. II. New insights from extended main-sequence turnoffs in seven star clusters. Astrophys. J. **737**, 3–21 (2011)
200. Rubele, S., Girardi, L., Kozhurina-Platais, V., Kerber, L., Goudfrooij, P., Bressan, A., Marigo, P.: The star formation history of the large magellanic cloud star clusters NGC 1846 and NGC 1783. Mon. Not. R. Astron. Soc. **430**, 2774–2788 (2013)
201. Li, C., de Grijs, R., Deng, L.: Not-so-simple stellar populations in the intermediate-age large magellanic cloud star clusters NGC 1831 and NGC 1868. Astrophys. J. **784**, 157–170 (2014)
202. Milone, A.P., Marino, A.F., Piotto, G., Bedin, L.R., Anderson, J., Aparicio, A., Cassisi, S., Rich, R.M.: A double main sequence in the globular cluster NGC 6397. Astrophys. J. **745**, 27–37 (2012)
203. Milone, A.P., Bedin, L.R., Piotto, G., Anderson, J., King, I.R., Sarajedini, A., Dotter, A., Chaboyer, B., Marín-Franch, A., Majewski, S., Aparicio, A., Hempel, M., Paust, N.E.Q., Reid, I.N., Rosenberg, A., Siegel, M.: The ACS survey of galactic globular clusters. III. The double subgiant branch of NGC 1851. Astrophys. J. **673**, 241–250 (2008)
204. Kraft, R.P.: On the nonhomogeneity of metal abundances in stars of globular clusters and satellite subsystems of the galaxy. Ann. Rev. Astron. Astrophys. **17**, 309–343 (1979)
205. Carretta, E., Bragaglia, A., Gratton, R.G., Lucatello, S., Catanzaro, G., Leone, F., Bellazzini, M., Claudi, R., D'Orazi, V., Momany, Y., Ortolani, S., Pancino, E., Piotto, G., Recio-Blanco, A., Sabbi, E.: Na-O anticorrelation and HB. VII. The chemical composition of first and second-generation stars in 15 globular clusters from GIRAFFE spectra. Astron. Astrophys. **505**, 117–138 (2009)
206. Massari, D., Lapenna, E., Bragaglia, E., Dalessandro, E., Ramos, R. C., Amigo, P.: Multiple stellar populations in the globular cluster M3 (NGC 5272): a Strömgren perspective. Monthly Not. R. Astron. Soc. (2016). arXiv:1603.02827
207. Norris, J., Freeman, K.C.: The cyanogen distribution of the giants in 47 Tucanae. Astrophys. J. Lett. **230**, L179–L182 (1979)
208. Norris, J., Freeman, K.C.: The anticorrelation of Carbon and Nitrogen on the horizontal branch of 47 Tucanae. Astrophys. J. **254**, 143–148 (1982)
209. Norris, J., Freeman, K.C., Da Costa, G.S.: The anticorrelation of Cyanogen and CH on the giant branch of 47 Tucanae. Astrophys. J. **277**, 615–622 (1984)
210. Anderson, J., Piotto, G., King, I.R., Bedin, L.R., Guhathakurta, P.: Mixed populations in globular clusters: Et Tu, 47 Tuc? Astrophys. J. Lett. **697**, L58–L62 (2009)
211. Monelli, M., Milone, A.P., Stetson, P.B., Marino, A.F., Cassisi, S., del Pino Molina, A., Salaris, M., Aparicio, A., Asplund, M., Grundahl, F., Piotto, G., Weiss, A., Carrera, R., Cebrin, M., Murabito, S., Pietrinferni, A., Sbordone, L.: The SUMO project I. A survey of multiple populations in globular clusters. Mon. Not. R. Astron. Soc. **431**, 2126–2149 (2013)
212. Nataf, D.M., Gould, A., Pinsonneault, M.H., Stetson, P.B.: The Gradients in the 47 Tuc Red giant branch bump and horizontal branch are consistent with a centrally concentrated helium-enriched second stellar generation. Astrophys. J. **736**, 94–101 (2011)

213. Cordero, M.J., Pilachowski, C.A., Johnson, C.I., McDonald, I., Zijlstra, A.A., Simmerer, J.: Detailed abundances for a large sample of giant stars in the globular cluster 47 Tucanae (NGC 104). Astrophys. J. **780**, 94–108 (2014)
214. Langer, G.E., Hoffman, R., Sneden, C.: Sodium-Oxygen abundance anticorrelations and deep-mixing scenarios for globular-cluster giants. Publ. Astron. Soc. Pac. **105**, 301–307 (1993)
215. Decressin, T., Baumgardt, H., Kroupa, P.: The evolution of two stellar populations in globular clusters. I. The dynamical mixing timescale. Astron. Astrophys. **492**, 101–109 (2008)
216. D'Ercole, A., Vesperini, E., D'Antona, F., McMillan, S.L.W., Recchi, S.: Formation and dynamical evolution of multiple stellar generations in globular clusters. Mon. Not. R. Astron. Soc. **391**, 825–843 (2008)
217. Vesperini, E., McMillan, S.L.W., D'Antona, F., D'Ercole, A.: Dynamical evolution and spatial mixing of multiple population globular clusters. Mon. Not. R. Astron. Soc. **429**, 1913–1921 (2013)
218. Cioni, M.-R.L., Clementini, G., Girardi, L., et al.: The VMC survey I. Strategy and first data. Astron. Astrophys. **527**, 116–138 (2011)
219. Irwin, M. J., Lewis, J., Hodgkin, S., Bunclark, P., Evans, D., McMahon, R., Emerson, J. P., Stewart, M., Beard, S.: vista data flow system: pipeline processing for WFCAM and VISTA. Optimizing scientific return for astronomy through information technologies. In: Quinn, P.J., Bridger, A (ed.) Proceedings of the SPIE. **5493**, 411–422 (2004)
220. Cross, N.J.G., Collins, R.S., Mann, R.G., Read, M.A., Sutorius, E.T.W., Blake, R.P., Holliman, M., Hambly, N.C., Emerson, J.P., Lawrence, A., Noddle, K.T.: The VISTA science archive. Astron. Astrophys. **548**, 119–130 (2012)
221. McLaughlin, D.E., Anderson, J., Meylan, G., Gebhardt, K., Pryor, C., Minniti, D., Phinney, S.: Hubble space telescope proper motions and stellar dynamics in the core of the globular cluster 47 Tucanae. Astrophys. J. Suppl. **166**, 249–297 (2006)
222. Goldsbury, R., Richer, H.B., Anderson, J., Dotter, A., Sarajedini, A., Woodley, K.: The ACS survey of galactic globular clusters. X. New determinations of centers for 65 clusters. Astron. J. **140**, 1830–1837 (2010)
223. Harris, W. E.: A new catalog of globular clusters in the milky way (2010). arXiv:1012.3224
224. Harris, W.E.: A catalog of parameters for globular clusters in the milky way. Astron. J. **112**, 1487–1488 (1996)
225. Lane, R.R., Küpper, A.H.W., Heggie, D.C.: The tidal tails of 47 Tucanae. Mon. Not. R. Astron. Soc. **423**, 2845–2853 (2012)
226. Valcarce, A.A.R., Catelan, M., Sweigart, A.V.: Effects of Helium enrichment in globular clusters. I. Theoretical plane with PGPUC stellar evolution code. Astron. Astrophys. **547**, 5–23 (2012)
227. Zoccali, M., Renzini, A., Ortolani, S., Bragaglia, A., Bohlin, R., Carretta, E., Ferraro, F.R., Gilmozzi, R., Holberg, J.B., Marconi, G., Rich, R.M., Wesemael, F.: The white dwarf distance to the globular cluster 47 Tucanae and its age. Astrophys. J. **553**, 733–743 (2001)
228. di Criscienzo, M., Ventura, P., D'Antona, F., Milone, A., Piotto, G.: The Helium spread in the globular cluster 47 Tuc. Mon. Not. R. Astron. Soc. **408**, 999–1005 (2010)
229. McDonald, I., Boyer, M. L., van Loon, J. Th., Zijlstra, A. A., Hora, J. L., Babler, B., Block, M., Gordon, K., Meade, M., Meixner, M., Misselt, K., Robitaille, T., Sewi?o, M., Shiao, B., Whitney, B.: Fundamental parameters, integrated red giant branch mass loss, and dust production in the galactic globular cluster 47 Tucanae. Astrophys. J. Suppl. **193**, 23–43 (2011)
230. Schlegel, D.J., Finkbeiner, D.P., Davis, M.: Maps of dust infrared emission for use in estimation of reddening and cosmic microwave background radiation foregrounds. Astrophys. J. **500**, 525–553 (1998)
231. Schlafly, E.F., Finkbeiner, D.P.: Measuring redding with sloan digital sky survey stellar spectra and recalibrating SFD. Astrophys. J. **737**, 103–116 (2011)
232. For, B.-Q., Sneden, C.: The chemical compositions of non-variable red and blue field horizontal branch stars. Astron. J. **140**, 1694–1718 (2010)
233. Salaris, M., Held, E.V., Ortolani, S., Gullieuszik, M., Momany, Y.: Deep near-infrared photometry of the globular cluster 47 Tucanae. Reconciling theory and observations. Astron. Astrophys. **476**, 243–253 (2007)

234. Momany, Y., Saviane, I., Smette, A., Bayo, A., Girardi, L., Marconi, G., Milone, A.P., Bressan, A.: The VLT/VISIR Mid-IR view of 47 Tucanae. A further step in solving the puzzle of RGB mass loss. Astron. Astrophys. **537**, 2–16 (2010)
235. Boyer, M.L., van Loon, J.T., McDonald, I., et al.: Is dust forming on the red giant branch in 47 Tuc? Astrophys. J. Lett. **711**, L99–L103 (2010)
236. Bonatto, C., Campos, F., Kepler, S.O.: Mapping the differential reddening in globular clusters. Mon. Not. R. Astron. Soc. **435**, 263–272 (2013)
237. Marino, A.F., Sneden, C., Kraft, R.P., Wallerstein, G., Norris, J.E., da Costa, G., Milone, A.P., Ivans, I.I., Gonzalez, G., Fulbright, J.P., Hilker, M., Piotto, G., Zoccali, M., Stetson, P.B.: The two metallicity groups of the globular cluster M 22: a chemical perspective. Astron. Astrophys. **532**, 8–32 (2011)
238. Marino, A.F., Milone, A.P., Sneden, C., Bergemann, M., Kraft, R.P., Wallerstein, G., Cassisi, S., Aparicio, A., Asplund, M., Bedin, R.L., Hilker, M., Lind, K., Momany, Y., Piotto, G., Roederer, I.U., Stetson, P.B., Zoccali, M.: The double sub-giant branch of NGC 6656 (M 22): a chemical characterization. Astron. Astrophys. **541**, 15–33 (2012)
239. Brown, J.A., Wallerstein, G.: High-resolution CCD spectra of stars in globular clusters. VII - Abundances of 16 elements in 47 Tuc, M4, and M22. Astron. J. **104**, 1818–1830 (1992)
240. Carretta, E., Gratton, R.G.: Abundances for globular cluster giants. I. Homogeneous metallicities for 24 clusters. Astron. Astrophys. Suppl. **121**, 95–112 (1991)
241. Koch, A., McWilliam, A.: A new abundance scale for the globular cluster 47 Tuc. Astron. J. **135**, 1551–1566 (2008)
242. Gratton, R.G., Bragaglia, A., Carretta, E., Clementini, G., Desidera, S., Grundahl, F., Lucatello, S.: Distances and ages of NGC 6397, NGC 6752 and 47 Tuc. Astron. Astrophys. **408**, 529–543 (2003)
243. Marín-Franch, A., Aparicio, A., Piotto, G., et al.: The ACS survey of galactic globular clusters VII. Relative ages. Astrophys. J. **694**, 1498–1516 (2009)
244. Dotter, A., Sarajedini, A., Anderson, J., et al.: The ACS survey of galactic globular clusters. IX. Horizontal branch morphology and the second parameter phenomenon. Astrophys. J. **708**, 698–716 (2010)
245. VandenBerg, D.A., Brogaard, K., Leaman, R., Casagrande, L.: The ages of 55 globular clusters as determined using an improved $\Delta V_{\rm TO}^{\rm HB}$ method along with color-magnitude diagram constraints, and their implications for broader issues. Astrophys. J. **775**, 134–181 (2013)
246. Ventura, P., Criscienzo, M.D., D'Antona, F., Vesperini, E., Tailo, M., Dell'Agli, F., D'Ercole, A.: The formation of multiple populations in the globular cluster 47 Tuc. Mon. Not. R. Astron. Soc. **437**, 3274–3282 (2014)
247. Longmore, S.N., Kruijssen, J.M.D., Bastian, N., Bally, J., Rathborne, J., Testi, L., Stolte, A., Dale, J., Bressert, E., Alves, J.: The formation and early evolution of young massive clusters. In: Protostars and Planets VI, University of Arizona Press, Tucson, vol. 914, pp. 291–314 (2014)
248. Glatt, K., Grebel, E.K., Sabbi, E.: Age determination of six intermediate-age small magellanic cloud star clusters with HST/ACS. Astron. J. **136**, 1703–1727 (2008)
249. Keller, S.C., Mackey, A.D., Da Costa, G.S.: Extended star formation in the intermediate-age large magellanic cloud star cluster NGC 2209. Astrophys. J. Lett. **761**, L5–L9 (2012)
250. Keller, S.C., Mackey, A.D., Da Costa, G.S.: The extended main-sequence turnoff clusters of the large magellanic cloud?missing links in globular cluster evolution. Astrophys. J. **731**, 22–31 (2011)
251. Goudfrooij, P., Puzia, T.H., Kozhurina-Platais, V., Chandar, R.: Population parameters of intermediate-age star clusters in the large magellanic cloud. I. NGC 1846 and its wide main-sequence turnoff. Astron. J. **137**, 4988–5002 (2009)
252. D'Antona, F., Di Criscienzo, M., Decressin, T., Milone, A.P., Vesperini, E., Ventura, P.: The extended main-sequence turn-off cluster ngc 1856: rotational evolution in a coeval stellar ensemble. Mon. Not. R. Astron. Soc. **453**, 2637–2643 (2015)
253. Meynet, G., Maeder, A.: Stellar evolution with rotation. V. Changes in all the outputs of massive star models. Astron. Astrophys. **361**, 101–120 (2000)

254. Brandt, T.D., Huang, C.X.: Rotating stellar models can account for the extended main-sequence turnoffs in intermediate-age clusters. Astrophys. J. **807**, 27–32 (2015)
255. Daivs, L. E.: A reference guide to the IRAF/DOLPHOT package (1994). http://iraf.noao.edu/iraf/web/docs/recommend.html
256. Dolphin, A.: DOLPHOT/WFC3 User's Guide, Version 2.0 (2011). http://americano.dolphinsim.com/dolphin/dolphinWFC3.pdf
257. Dolphin, A.: DOLPHOT User's Guide, Version 2.0 (2013). http://americano.dolphinsim.com/dolphin/dolphin.pdf
258. Dirsch, B., Richtler, T., Gieren, W.P., Hilker, M.: Age and metallicity for six LMC clusters and their surrounding field population. Astron. Astrophys. **360**, 133–160 (2000)
259. Grocholski, A.J., Sarajedini, A., Olsen, K.A.G., Tiede, G.P., Mancone, C.L.: Distances to populous clusters in the large magellanic cloud via the k-band luminosity of the red clump. Astrophys. J. **134**, 680–693 (2007)
260. Elson, R.A.W., Fall, S.M., Freeman, K.C.: The stellar content of rich young clusters in the large magellanic cloud. **336**, 734–751 (1989)
261. Chabrier, G.: The galactic disk mass budget. I. Stellar mass function and density. Astrophys.J. **554**, 1274–1281 (2001)
262. Tayar, J., Pinsonneault, M.H.: Implications of rapid core rotation in red giants for internal angular momentum transport in stars. Astrophys. J. Lett. **775**, L1–L5 (2013)
263. Deheuvels, S., Ballot, J., Beck, P.G., Mosser, B., Østensen, R., García, R.A., Goupil, M.J.: Seismic evidence for a weak radial differential rotation in intermediate-mass core helium burning stars. Astron. Astrophys. **580**, A96–A111 (2015)
264. McLaughlin, D.E., van der Marel, R.P.: Resolved massive star clusters in the milky way and its satellites: brightness profiles and a catalog of fundamental parameters. Astrophys. J. Suppl. **161**, 304–360 (2005)
265. King, I.: The structure of star clusters. I. an empirical density law. Astron. J. **67**, 471–485 (1962)
266. Schönberner, D., Herrero, A., Becker, S., Eber, F., Butler, K., Kudritzki, R.P., Simon, K.P.: A non-LTE stellar atmosphere study of nitrogen-rich early-type stars. Astron. Astrophys. **197**, 209–222 (1988)
267. Gies, D.R., Lambert, D.L.: Carbon, Nitrogen, and Oxygen Abundances in early B-type stars. Astrophys. J. **387**, 673–700 (1992)
268. Niederhofer, F., Bastian, N., Kozhurina-Platais, V., Hilker, M., de Mink, S.E., Cabrera-Ziri, I., Li, C., Ercolano, B.: Controversial age spreads from the main sequence turn-off and red clump in intermediate-age clusters in the LMC. Astron. Astrophys. **586**, 148–164 (2016)
269. Piatti, A.E., Bastian, N.: Extended main sequence turn-offs in low mass intermediate-age clusters. Astron. Astrophys. **590**, 50–61 (2016)
270. Geller, A.M., Mathieu, R.D.: WIYN open cluster study. XLVIII. The hard-binary population of NGC 188. Astron. J. **144**, 54–76 (2012)
271. Baumgardt, H., Parmentier, G., Anders, P., Grebel, E.K.: The star cluster formation history of the LMC. Monthly Not. R. Astron. Soc. **430**, 676–685 (2013)
272. de Grijs, R., Goodwin, S.P., Anders, P.: No compelling evidence of significant early star cluster disruption in the large magellanic cloud. Monthly Not. R. Astron. Soc. **436**, 136–149 (2013)
273. D'Souza, R.: Rix, hans-walter: mass estimates from stellar proper motions: the mass of ω centauri. Monthly Not. R. Astron. Soc. **429**, 1887–1901 (2013)
274. Larsen, S.S., Strader, J., Brodie, J.P.: Constraints on mass loss and self-enrichment scenarios for the globular clusters of the fornax dSph. Astron. Astrophys. **544**, L14–L18 (2012)
275. Dalessandro, E., Massari, D., Bellazzini, M., Miocchi, P., Mucciarelli, A., Salaris, M., Cassisi, S., Ferraro, F.R., Lanzoni, B.: First evidence of fully spatially mixed first and second generations in globular clusters: the case of NGC 6362. Astrophys. J. Lett. **791**, L4–L9 (2014)
276. Jiang, D.-K., Han, Z.-W., Ge, H.-W., Yang, L.-H., Li, L.-F.: The short-period limit of contact binaries. Monthly Not. R. Astron.Soc. **421**, 2769–2773 (2012)
277. Stepien, K.: The low-mass limit for total mass of W UMa-type binaries. Acta Astronomica **56**, 347–364 (2006)

278. Li, C.-Y., de Grijs, R., Deng, L-C.: Stellar populations in star clusters. Res. Astron. Astrophys. (2016)
279. Popescu, B., Hanson, M.M., Elmegreen, B.G.: Age and mass for 920 large magellanic cloud clusters derived from 100 million monte carlo simulations. Astrophys. J. **751**, 122–136 (2012)
280. Smith, L.J., Westmoquette, M.S., Gallagher, J.S., O'Connell, R.W., Rosario, D.J., de Grijs, R.: HST/STIS optical spectroscopy of five super star clusters in the starburst galaxy M82. Monthly Not. R. Astron. Soc. **370**, 513–527 (2006)